UILU-ENG 84-3613

Report No. 113

A FATIGUE LIFE PREDICTION METHOD FOR TENSILE-SHEAR SPOT WELDS

by

Pei-Chung Wang and F. V. Lawrence
Department of Metallurgy and Mining Engineering

A Report of the
MATERIALS ENGINEERING - MECHANICAL BEHAVIOR
College of Engineering, University of Illinois at Urbana-Champaign
October 1984

A FATIGUE LIFE PREDICTION METHOD FOR TENSILE-SHEAR SPOT WELDS

ABSTRACT

An empirical Three Stage Initiation-Propagation (TSIP) model has been developed which predicts the fatigue resistance of tensile-shear spot welds under constant amplitude loading test. The TSIP model consists of Stage I - fatigue crack initiation and early crack growth, Stage II - through sheet thickness crack propagation, and Stage III - across sheet width crack propagation. The improvements of tensile-shear spot weld fatigue resistance through manipulation of geometry, residual stress and material property variables are discussed with the aid of the model. The TSIP model suggests that, in addition to the influence of geometry, residual stresses at the site of crack initiation greatly influence the fatigue resistance of tensile-shear spot welds. The TSIP model predicts the subtle role of material properties in determining the fatigue resistance of tensile-shear spot welds.

Tensile-shear spot welds of low carbon and HSLA steel sheet spot welds have been tested to determine the effect of change in nugget shape, preloading and coining post-weld treatments. The effect of these treatments on the fatigue resistance of spot welds was determined using constant amplitude and variable load histories. The experimental results were compared with predictions made using the TSIP model.

ACKNOWLEDGEMENTS

The author wishes to express his sincere to Professor F. V. Lawrence Jr. and H. T. Corten for their help, guidance and patience during the course of this research project.

Special thanks are also extended to Professor D. F. Socie of the Department of Mechanical Engineering and Dr. S. D. Downing for bulding the function generator for the variable loading test, to K. M. Ewing of General Motors Technical Center for assisting in the welding of the spot weld, to R. Landgraf of Ford Motor Co. for donating the Ford weld history, to R. Evans of Caterpillar Tractor Co. for measuring the residual stresses, to G. Miller of Bethlehem Steel and J. Davidson U. S. Steel Corp. for donating the materials used, and P. Griffis for typing the manuscript.

The author would like to thank his wife, Jenny, for spiritual support and abundant encouragement.

Funds to help support this research were provided by the American Iron and Steel Institute (Grant No. 1201-448) and Fracture Control Program, College of Engineering, University of Illinois at Urbana-Champaign.

TABLE OF CONTENTS

Page

NOMENCLATURE

a	Crack depth, major axis of ellipse
$\underline{a}$	Peterson's material constant
a_I	Initial crack length
a_f	Final crack length
B	Crack growth rate material constant
b	Fatigue strength exponent
C	Crack growth rate material constant
c	Half crack length
D	Nugget diameter
E	Young's modulus
ΔE	Stiffness parameter of SFD method
$\Delta\varepsilon$	Range of local strain
F_t	Surface correction factor
K_f	Fatigue notch factor
K_{fmax}	Maximum fatigue notch factor
K_t	Theoretical stress concentration factor
ΔK	Range of stress intensity factor
K_I	Mode I stress intensity factor
K_{II}	Mode II stress intensity factor
ΔK_{th}	Threshold stress intensity factor
M	Bending moment per unit thickness
M_w	Finite-width correction factor
m	Crack growth rate constant
N_I	Crack initiation life
N_{pt}	Through sheet thickness crack propagation life
N_{pw}	Across the sheet width crack propagation life

N_T	Total fatigue life
R_F	Reliability factor
γ	Notch root radius
S	Nominal stress
ΔS	Nominal stress range
S_D	Maximum stress range
S_N	Constant cycle stress range
S_u	Ultimate tensile strength
S_y	Yield strength
t	Sheet thickness
W	Sheet width
Y_t	Geometrical factor for front and back surface
Y_W	Geometrical factor accounting for finite-width
σ_f'	Fatigue strength coefficient
$\sigma_{o,i}$	Initial mean stress
σ_γ	Residual stress
σ_t	Maximum tangential stress along the surface of blunt crack tip
σ_x	Stress field of blunt crack tip in X direction
σ_y	Stress field of blunt crack tip in Y direction
σ_z	Stress field of blunt crack tip in Z direction
η	Non-dimensional parameter
λ	Non-dimensional parameter
ξ	Random load factor
ν	Possion's Ratio

I. INTRODUCTION

1.1 Resistance Spot Welding

Resistance Spot Welding is a process in which workpieces are pressed together between electrodes, and electrical resistance at the interface produces the welding heat when current is applied. A schematic of the spot welding process is shown in Fig. 1. (1).

1.2 The Fatigue Resistance of Tensile-Shear Spot Welds

Spot welding has recently assumed a greater importance in the manufacture of automobiles because of changes in manufacturing practice. Interest in their mechanical behavior and in particular their fatigue resistance has increased. During the past decade, many studies (2-8) have been made to better understand fatigue performance of spot-welded sheet steels. Although numerous studies have measured the influence of variables such as sheet thickness and width, nugget diameter, load ratio, and loading history on fatigue resistance of spot welds, relatively little work have been done on developing an analytical model to reflect the combined effects of all those possible variables. Since fatigue testing is expensive and time consuming, models that predict the fatigue life have great potential for reducing the need for testing programs and for assisting the design engineer in optimizing those variables which influence the fatigue resistance of welds.

Motivated by fuel economy and weight considerations, the automotive industry has used increasing amounts of high strength low alloy (HSLA) steels in car design. To justify use of the HSLA steels their spot weld fatigue resistance must be better than that of mild steel. However, most of the experimental data generated to date (9-13) suggests that the high cycle fatigue strength is not improved and may actually be slightly reduced

for equivalent welds in the same thickness. Thus, the need for improving fatigue resistance of HSLA is being increasingly recognized.

1.3 Effect of Spot-Weld Variables on Fatigue Resistance

1.3.1 Effect of Sheet Thickness

Sperle (15) performed an extensive study of influence of sheet thickness on strength and showed that there is no significant thickness effect on both static and fatigue strength of spot welded joints for a given nugget diameter. Cappelli et al. (3) also examined the effects of three different thickness, 1.5 mm (.059 in.), 2 mm (.078 in.) and 2.5 mm (.098 in.) on fatigue strength using the same electrode and found that no noticeable increase in strength can be observed for thicker material at 10^7 cycles. Cappelli et al. explained that this is probably due to the presence of combined bending and tensile stresses introduced by insufficient rigidity of the specimen, allowing its rotation during testing. However, work done by Overbeeke and Draisma (16) on 7 mm (.28 in.) thick plate of spot welds indicated that increasing the plate thickness increased the life devoted to the propagation of the fatigue crack through the thickness of the plate. The work of Iwasaki et al. (17) also showed the fatigue strength of spot welded joints tends to increase with an increase in sheet thickness. This tendency is more pronounced in a low-cycle region involving the application of greater load. Davidson (18) developed a stiffness parameter to describe fatigue resistance of tensile-shear spot welds, found an increase in sheet thickness along with increasing nugget size resulted in stiffer joints. As expected, an increase in joint stiffness improved the fatigue resistance. This stiffness concept is a useful index to characterize the fatigue resistance

of spot welds.

1.3.2 Effect of Sheet Width

Orts (2) examined the sheet width effect on fatigue strength of a single tensile shear spot weld in HSLA (222.4 kN (50 Ksi) yield strength) steel and found that when the sheet width exceeded 50 mm (1.97 in.), there was little effect of sheet width. Width 25mm (.98 in.) showed reduced fatigue strength over the entire range of lives. The work of Davidson (18) showed that the narrower the sheet width, the less stiff is the joint and, the lower will be the fatigue resistance of spot welds.

1.3.3 Effect of Nugget Diameter

Many investigators (3,16) have shown that increased nugget diameter increases both the static and fatigue strength of spot welded joints. DeFourny (21) observed that as much as a 50% increase in fatigue strength for HSLA cold-rolled steel at 10^7 cycles can be obtained when the electrode diameter was increased from 5 mm (.197 in.) to 8 mm (.315 in.). However, Overbeeke and Draisma (16) showed for 7 mm (.275 in.) thick plain carbon steel that when the nugget diameter exceeded 18 mm (.708 in.) there was no effect of nugget diameter on fatigue strength. An underwelded nugget reduces the fatigue strength in the low cycle regime, and interfacial nugget failure was observed. Davidson (18) showed that an increased nugget diameter increases the joint stiffness, but to a lesser degree than increasing the sheet thickness. Nugget diameter also plays a major role in determining the propensity for pull-out or interfacial failure.

1.3.4 Effect of Welding Condition

Lawrence et al. (22) have conducted an extensive study on the influence of welding schedule on fatigue resistance of tensile-shear spot welds. Low current (underweld) diminished significantly the fatigue resistance whereas, high current welding (expulsion) did not greatly alter the fatigue resistance. Kimchi (23) found that .97 mm (.038 in.) thick bare HSLA and low carbon steel spot welds made with current levels above the initial expulsion point showed significant improvement (up to 68%) in fatigue life due to an increase in nugget diameter. However, welding under expulsion conditions causes rapid electrode deterioration. The extent and consequences of electrode deterioration are dependent on electrode geometry.

One effective technique for improving the fatigue strength, which has been found by Shinozaki et al. (24), is to generate moderate expulsion by welding with a current just above the upper lobe curve. Fatigue strengths (10^7 cycles) of a dual-phase steel sheet were increased by about a factor of two as compared with those of the normal welding method. This improvement in fatigue strength is due to the increase in effective area of 'corona bond', and due to the increase in compressive residual stresses around the nugget.

1.3.5 Effect of Base Metal Strength

Many studies on the static strength of the spot welded joint have been made, and it has been widely accepted that tensile-shear spot weld strength increases with the tensile strength of the base materials (25). Also the low cycle (10^3 -10^4) fatigue strength of spot welded joints improve with increasing base metal strength, however the (10^6 -10^7) cycle fatigue strength does not exhibit a dependence on the base metal strength and is nearly identical for all materials (2,9,10,12).

1.3.6 Effect of Galvanized Coating

The effect of galvanization on the fatigue resistance of spot welds was investigated by Lawrence et al. (22), Freytag (26) and Orts (2). Lawrence et al. showed that galvanization of low carbon and HSLA steel sheets prior to spot welding does not seem to alter the fatigue resistance. Freytag, however, found that an improvement in fatigue resistance on low carbon steel as a result of coating. The work of Orts also indicated an improvement in fatigue resistance on aluminzed steel.

1.3.7 Effect of Oiled Surface

Matsoukas, Stevens and Mai (27) studied the effect of an oil coating on the fatigue resistance of stainless steel sheet. They showed that the presence of oil on the surface has a beneficial effect and increased the fatigue life of the welded joint. They also conducted an experiment on fatigue crack propagation of parent metal in air and in oil and found oil did not affect da/dn for the same ΔK in the region II fatigue crack growth. The threshold stress intensity (K_{th}) is higher in an oil environment than in air. Thus, this increase in life is ascribed to the increasing the number of fatigue cycles required for crack initiation when

oil is present.

Similarily, Overbeeke and Draisma (16), Frost (28) indicate that oil greatly extends the fatigue life of the spot-welded lap joints. Frost suggested that this life improvement is because the presence of oil on the surface of the spot welds inhibits atmospheric corrosion.

1.3.8 Effect of Post-Weld Treatment

Choquet et al. (29) extensively studied the effects of tensile preloading on fatigue resistance of spot welds and found that applying a order of 75% of their ultimate tensile load to a row of stainless spot welds increased as much as 400% in strength at 10^7 cycles. This application of tensile preloading should result in a more even distribution of subsequent fatigue stresses among the spots, therely improving their fatigue characteristics. In addition, Lawrence et al. (30) also found tensile preloading the single spot weld prior to fatigue testing caused a substantial improvement in the fatigue resistance which was most marked for the HSLA steel.

Welter and Choquet (31) showed that a hydrodynamic compression treatment of single stainless spot weld which yields above 400% fatigue strength improvement at 10^7 cycles. Chandel (32) also found that the introduction (or relief) of residual stresses around spot welds by plastic deformation significantly increases their fatigue strength and endurance limits.

Balasubramanian (33) studied the effects of spot weld heat treatment on the fatigue strength of spot welds in plain carbon steel and found that heat treating both in situ in the welding machine and in the furnace improved considerably their fatigue resistance. Hiratsuka and Ito (34) proposed a method for determining the tempering cycle condition for spot

welds on anti-corrosion high strength steels and based on the following principles: The electrical resistance of the steels rises with the temperature but, during the austenite transformation, this temperature drops remarkably. When the weld periphery has been properly tempered, the center is heated above the austenitizing temperature. Consequently, the resistance of the weld during post-heating increases first and then decreases slowly or rapidly depending on the post-heat current. Thus, by analyzing the resistance characteristics, it is possible to select the optimum post-heating conditions. To check the validity of this method, fatigue strength tests were carried out. The results are in fairly good agreement with temper schedule selected. The improvement by the temper treatment will be caused by the generation of residual compressive stresses at 'corona bond' and indentation. The residual compressive stresses are probably generated by the tempering of martensite in nugget and plastic deformation of metal around the nugget by the electrode force. Similarily, Shinozaki et al.(24) also conducted a controlled tempering treatment during the welding schedule on the fatigue strength of spot welded joints in a precipitation-hardened steel having relatively high carbon content (.12 %). By this treatment, fatigue strengths at 10^7 cycles increased by about a factor of two compared with those obtained using conventional welding methods.

1.4. Scope

This study was devoted to finding means of substantially improving the fatigue resistance of both high strength low alloy (HSLA) and plain carbon steel spot welds. The post-weld treatments (change nugget shape, pre-loading and coining) have been investigated. Fatigue tests of spot welds having elliptical nugget shape with stress ratio R=-1 were conducted. Fatigue tests of pre-loaded and coined spot welds with stress ratio R=-1 and a variable load history were also performed.

To assist in improving the fatigue resistance, a Three-Stage model (I-P model) was developed for estimating the fatigue resistance of tensile-shear spot welds. Low cycle fatigue concepts combined with the results of crack propagation experiments on spot welds and existing stress intensity factor solutions were used to form this Three Stage model.

A three-dimensional stress analysis was performed and the stress intensity factor (K_I) was calculated for tensile-shear spot welds. Thickness, width and nugget diameter effects on stress intensity factor (K_I) were determined using a stiffness derivative technique (35).

The Munse Fatigue Criterion (36,37) was used and combined with the constant amplitude fatigue test data to estimate the maximun fatigue design stress for spot welds under the variable load history.

II. THE THREE STAGE INITIATION-PROPAGATION MODEL FOR TENSILE-SHEAR SPOT WELDS

2.1. Total Fatigue Life of Tensile-Shear Spot Welds

The Three Stage Initiation-Propagation model (TSIP) considers the total fatigue life of tensile-shear spot welds to consist of three stages: Stage I - fatigue crack initiation life and early growth (N_I), Stage II - crack propagation life involved in the propagation of a crack through the sheet thickness (N_{pt}), and Stage III - crack propagation life spent in the growth of a nugget-size crack across the specimen width (N_{pw}):

$$N_T = N_I + N_{pt} + N_{pw} \tag{1}$$

In Section 2.2, the elastic stress concentration factor (K_t) for tensile-shear spot welds will be computed as a means of estimating K_{fmax} and the Stage I crack initiation life (N_I) which will be dealt with in Section 2.3. The fatigue crack propagation life is estimated in Section 2.4, 2.5 and 2.6 in two segments, propagation through the sheet thickness (Stage II) and widthwise propagation (Stage III), corresponding to N_{pt} and N_{pw} in Eq. 1.

2.2. Estimation of Elastic Stress Concentration Factor (K_t) for a Tensile-Shear Spot Weld

Stress intensity factors for the tensile-shear spot weld have been derived by Pook (38). For a single spot weld, the expressions for the mode I and II stress intensity factors are

$$K_I = \frac{P}{D^{1.5}}\{.964(D/t)^{.397}\} \tag{2}$$

$$(D/t < 10)$$

$$K_{II} = \frac{P}{D^{1.5}}\{.798 + .458\,(D/t)^{.710}\} \tag{3}$$

where P is the load applied to the spot weld, D is the nugget diameter and t is sheet thickness. The above stress intensity factor expressions for point A in Fig. 2 are based on small deformation elasticity; and, thus, finite deformations such as nugget rotation have not been included.

The expressions developed by Pook for the stress intensity factor, (K_I), for sharp crack have been modified to predict the elastic stress concentration factor (K_t) associated with notches having a finite radius (39). The hyperbolic blunt crack shown in Fig. 3 has a finite crack-tip (r). A polar system of coordinates centered at O was used where $\rho\cos\theta = (\eta + 1/2)r$, and $\rho\sin\theta = \lambda r$. The quantities η and λ are non-dimensional parameters which define the position of a point relative to the crack tip.

The stress field ahead of the blunt crack tip is (39):

For Mode I:

$$\begin{pmatrix}\sigma_x\\ \sigma_y\\ \tau_{xy}\end{pmatrix} \frac{K_I}{(2\pi\rho)^{1/2}} \left[\begin{pmatrix}f_1(\theta)\\ f_2(\theta)\\ f_3(\theta)\end{pmatrix} \begin{matrix}-\\ +\\ -\end{matrix} \frac{r}{2\rho} \begin{pmatrix}\cos\frac{3}{2}\theta\\ \cos\frac{3}{2}\theta\\ \sin\frac{3}{2}\theta\end{pmatrix}\right] \tag{4}$$

For Mode II:

$$\begin{pmatrix}\sigma_x\\ \sigma_y\\ \tau_{xy}\end{pmatrix} \frac{K_{II}}{(2\pi\rho)^{1/2}} \left[\begin{pmatrix}f_4(\theta)\\ f_5(\theta)\\ f_6(\theta)\end{pmatrix} \begin{matrix}+\\ -\\ -\end{matrix} \frac{r}{2\rho} \begin{pmatrix}\sin\frac{3}{2}\theta\\ \sin\frac{3}{2}\theta\\ \cos\frac{3}{2}\theta\end{pmatrix}\right] \tag{5}$$

where:
$$f_1(\theta) = \cos\frac{\theta}{2}\left[1 - \sin\frac{\theta}{2}\sin\frac{3}{2}\theta\right]$$
$$f_2(\theta) = \cos\frac{\theta}{2}\left[1 + \sin\frac{\theta}{2}\sin\frac{3}{2}\theta\right]$$
$$f_3(\theta) = \sin\frac{\theta}{2}\cos\frac{\theta}{2}\cos\frac{3}{2}\theta$$
$$f_4(\theta) = -\sin\frac{\theta}{2}\left[2 + \cos\frac{\theta}{2}\cos\frac{3}{2}\theta\right]$$

$$f_5(\theta) = \sin\frac{\theta}{2}\cos\frac{\theta}{2}\cos\frac{3\theta}{2}\theta$$

$$f_6(\theta) = \cos\frac{\theta}{2}\left[1 - \sin\frac{\theta}{2}\sin\frac{3}{2}\theta\right]$$

The maximum tangential stress along the interior surface of the blunt crack tip due to a remotely applied load P is:

$$\sigma_t = \frac{2K_I}{(\pi\gamma)^{1/2}}\cos\frac{2\theta}{2} - \frac{K_{II}}{(\pi\gamma)^{1/2}}\sin\theta \qquad (6)$$

Upon substitution of the stress intensity factors of Pook (Eq. 2,3) into Eq. 6 the maximum value of σ_t, is found to occur at an angle θ of $-51°$ for $D/t = 4.7$. The initial angle of crack growth from this point of maximum stress is predicted to be 66° from the horizontal: see Fig. 4.

If one defines the elastic stress concentration factor (K_t) as the ratio of the peak notch tip stress (σ_t at $\theta = -51°$) to the remote average tensile stress in the sheet (P/Wt), then K_t for a tensile-shear spot weld becomes from Eqs. 2,3 and 6:

$$K_t = \frac{Wt}{(\pi\gamma)^{1/2}D^{1.5}}\left[1.61(D/t)^{.397} + .593 + .34(D/t)^{.710}\right] \qquad (7)$$

The above value of K_t will be used to estimate the number of cycles for initiation of a crack in the next section.

2.3 Stage I Fatigue Crack Initiation Life Estimation

The Stage I crack initiation life consists of the crack initiation and early crack growth. For long life fatigue ($N_I >> N_{tr}$), cyclic hardening and softening effects can usually be ignored. In such cases. N_I can be estimated using the empirical Basquin equation (40) and the linear damage summation rule (41):

$$\int_1^{2N_I}\left[(\sigma_f/\Delta\sigma/2)(1-\sigma_{o,i}(2N)^k/\sigma'_f\right]^{-1/b}dN = 1 \qquad (8)$$

Where N_I = fatigue crack initiation life

σ'_f = the fatigue strength coefficient

b = the fatigue strength exponent

k = the mean stress relaxation exponent

$\sigma_{o,i}$ = the local initial mean stress

$\Delta\sigma$ = the local stress range

When the test results are unavailable, the fatigue properties and relaxation constant can be estimated from the hardness measurements of the region where the fatigue crack initiates (42).

The notch root stress ($\Delta\sigma$), i.e. the stress at the critical region in the weld (point A in Fig.8) can be obtained using Neuber's rule (43) and a " set up cycle" analysis (44,45):

$$\Delta\sigma\Delta\varepsilon = (K_f\Delta S)^2/E \qquad (9)$$

where: Δs is the remote nominal stress range which is in the elastic region and K_f is the fatigue notch factor.

To proceed with the calculation suggested by Eq. 9 the appropriate value of K_f for the critical region in the weld is needed. A difficulty arises from the fact that the notch-root radius of a discontinuity such as weld toe is unknown and variable. Microscopic examination of weld toes reveals that practically any and all value of radius are observed. To analyze notches such as weld toes which exhibit all possible values of notch-root radius, the concept of using the maximum value of K_f , K_{fmax} has been developed (41). K_f can be estimated using Peterson's equation (47):

$$K_f = 1 + \frac{K_t - 1}{1 + \frac{a}{r}} \tag{10}$$

where K_t is the elastic stress concentration factor, a is material parameter ($\sim 1.08 \times 10^5 Su^{-2}$)(46), for steel (mm), r is the notch root radius (mm), and Su is the ultimate strength (Mpa). K_{fmax} is K_f evaluated for a notch root radius (r) equal to the material constant (a) in Peterson's equation (47). Since K_t is in the range 10-30, (K_t-1) in Eq. 7 is assumed approximately equal to K_t. Substituting Eq. 7 into Eq. 10, thus, K_{fmax} for tensile-shear spot weld is

$$K_{fmax} \cong 1 + 2.41 \times 10^{-3} \, WS_u D^{-1} t^{1/2} f(t/D) \qquad \text{(MPa - mm units)} \tag{11}$$

where

$$f(t/D) = .569(t/D)^{.103} + .209(t/D)^5 + .12(t/D)^{-.21} \tag{12}$$

Substituting Eq. 11 into Eq. 9, the notch root stresses can be calculated. Then, the crack initiation life (N_I) can be estimated using Eq. 8.

2.4. Fatigue Crack Propagation Life Estimation

Fatigue crack propagation characteristics are conveniently represented in the form of a power law (48):

$$\frac{da}{dN} = c(\Delta K)^m \tag{13}$$

Where $\frac{da}{dN}$ is the rate of crack extension and ΔK is the range of K_I. Rearranging Eq. 13 gives,

$$N_p = \int_{a_I}^{a_f} \frac{da}{C(\Delta K)^m} \tag{14}$$

where C and m are material constants, a_I and a_f are initial and final crack lengths. The range of K_I is conveniently expressed in terms of the stress range ΔS as

$$\Delta K = Y\Delta S\sqrt{\pi a} \tag{15}$$

where Y is a combination of geometric correction factors for crack shape, finite plate dimensions and other geometry (49).

A fatigue crack propagation expression which has been derived by Zheng and Hirt (50) is:

$$\frac{da}{dN} = B(\Delta K - \Delta K_{th})^2 \tag{16}$$

where B is a material constant and ΔK_{th} is the threshold stress intensity factor. For HSLA, B is equal to $6.65\text{x}10^{-10}$ MPa^{-2} and ΔK_{th} is equal to 10.10 MPa $\sqrt{m}$ (50).

The negative inverse slopes of regression analysis of tensile-shear spot weld S-N curve in the life range 10^4 to $3\text{x}10^6$ cycles for B60XK G-90 (HSLA) and 10^5 to $2\text{x}10^7$ cycles for galvanized SAE 960X (HSLA) are 5.2 and 5.6, respectively. Thus, the value of 5 is assumed equal to the exponent m in Eq. 13 and Eq. 13 becomes

$$\frac{da}{dN} = C(\Delta K)^5 \tag{17}$$

The material constant C can be obtained numerically by setting

$$\frac{da}{dN} = B(\Delta K - \Delta K_{th})^2 = C(\Delta K)^5 \tag{18}$$

The fatigue crack propagation life of tensile-shear spot weld consists of first the life required to propagate a crack through the sheet thickness until it reaches the specimen surface and then the life spent to grow a nugget-size crack laterally towards side of the sheet until specimen separation occurs. These two parts were defined as N_{pt} and N_{pw} in Eq. 2.1 and will be considered in turn.

2.5 Stage II Crack Propagation Life (N_{pt}) Estimation

Since a spot weld has a three-dimensional geometry, Emery's solution (51) does not work for obtaining the stress intensity factor. The finite element method (FEM) was attempted to estimate the stress intensity factor for various crack lengths by using stiffness derivative technique (35). Then, this stress intensity factor is substituted into the Paris law to estimate Stage II crack propagation life. However, efforts to obtain the stress intensity factor for various crack depths have been discontinued due to the fact that solving this problem using FEM is simply too costly.

Smith (52) has carried out a study of crack depth versus life for different load levels for a series of spot weld specimens. Fig. 5 shows the crack depth versus life data for four different load levels and the curve fitted relationship (solid line) for each load level. The calculated stress intensity factor range for four different load levels can be obtained by taking the derivative of 2.22 kN (500 lbs.) curve to estimate da/dn and by using the material constant ($C = 1.0 \times 10^{-13}$ MPa^{-5} $m^{-3/2}$, $m = 5$ for HSLA steel). The value of ΔK is computed from Eq. 11. Since the stress intensity factor range depends upon the load range applied, $\Delta K/P$ versus crack depth (a) is graphed in Fig. 6. This relationship should be the same for each load level. However, as seen in Fig. 6, the curves for the four different load levels

do not coincide. The probable reasons for this difference are the inconsistency of welding schedule, crack measurements and test environment. The dashed lines shown in Fig. 5 represent the calculated (based on Eq. 17) crack depth versus life for four different load levels using 2.22 kN (500 lbs.) data and .08 mm (.003 in.) for the a_I.

The 2.22 kN (500 lbs.) load range was chosen to characterize crack propagation behavior in stage II growth. Consequently, the empirical geometrical factor Y ($\Delta K/\Delta S \sqrt{\pi a}$) is a function of a and curve fitting was used to obtain the relationship below:

$$Y = -8.96(a/t)^3 + 20.03(a/t)^2 - 16.2(a/t) + 8.20 \qquad (19)$$

When Y is substituted into Eq. 15 and .254 mm (.01 in.) and sheet thickness t are used for a_I and a_f, the life N_{pt} can be calculated. The .254 mm (.01 in.) was used for a_I because the crack depth which is less than .254 mm (.01 in.) is dominated by mode I and mode II. The .254 mm (.01 in.) was used simply to avoid the complexity of mixed mode I and II crack propagation behavior.

2.6 Stage III Crack Propagation Life (N_{pw}) Estimation

As shown in Fig. 7, a crack emanating from a hole loaded axially with a centrally located force at the hole and an equal and opposite distributed force at the opposite edge represents the axial loading as the crack propagates across the sheet width (53). Note that P is the force per unit plate thickness. The hole should be small with respect to the crack. The stress intensity factor at this stage has been derived by using elastic superposition (54). According to Fig. 7 the desired case can be obtained from a superposition of three others. Thus,

$$\Delta K_{IA} = \Delta K_{IB} + \Delta K_{ID} - \Delta K_{IE} \tag{20}$$

Since it is obvious that $\Delta K_{IA} = \Delta K_{IE}$, the stress intensity follows from:

$$\Delta K_{IA} = .5(\Delta K_{IB} + \Delta K_{ID}) \tag{21}$$

The spot weld actually experiences both axial and bending stresses. Because bending stresses have a direction parallel to the axial load and normal to the crack surface, they are superimposed on the stresses due to the axial load. The stress intensity factor for combined axial and bending loads can be obtained again by using superposition (54).

$$\Delta K_{IA} = .5(\Delta K_{IBa} + \Delta K_{IBb} + \Delta K_{IDa} + \Delta K_{IDb}) \tag{22}$$

where subscript a and b stand for axial and bending. See Appendix A for the stress intensity factor solution of ΔK_{IBa}, ΔK_{IBb}, ΔK_{IDa}, ΔK_{IDb}. When ΔK_{IA} is substituted for ΔK in Eq. 17 and the nugget diameter and sheet width are used for a_I and a_f, the life N_{pw} can be calculated.

Thus, an analytical model for estimating the total fatigue life of spot welds has been developed in which the total fatigue life of a spot weld (N_T) is the sum of the initiation (Eq. 8) and propagation stages (Eq. 17) given by

$$N_T = N_I + N_{pt} + N_{pw} \tag{23}$$

Eq. 23 is used to estimate total fatigue life of spot welds for comparison with experiments in Section V, Results and Predictions.

2.7 Assumptions and Approximations of The Three Stage Initiation-Propagation Model

Stage I:

1. Root of nugget may be considered to be blunt notch.
2. No cyclic hardening and softening occur.
3. The Basquin equation with mean stress correction valid.
4. Linear damage rule was assumed to be valid.
5. Mean stress relaxation was assumed to occur as a function of life.
6. Residual stress was assumed to be equal to the yield strength of the base metal in the as-welded state.
7. The cyclic properties were estimated from hardness measurements (DPH).

Stage II:

1. Direct observation of crack development in tensile-shear spot welds was used as a guide to modelling and a source for the stress intensity factor.
2. The Paris power law was assumed to apply.
3. The crack aspect ratio was assumed to be constant.
4. The material properties of the HAZ were taken as $m = 5$, $C = 1.0 \times 10^{-13}$ MPa^{-5} $m^{3/2}$.
5. The initial crack length was assumed to be .254 mm (.01 in.).
6. The final crack length was assumed to be sheet thickness.
7. The effect of residual stress was assumed to be

negligible.

Stage III:

1. A model for a crack emanating from a loaded rivet hole was taken to model the tensile-shear spot welds.
2. The Paris power law was assumed to apply.
3. The initial crack length was taken as the nugget diameter.
4. The final crack length was taken as the sheet width.
5. The effect of residual stress was assumed to be negligible.

III EXPERIMENTAL PROCEDURES

3.1. Materials and Specimen Preparation

Three galvanized sheet steels were used in this investigation. A low-carbon galvanized sheet steel 1.14 mm (.045 in.) thick designated DQSK G-90 was donated by the U. S. Steel Corporation. A high strength low alloy (HSLA) galvanized sheet steel 1.29 mm (.051 in.) designated B60XK G-90 was donated by the Bethlehem Steel Corporation. A galvanized high strength low alloy sheet steel 1.40 mm (.055 in.) designated SAE 960X (HI-FORM 60) was donated by General Motors Corporation. The chemical composition and average tensile properties for these steels are shown in Tables 1 and 2. The Heat-Affected-Zone (HAZ) fatigue properties estimated from hardness measurements (55,56) for these three materials are listed in Table 3.

The specimens were fabricated from 38.1 x 69.8 mm and 38.1 x 44.4 mm (1.5 x 2.75 in. and 1.5 x 1.75 in.) coupons sheared from sheet with their longer dimensions parallel to the longitudinal orientation. The specimen is shown in Fig. 8. A fixture was used to ensure consistency in weld location, as shown in Fig. 9.

Specimens were welded at the General Motors Technical Center using Fisher Body division recommended procedures (57,58). The spot welds were prepared with a single-phase, microprocessor-controlled AC electrical resistance spot welding unit. The optimum welding conditions for the DQSK G-90, B60XK G-90 and galvanized SAE 960X steel were listed in Table 4. The welding lobe diagrams for DQSK G-90, B60XK G-90 and galvanized SAE 960X were given in Fig. 10. The welding lobe diagram is a plot of the welding time in cycles (one cycle equals 1/60 second.) versus the welding current in thousands of amperes (Kilo amperes). In each of the three diagrams, the

open circle represents the optimum welding condition.

3.2. Post-Weld Treatment To Enhance Fatigue Resistance

Three variations in specimen preparation procedure designed to enhance the fatigue life were assessed for their influence on the fatigue life of tensile-shear spot welds. These included change of nugget shape, mechanical preloading and coining.

3.2.1 Change in Nugget Shape

Tensile-shear spot welds were manufactured using an elliptical and a rectangular cross sectional electrodes. The same welding conditions were applied except higher current was used to reach the desired nugget dimensions. These welding processes resulted in roughly elliptical nugget shapes having an approximate aspect ratio of 1.7 : 1.0. The influence of nugget orientation is considered in Section 6.5.1.

3.2.2 Preload

Specimens were preloaded in tension to 50% and 75% of their anticipated maximum static strength prior to fatigue testing.

3.2.3 Coining

Coining technique was used to stress-relieve or introduce compressive residual stresses to the spot weld region through the application of a high compressive load to the nugget of the spot weld, normal to the specimen face.

Specimens were 'coined' using a die which fitted into the dimple surface of spot welds. A jig of two steel blocks was used to facilitate the accurate positioning of spot weld. The load was applied through a 6.35 mm (.25 in.) diameter steel rod with a flat tip which covers the weld

nugget. A RIEHLE machine was used for the compression. The optimum coining treatment were determined by trial and error. This coining operation was carried out using two levels of compressive load: 22 kN (5,000 lbs.) and 44 kN (10,000 lbs.). To avoid upsetting the back face of the specimen or bending the specimen, an insert was used to support the nugget and to apply force equally to both sides of the nugget. Specimens were coined with and without the use of a lubricating oil. The lubricating oil was used to facilitate the lateral plastic flow of the material during the compression. A schematic drawing of the coining pretreatment is shown in Fig. 11.

3.3. Fatigue Testing Program

The specimens were gripped with self-aligning hydraulic grips, as shown in Fig. 12 (59) and tested in a 3 kip capacity MTS testing machine. The design of the specimens (60) and the grips were such that the specimen sustained 6.7 kN (1,500 lbs.) compression without buckling. To minimize bending stresses during testing, both ends of the specimens were reinforced by welding two filler plates of the same thickness. As seen in Fig. 8, two small holes were drilled in the specimen for alignment purposes. Thus, it was possible to carry out tension-to-compression (R=-1) load cycle tests. All constant amplitude fatigue tests were performed at 5 to 20 Hz frequency under ambient laboratory conditions.

Fatigue tests using a variable load history in which life was measured were also carried out. Fig. 13 shows a load history which was donated by the Ford Motor Company. A histogram of this load histoy which contains 18,844 events is shown in Fig. 14. The events of the Ford history were stored in a function generator which replayed the variable load history to the fatigue testing apparatus. The test matrix of B60XK G-90, DQSK G-90

and galvanized SAE 960X steel spot welds is shown in Table 5.

In both the constant amplitude and variable load history tests, pull-out failure and/or complete separation of the test piece into two pieces was defined as failure. Thus, the test results reflect crack initiation at the circumference of the weld nugget plus early crack growth through the thickness and later crack growth laterally across the specimen until final separation occurred.

IV. FINITE ELEMENT ANALYSIS OF TENSILE-SHEAR SPOT WELD

The application of the finite element method (FEM) to the determination of notch-tip stress fields has led to rapid progress. The method has great versatility: it allows the analysis of complicated geometries (welded structures), it enables treatment of three-dimensional problems, and it also permits the use of elastic-plastic elements to include notch tip plasticity.

4.1 Stress Analysis of Tensile-Shear Spot Weld

The 20-node brick element was used to model the geometry of the tensile-shear spot weld. The element grid was plotted by using a mesh generator (61) and is shown in Fig. 15. Because of symmetry, only one-half of the specimen was analyzed.

The stress analyses were performed using the ABAQUS finite element program, developed by Hibbitt and associates (63). All computations were performed on a Cyber 175 computer of University of Illinois.

The results of this analysis for the tensile-shear spot weld are shown in Figs. 16 and 17. Figure 16 shows the notch-root stresses as a function of position around the periphery of the spot weld nugget. It was assumed that the root of the weld nugget had a very small but defined radius. Around the notch root radius, Fig. 17 shows the profile of the magnitude of the stress concentration factor of the weld nugget. The maximum stress concentration factor occurs approximately 70° above or below the horizontal for the geometry studied, suggesting that fatigue cracks should initiate and propagate in this initial direction as has been shown by experiment. Fig. 18 shows a comparison of the calculated stress concentration factor using Eq. 7 and computed stress concentration factor using finite element

method (FEM) for various ellipticity. The stress concentration factors (K_t) calculated using Eq. 7 and computed using FEM agree within 25%. This encouraging agreement gave confidence in using Eq. 10 to obtain the fatigue notch factor and, thus, to estimate the fatigue initiation life of tensile-shear spot welds.

Finite element analyses were used to determine if nugget shapes other than circular could have a benefical influence upon the fatigue resistance of tensile-shear spot welds. Figure 19 shows the calculated maximum stress concentration factor (K_t) for tensile-shear spot welds having circular and elliptical nugget shapes. In these calculations, the nugget cross-sectional area was maintained constant, and the K_t of the circular nugget was compared with the K_t of various shapes of elliptical nuggets. The calculations indicate that elliptical nuggets having their major axes perpendicular to the load should have a K_t at their notch root substantially less than that of a circular nugget. Conversely, the elliptical nuggets have higher K_t at their notch root than that of a circular nugget when the major axes are parallel to the loading direction. The nugget shape effects on fatigue resistance of tensile-shear spot welds will be discussed in Section 6.5.1.

4.2. Stress Intensity Factor (K_I) of Tensile-Shear Spot Weld

Three-dimensional finite element analyses for various specimen dimensions were carried out to obtain the values of stress intensity factor of a tensile-shear spot weld using a stiffness derivative technique (35). The dashed lines in Figs. 20 to 22 give the K_I values with Pook's solution for changing the sheet width, thickness and nugget diameter, respectively. The solid lines were obtained by connecting the K_I values from finite element analyses for changing the dimensions of the specimen. Combining

Figs. 20 to 22 , the curve fitted stress intensity factor solution (K_I) of a tensile-shear spot weld can be expressed as:

$$K_I = \frac{P}{D^{1.5}} \{2.37(\frac{D}{t})^{.27} (\frac{D}{W})^{.285}\} \quad (24)$$

As seen in Fig. 20, Pook's stress intensity factor (38) (K_I) deviates from the stress intensity factor of FEM in the range $W/D<6$. This disagreement is because the free edges affect the stress intensity factor in the finite element study when the width becomes narrow. Fig. 21 shows the thickness effect on stress intensity factor of spot welds. The stress intensity factor of FEM is approximately 20% higher than that of Pook in the range $1/60< t/W< 1/10$. The stress intensity factor of Pook and FEM agree with each other reasonably well for the nugget diameter within the range $1.25< D/t<10$.

Generally speaking, the stress intensity factor of Pook agrees with the empirical stress intensity factor (K_I) from finite element analyses except at narrow sheet widths ($W/D<6$).

4.3. Fracture Mechanics Analysis of The Fatigue Behavior of Spot Welds

Plotting fatigue test results of tensile-shear spot weld in terms of initial stress intensity factor can reduce the scatter (62). It seems interesting to study the initial value of stress intensity factor for various spot welds. The designer can easily use this initial stress intensity factor to judge the fatigue resistance of different spot welds.

Fig. 23 shows the values of initial stress intensity factor for three different spot welds. A is a spot weld having sheet thickness t; B is a spot weld having two different thicknesses t and t/2; and C is for two spot

welds consisting of three sheets having sheet thickness t. As seen in Fig. 23, the spot weld C has a substantially reduced stress intensity factor. The spot weld C has a K_I/S of approximately 3 and 3.4 at point U and V. The stress intensity factor of spot weld A has a K_I/S of about 11 at U and V. According to this analysis, the spot weld C should have a much higher fatigue resistance than spot weld A. Fig. 24 shows the experimental results of spot A and spot C for galvanized SAE 960X (HSLA). The spot weld C consists of two spot welds: because of the two spot welds it is anticipated that the fatigue strength will be at least two times that of spot weld A. In fact, weld C exceeded weld A by a factor of three as can be seen in Fig. 23. This difference is due to the fact that spot weld A has a large nugget rotation and bending which is almost absent for spot weld C when the load is applied. Thus, if a spot weld having little or no nugget rotation and bending can be prepared, significantly improved fatigue resistance may be expected (20).

An analysis of spot weld B also is included in Fig. 23. Although it is difficult to establish a standard for comparison of the weldment of dissimilar sheet thickness with the weld of equal sheet thickness, there does appear to be some unusual effects involved as shown by curve B in Fig. 23. The stress intensity factor, K_I/S has a value of approximately 17 at point V and 5.6 at point U. The value of stress intensity factor (K_I) gradually increases along the notch root. This implies that the spot weld B will fail at the thinner sheet. Comparing spot weld B with spot weld A and C, spot weld B has the poorest fatigue resistance. The results indicate that the geometry of tensile-shear spot weld exerts one of the most important influences on the fatigue resistance of spot welds.

V. RESULTS AND PREDICTIONS

5.1 Results for Constant Amplitude Loading Fatigue Tests

The constant amplitude fatigue test results and life predictions for the as-welded B60XK G-90 (HSLA), DQSK G-90 (low carbon) and galvanized SAE 960X (HSLA) tensile-shear spot welds are given in Tables 6 to 8 and shown in Figs. 25 to 27. B60XK G-90 and DQSK G-90 spot welds were tested under R=-1 loading condition and galvanized SAE 960X spot welds were tested under R=0 loading condition. The vertical axis represents the applied axial stress range which is defined as the load range divided by the cross sectional area of the sheet. Each of the solid lines represents the total life predictions based on Eq. 23.

A 'pull-out' failure in which the fatigue crack initiated at the weld nugget and propagated rapidly into the base metal sheet was observed in specimens at short lives (less than 10^6 cycles). A specimen separation where the crack has progressed to the outer surface of the specimen and has subsequently advanced away from the nugget and across the width was observed in specimens at long lives (particularly longer than 10^6 cycles). The interfacial failure in which the crack propagated through the weld nugget was seldom observed in this study. The general appearances of the pull-out failure and specimen separation are shown in Fig. 28. Fig. 29 shows a comparison between the number of cycles to failure observed and the number of cycles to failure predicted for B60XK G-90, DQSK G-90 and galvanized SAE 960X using the TSIP model.

5.2 Results for Variable Load History Fatigue Tests

Tables 9 to 10 and Figs. 30 and 31 give the fatigue test results and predictions using the Munse Fatigue Criterion (see Appendix B) for B60XK G-90 (HSLA) and DQSK G-90 (low carbon) tensile-shear spot welds subjected to the Ford variable load history. The nominal stresses shown in the figure were computed from the largest absolute load value of the Ford weld history, and the life was represented as blocks (18,844 reversals in one block). The data in both of these diagrams range from approximately 10 blocks to over 600 blocks. The dashed and solid lines shown in Figs. 30 and 31 are predictions for 50% reliability (the central tendency of the fatigue data) and 95% reliability made using the Munse Fatigue Criterion (36,37). The slope of the S-N regression analysis line, uncertainity, random load factor and reliability factor for B60XK G-90 samples and DQSK G-90 samples are given in Table 11. Fig. 32 shows a comparison between the number of blocks to failure observed in these experiments and the number of blocks to failure predicted using Munse Fatigue Criterion at 50% reliability. The dashed lines are a factor of two in life. As seen in Fig. 32, the Munse Fatigue Criterion at 50% reliability slightly overestimated the fatigue life. A conservative life predication will be obtained if the Munse Fatigue Critetion at 95% reliability is used.

5.3 Improvement of Spot Weld Fatigue Resistance

5.3.1 Results of Changing Nugget Shape

As shown in Fig. 33, a and b stand for the axes of ellipse parallel and perpendicular to the loading direction. Spot welds having elliptical nuggets with the major axis aligned perpendicular to the load, that is b/a=1.7, and parallel to the load, that is b/a=.6, were tested. The

results of these R=-1 tests on B60XK G-90 (HSLA) are shown in Table 12 and Fig. 33. The dashed line stands for the fatigue resistance of as-welded B60XK G-90 circular spot welds which have the same nugget area. From these tests, it seem that the introduction of different ellipticity does not appreciably improve the fatigue life of spot welds.

5.3.2. Results of Pre-Loading

The improvement of fatigue life due to pre-loading in tension prior to fatigue testing was substantial. Fig. 34 shows the monotonic load-displacement curve for B60XK G-90 (HSLA) and DQSK G-90 (low carbon) tensile-shear spot welds. The 75% of the ultimate tensile load, which is 11.1 kN (2,500 lbs.) for B60XK G-90 and 9.2 kN (1,620 lbs.) for DQSK G-90, is shown by an arrow on each curve. These specimens were tested under R=-1 loading condition and results of these tests are listed in Tables 13 to 14 and shown with predictions in Figs. 35 to 36 for B60XK G-90 and DQSK G-90 steel, respectively. The dashed lines are the fatigue resistance of as-welded spot welds from Figs. 25 and 26. As seen in Figs. 35 and 36, the preloading to 75% of their ultimate tensile load does increase the fatigue strength ($2x10^6$ cycles) as much as 95% for B60XK G-90 and 73% for DQSK G-90. However, this preload only resulted in 13% increase in strength for both materials at 10^4 cycles. Predictions of the total fatigue lives were made by assuming the maximum compressive residual stresses which are equal to base metal yield strength at the notch root.

Results of B60XK G-90 and DQSK G-90 which were subjected to the Ford weld history are given in Tables 15 to 16 and shown in Figs. 37 to 38. The strength at 700 blocks increased 61% for B60XK G-90 and 28% for DQSK G-90 when preloading of 75% of their ultimate tensile load was applied. This preload only resulted in 1% and 8% increase in strength at 10 blocks

for B60XK G-90 and DQSK G-90, respectively.

5.3.3 Results of Coining

The test results and predictions for B60XK G-90 (HSLA) specimens which were subjected to the coining operation under R=-1 conditions are given in Table 17 and Fig. 39. The dashed line represents the fatigue resistance of as-welded B60XK G-90 spot welds. As much as 50% increase in strength at $2x10^6$ cycles can be obtained by applying 44.4 kN (10,000 lbs.) compressive load. However, this compressive load only resulted in a 24% increase in fatigue strength at 10^4 cycles. The maximum compressive residual stresses which equal to base metal yield strength at the notch root was used to estimate the total fatigue life (N_T).

Results of B60XK G-90 spot welds which were subjected to the Ford weld history are given in Table 18 and Fig. 40. The 56% increase in strength at 700 blocks can be obtained by applying 44.4 kN (10,000 lbs.) compressive load. This compressive load only resulted in 15% increase in strength at 10 blocks. Table 17 and Fig. 39 clearly demonstrate that the higher load level (44.4 kN) resulted in substantial improvement in the fatigue life of the B60XK G-90 steel. From these tests, it seemed that the introduction of the lubricating oil did not appreciably improve much the effect of this pretreatment.

VI. DISCUSSION

6.1 Comparison of TSIP Model Predictions with Experimental Results

The stages of the TSIP model are: Stage I - crack initiation and early crack growth, and Stage II - through thickness crack propagation, and Stage III - lateral crack propagation. For Stage I, the Pook's stress intensity factor solution for the tensile-shear spot weld and Creager's blunt notch tip stress field were used to evaluate the notch root stresses. The life spent in crack initiation and early crack growth can be estimated using smooth specimen fatigue data. For Stage II, estimates of the life involved in the propagation of a crack through the sheet thickness (N_{pt}) were based on the crack growth studies (52) for tensile-shear spot welds. For Stage III, the life spent in the growth of a nugget-size crack across the width of the specimen (N_{pw}) was evaluated using existing and estimated stress intensity factor solutions (as described in Appendix A). Predictions of the total fatigue life (N_T) were made by adding the separate estimates of crack initiation life (N_I) Stage I and the crack propagation lives Stage II and Stage III.

The fatigue life predictions for as-welded, pre-loaded and coined tensile-shear spot welds were made and compared with experimental results from this study. The principal difficulty in applying the TSIP model was determining appropriate values of HAZ fatigue properties. Because of the buckling problem in the testing of thin sheet materials, obtaining the strain-controlled fatigue properties for these HAZ is extremely difficult. Thus, the fatigue properties used in this study were estimated from hardness measurements of HAZ (55,56). Fig. 41 shows the hardness profile of B60XK G-90 (HSLA) and DQSK G-90 (low carbon). Detail of the predictions of total fatigue life (N_T) are described in Chap. II.

Figure 29, compares of the predicted total fatigue lives with the observed total fatigue lives. The predictions of total life agree with the experimental results within a factor of two.

6.2 Effects of Geometry on Tensile-Shear Spot Welds

6.2.1 Width Effects

The effect of width (W) predicted by the TSIP model on tensile-shear spot weld fatigue life is diagrammed in Fig. 42 for B60XK G-90 (HSLA) steel. Since the Pook stress intensity factor solution is not a function of width, the stress intensity factor solution which was developed using the finite element method for a finite width specimen was used to estimate the notch severity. The elastic stress concentration factor is:

$$K_t = \frac{Wt}{(\pi r)^{1/2} D^{1.5}} \{3.96(D/t)^{.27}(D/W)^{.285} + .593 + .34(D/t)^{.710}\} \qquad (25)$$

The fatigue notch factor can be obtained by substituting Eq. 25 into Eq. 10. As seen in Fig. 42, the initiation life drops drastically when the width is less than 38.1 mm (1.5 in.) because the proximity of the free edges results in a higher stress concentration around the notch root and, thus, decreases initiation life. The initiation life is insensitive to the width when the width is larger than 50.8 mm (2 in.). As shown in Fig. 20, the stress intensity factor (K_I) at the notch root is essentially independent of sheet width when (W/D)>12 due to the fact that the free edge effects diminish.

The Stage II crack propagation life (N_{pt}) was estimated from crack propagation experiments on tensile-shear spot welds having a width 38.1 mm (1.5 in.). A finite width correction factor was needed to account for the width effect on the stress intensity factor range during this stage. The

range of stress intensity factor ΔK of Stage II is:

$$\Delta K = Y_w \Delta S \sqrt{\pi a} \tag{26}$$

where Y_w is the geometrical factor accounting for finite-width and can be expressed as:

$$Y_w = Y \frac{M_w}{M_t} \tag{27}$$

M_w is the finite-width correction factor for an embedded elliptical crack is (64):

$$M_w = \sqrt{\sec\left(\frac{\pi c}{w}\sqrt{\frac{a}{t}}\right)} \tag{28}$$

where c is the crack length, a is the crack depth, Y is a geometrical factor and M_t is a finite-width correction factor for an embedded elliptical crack in a 38.1 mm (1.5 in.) wide specimen. From failure surface observations, the ratio of c/a is about 2.5. Thus, the Stage II propagation life due to various widths can be evaluated by using Eq. 14. As shown in Fig. 42, the Stage II propagation life becomes more important when the width increases. Also in Stage III, increases in sheet width result in an increase in the life devoted to the propagation of a crack across the width of the sheet.

The TSIP model predicts that the fatigue resistance of tensile-shear spot welds is relatively insensitive to specimen width except at narrow widths.

6.2.2 Thickness Effects

The effect of thickness (t) predicted by the TSIP model on tensile-shear spot welds fatigue life is shown in Fig. 43 for B60XK G-90 (HSLA) steel spot welds.

The crack initiation life gradually dominates the total life as thickness increases. An increase in thickness results in a decrease in stress concentration factor and an increase in crack initiation life.

For Stage II crack propagation, a correction factor for the front and back surface is needed to account for the thickness effect on stress intensity factor range. The range of stress intensity factor ΔK of Stage II is:

$$\Delta K = Y_t \Delta S \sqrt{\pi a} \tag{29}$$

where Y_t is the geometrical factor for front and back surface and can be expressed as:

$$Y_t = Y \frac{F_t}{F_S} \tag{30}$$

F_t is the surface correction factor (front and back) which was obtained by curve fitting from Kaju's (65) three-dimensional finite element results (c/a=2.5) and is given:

$$F_t = -2.63(\frac{a}{t})^3 + 3.87(\frac{a}{t})^2 - 1.15(\frac{a}{t}) + 1.23 \tag{31}$$

where Y and F_S are geometrical factor and free surface correction factor for an embedded elliptical crack in a 1.3 mm (.051 in.) thick specimen. Thus, the Stage II propagation can be evaluated for various thicknesses using Eq. 14.

For Stage III, crack propagation life increases with the thickness. Thus, an increase in thickness should result in a significant improvement in fatigue life. However, some investigators (3,15) have claimed no noticeable improvements in fatigue strength from increasing thickness. This observation is probably due to the fact that the changes in thickness studied were too small to show any significant effect. As far as vehicle weight savings and fuel economy are concerned, increasing sheet thickness in order to improve the fatigue resistance of spot welds is probably not a practical suggestion.

6.2.3 Nugget Diameter Effects

The effect of nugget diameter (D) predicted by the TSIP model on tensile-shear spot weld fatigue life is shown in Fig. 44. As seen in Figs. 42 to 44, within the practical range of width, thickness and nugget diameter included in this study the degree of life change caused by altering the nugget diameter is not as great as the thickness effect, but is larger than the width effect.

Increasing the nugget diameter results in a decrease of the stress concentration factor around the notch root, and thus, causes an improvement in the Stage I fatigue initiation life.

It has been assumed that through thickness crack propagation life (Stage II - N_{pt}) is the same for various nugget diameters.

The nugget diameter was assumed for the initial crack length (a_I) for the cross-width crack propagation (Stage III) study. Thus, the stage III crack propagation life decreases with an increase in nugget diameter.

Although the improvement in fatigue resistance due to the nugget diameter is not as effective as the thickness effect, increasing the nugget diameter would seem to be the most direct and practical means of increasing

fatigue resistance through changes in geometry.

6.3 The Mixture of Geometry Effects

For practical applications, it is important to know the 'trade off' between the geometrical variables on fatigue resistance of spot welds. Since fatigue resistance of spot weld is insensitive to the sheet width, this discussion will be focused on the nugget diameter and sheet thickness. High strength steel sheet has high static strength and allows thickness reduction and weight savings. However, the fatigue resistance of high strength steel spot welds is about the same as that of low carbon steel spot welds . Thus, a reduction in thickness needs to be balanced, in term of fatigue life, by increasing the nugget diameter. For example, the results predicted by the TSIP model indicate, for B60XK G-90 (HSLA) steel under load range 2.67 kN (600 lbs.), a thickness reduction from 1.91 mm (.075 in.) to 1.3 mm (.051 in.) could in terms of total fatigue life be compensated for by increasing the nugget diameter from 6.1 mm (.24 in.) to 9.9 mm (.39 in.). Conversely, a thickness increase from 1.02 mm (.04 in.) to 1.3 mm (.051 in.) could be balanced by decreasing the nugget diameter from 6.1 mm (.24 in.) to 4.8 mm (.19 in.).

According to Fisher Body recommended procedures (57), the nugget diameter (D) is usually proportional to the square root of the sheet thickness (t) for nominal spot welding condition. A given electrode produces larger nugget sizes in thicker sheet (15). Thus, an increase in sheet thickness will result in life improvement both due to increase in sheet thickness as well as attendant increase in nugget diameter. For example, the results predicted by TSIP model, for B60XK G-90 (HSLA) steel tensile-shear spot weld test using a load range 2.67 kN (600 lbs.) for a thickness increase from 1.3 mm (.051 in.) to 1.9 mm (.076 in.) and an

associated nugget diameter increase from 6.1 mm (.24 in.) to 7.5 mm (.29 in.) would result in fatigue life improvement from about $2x10^6$ to $5x10^7$ cycles. Increase in thickness alone will result in life improvement only from about $2x10^6$ to $9x10^6$ cycles.

6.4 Effects of Material Properties

It has been shown in many investigations that the high cycle fatigue resistance of spot welds seems to be independent of the static strength of the base metal (4,10,19,22). The tensile residual stress cancels out material property effects and thus, no life improvement occurs in the high cycle regime ($>10^6$ cycles). In the low cycle regime ($\sim10^4$ cycles), the tensile residual stresses may be partially 'washed out' by notch root plasticity; and high strength materials give a higher fatigue resistance (66,67).

The predicted effect of material properties on fatigue life for a given geometry and load range is shown in Fig. 45. In this analysis, the HAZ residual stresses of spot welds are assumed to be equal to the yield strength of the surrounding base materials (45). The yield strength of base material can be obtained from the ultimate tensile strength of the HAZ (55,56). The relationship $S_Y = .5\ S_u$ was used in this study (55). As seen in Fig. 45, the crack initiation life decreases slightly with increasing the HAZ strength. Barsom (68) showed that the region II fatigue-crack-growth-rate behavior of steels in a benign environment is essentially independent of mechanical and metallurgical properties. Thus, the HAZ material properties are presumed to have no influence on crack propagation life (N_{pt} and N_{pw}).

An increase in HAZ material strength results in a slight decrease in fatigue resistance because of the high tensile residual stresses associated with the weld in the high strength materials.

6.5. Improvement of Tensile-Shear Spot Weld Fatigue Resistance

The three most important factors which are inherent properties of the discontinuity (notch) causing fatigue failure in weldments are: geometry - the severity of the stress concentration; residual stress- the sign and magnitude of the residual stress at the root of the stress concentration; and material properties- the fatigue properties of the material at the root of the stress concentration. All methods of improving the fatigue resistance of weldments do so by altering one or more of the above-mentioned factors (69,70).

Thus, there are two main avenues for increasing tensile-shear spot weld fatigue resistance: altering weld geometry (increasing in sheet thickness, nugget diameter, decreasing nugget rotation through increase in specimen stiffness, altering nugget shape) and controlling residual stresses (altering of the welding parameters, changing in material properties through post-weld thermal or mechanical treatments).

6.5.1 Change in Nugget Shape

Finite element analyses were used to determine if nugget shapes other than circular could have a beneficial influence upon the fatigue resistance of tensile-shear spot welds. The FEM results show that elliptical nuggets having their major axes perpendicular to the load have a K_t at their notch root substantially less than that of a circular nugget. If this is so, the elliptical nuggets of shape b/a=2 should have a substantially improved initiation life (N_I).

However, tests made using spot welds having elliptical shape did not improve the fatigue life. It seems that any improvement in initition life (N_I) must have been offset by decreases in propagation life ($N_{pt} + N_{pw}$), so that the test results for spot welds having lives of approximately a million cycles indicated that circular spot welds and elliptical spot welds having a b/a ratio of about .6 and 1.7 all had about the same fatigue life. The data spans the range of approximately 10^5 cycles to $3x10^6$ cycles. Further tests would be required to determine if the different ellipticity can produce increases of life in the very long life region.

6.5.2 Preload

The TSIP model predicts that residual stresses have a large influence upon the fatigue life of a tensile-shear spot weld. It was thought that inducing compressive residual stresses in the locations at which fatigue crack initiation and early crack growth occur would substantially improve the fatigue resistance. As seen in Fig. 35 and 36, the introduction of compressive residual stresses resulted in a substantial improvement of fatigue resistance at $2x10^6$ cycles. In the low cycle region (10^3 to 10^4 cycles), this compressive residual stress did not improve fatigue resistance much because the notch root plasticity presumably 'washed-out' the residual stresses after a few cycles.

The increases in strength at $2x10^6$ cycles are 95% for B60XK G-90 (HSLA) and 73% for DQSK G-90 (low carbon) spot welds. Because B60XK G-90 (HSLA) has a high yield strength, a high compressive residual stress could be induced. Thus, tensile preloading causes a substantial improvement in fatigue resistance which was most beneficial to the high strength material. This observation is also confirmed by the work of Choquet (29).

If it is assumed that the whole of the fatigue life of a weld consists of crack propagation from pre-existing small crack-like defects then, as has been shown by Maddox (71), one would anticipate that the negative inverse slope of the S-N regression analysis line should be equal to the value of the index, m, in the Eq. 13. If there should be a significant crack initiation period, the slope would be less than m. As seen in Fig. 35 to 36 , the negative inverse slope of regression analysis line for as-welded spot welds is 5.2 and 5.5, and for pre-loaded specimens the slopes are 11.2 and 9.8 for B60XK G-90 (HSLA) and DQSK G-90 (low carbon), respectively. An reduction in slope of the test results possibly indicates a greater period of time spent in fatigue crack initiation and early crack growth. In addition, the negative inverse slope of the S-N diagram of as-welded specimens for B60XK G-90 (HSLA) and DQSK G-90 (low carbon) indicated that the fatigue life of spot welds is made up of significant contribution from fatigue crack initiation as well as fatigue crack propagation.

6.5.3 Coining

Coining treatment caused the fatigue resistance improvements by the introduction of compressive residual stresses or tensile residual stress-relieve at notch root. The factors which influence the degree of improvements are (1) the size of the compressed area of weld nugget. (2) the magnitude of the compressive load. (3) the shape of the tool tips used.

As seen in Fig. 39 and 40, the improvement in fatigue resistance caused by coining for B60XK G-90 (HSLA) is not as great as caused by the tensile preloading treatment. The 44.48 kN (10,000 lbs.) force applied and the size of the rod tip caused the entire nugget to be 'coined' but

these conditions are probably not the optimum combination of load and tip shape, and further improvements in fatigue resistance through coining may be possible.

The coining treatment resulted in a change of slope from 5.2 to 6.4 for the B60XK G-90 (HSLA) steel specimens. The degree of change in slope is not as great as produced by the tensile preload treatment.

The dimple surface residual stresses of B60XK G-90 (HSLA) and DQSK G-90 (low carbon) specimens were measured by the Caterpillar Tractor Company using X-ray technique to show that the state of residual stresses in the nugget and presumably at the notch root were altered by these mechanical pretreatments. Table 19 shows the residual stress measurements for as-welded, preloaded and coined nugget at the dimple surface. Although the existance of high compressive residual stresses at notch root has not been demonstrated for the coining and preloading treatments, these measurements do show that some stress relief and compressive residual stress have been induced at the nugget surface through coining and preloading treatments.

6.6. Comparison of The TSIP Model with The Method of Davidson et al.

Davidson and Imhof (20) developed a spot-weld fatigue design curve (termed here the SFD method) which relates the tensile shear spot weld fatigue life to a parameter ΔE:

$$\Delta E = \frac{\Delta P \Delta \Theta N^{1/2}}{t} \tag{32}$$

for the R=0 load condition. Where $\Delta\Theta N$ is the nugget rotation angle, t is the sheet thickness and ΔP is the load range applied to the spot weld. The SFD method is based upon the assumption that the fatigue of spot-welded

sheet is governed exclusively by fatigue crack growth. The SFD method uses the stiffness of the specimen as a index to characterize the fatigue resistance of tensile-shear spot welds. Using this stiffness parameter, the total life of tensile-shear spot weld were related to the stiffness parameter ΔE:

$$N_f = A(\Delta E)^{-3} \tag{33}$$

where A is equal to 1.84×10^6 when ΔE is in the unit of kN-deg$^{1/2}$/mm. Davidson hoped that the SFD method would apply to all single tensile-shear spot welds and would be independent of material properties (20).

The experimental data of of this study for galvanized SAE 960X (HSLA), B60XK G-90 (HSLA) and DQSK G-90 (low carbon) tensile-shear spot welds compared with the prediction of Eq. 33 were using the SFD stiffness parameter ΔE. Since the nugget rotation angle ($\Delta\theta N$) was not experimently determined for our specimens, a three-dimensional finite element stress analysis was carried out to obtain the nugget rotation angle by calculation. The angle was substituted into Eq. 32, and the data of this study was plotted and compared with Eq. 33 in Fig. 46.

As seen in Fig. 46, the SFD method works reasonably well for the R=0 loading condition but does not work well for the R=-1 loading condition.

The SFD method has the advantage of involving only the stiffness parameter in the calculation. However, the nugget rotation is a function of loading and specimen geometry, and the rotation angle measurement must be performed for each different loading and specimen geometry. Although rotation angle can be measured experimently, it is not an easy task.

The TSIP model has the disadvantage of requiring three separate analyses. The HAZ material properties must be determined from hardness measuremens in the HAZ. However, the advantage that TSIP model can be used to estimate the influence of residual stresses and stress ratio on the fatigue resistance of tensile-shear spot welds offsets these difficulties.

VII. CONCLUSIONS

1. The fatigue resistance of tensile-shear steel spot welds strongly depends upon the specimen geometry. The separate or joint changes in sheet thickness, width and nugget diameter will influence the stress intensity factor (or stiffness) of the spot welds. The lower the initial stress intensity factor, the greater the joint stiffness is the spot welds and the higher will be the fatigue resistance of spot welds. Material properties have little effect on fatigue resistance for life greater than 10^6 cycles for the as-welded condition.

2. Preloading and coining post-weld mechanical treatment greatly improve the fatigue resistance of tensile-shear spot welds under both constant amplitude and Ford variable load history. Both preloading and coining were more beneficial for the high strength material due to the higher compressive residual stresses induced. Thus, material properties are important in determining the effect of post-weld mechanical treatments.

3. The stress intensity factor (K_I) developed by Pook agrees with the empirical stress intensity factor (K_I) from finite element analysis except at narrow sheet width ($W/D<6$).

4. The Three-Stage model (TSIP) predicted the fatigue life of tensile-shear spot welds for the as-welded, preloaded and coined test condition under constant amplitude loading. The TSIP model suggestes that a significant portion of N_T is spent in Stage I - crack initiation and early growth in the high cycle region ($> 3x10^6$ cycles). Stage II - through thickness crack propagation dominates the total life in the low

and medium life region, and Stage III - cross sheet width propagation is important when the sheet width becomes large.

5. Using constant amplitude test results, the Munse Fatigue Criterion provided good estimates of the fatigue strength of tensile-shear spot welds subjected to Ford variable load history.

REFERENCES

1. Dickinson, D. W., Welding in The Automotive Industry, Report SG 81-5 , Republic Steel, Aug. 1981.

2. Orts, D. H., 'Fatigue Strength of Spot Welded Joints in HSLA Steel', SAE Paper 810355, 1981.

3. Cappelli, P. G., Castagna, M., and Ferrero, P., 'Fatigue Strength of Spot-Welded Joints of HSLA Steels', Welding of HSLA Structure Steels (Proc. Conf.) Rome, Italy., Nov. 1976.

4. Wilson, R. B. and Fine, T. E., 'Fatigue Behavior of Spot-Welded High-Strength Steel Joints', SAE Paper 810354, 1981.

5. Overbeeke, J. L. and Draisma, J., 'The Influence of Stress Relieving on The Fatigue of Heavy-Duty Spot Welded Lap Joints', Welding Research International, Volume 7, Number 3, pp 241-253, 1977.

6. Overbeeke, J. L., 'The Fatigue Behavior of Heavy-Duty Spot Welded Lap Joints Under Random Loading Conditions', Welding Research International, Volume 7, Number 3, pp254-276, 1977.

7. Overbeeke, J. L., 'Random Fatigue of Spot Welded Lap Joints', Metal Construction, pp 81-83, Feb. 1979.

8. Davidson, J. A., 'A Review of The Fatigue Properties of Welded Sheet Steel', SAE Paper 830033, Feb. 1983.

9. Sawhill, J. M. and Baker, J. C., 'Spot Weldability of High Strength Sheet Steel', Welding J. 59 (1), pp 195-205, 1980.

10. Pollard, B. 'Spot Welding Characterictics of HSLA for Automotive Application', Welding Journal 53(8), 343-350s, 1974.

11. Mitchell, J. W. and Chang, U. I., in 'Micro-Alloying' Conference, Washington, DC, pp. 599-609, October 1975.

12. Pollard, B. and Goodenow, R. H., 'Spot Weldability of Dual-Phase Steel', SAE Paper 790006, 1979.

13. Lawrence, F. V., Jr., Wang, P. C. and Corten, H. T., 'An Empirical Method for Estimating the Fatigue Resistance of Tensile-Shear Spot Welds', SAE Paper 830035, 1983.

14. Lawrence, F. V., Wang, P. C. and Corten, H. T., 'Improvement of Spot Weld Fatigue Resistance', SAE Paper 840112, 1984.

15. Sperle, J-O., 'Strength of Spot Welds in High Strength Steel Sheet', Metal Construction, pp 200-203, April, 1983.

16. Overbeeke, J. L. and Draisma, J., 'Fatigue Characteristics of Heavy-Duty Spot Welded Lap Joint', Metal Construction and British Welding J., pp 213-219, July, 1974.

17. Iwasaki, T., Tanaka, J., Kabasawa, M., and Nagae, M., 'Fatigue Strength of Base Metal and Spot Welded Joints in HSLA Steels for Automotive Applications', Nippon Kokan Technical Report, Overseas No. 34, 1982.

18. Davidson, J. A., 'Design-Related Methodology to Determine the Fatigue Life and Related Failure Mode of SPot-Welded Sheet Steels', Proceedings of Technology and Applications of HSLA Steels, PA., Oct. 1983.

19. Davidson, J. A. and Imhof, E. J., Jr., 'A Fracture-Mechanics and System Stiffness Approach to Fatigue Performance of Spot-Welded Sheet Steels', SAE Paper 830034, Feb. 1983.

20. Davidson, J. A. and Imhof, E. J., 'The Effect of Tensile Strength on The Fatigue Life of Spot-Welded Sheet Steels', SAE Paper 1984.

21. Defourny, J., D'Haeyer, and Brayard, A., 'Spot Welding of High Strength Steel Sheets for Deep Drawing', IIW Document III, 1980.

22. Lawrence, F. V., Jr., Wang, P. C. and Corten, H. T., 'The Fatigue Resistance of Thin Gauge Automotive Weldments', Technical Reports to General Motors Corporation, Dec. 1982.

23. Kimchi, M., 'Spot Weld Properties When Welding with Expulsion- A Comparative Study', Welding J., pp 58-63s, Feb. 1984.

24. Shinozaki, M., Kato, T., Irie, T. and Takahashi, I., 'Fatigue of Automotive High Strength Steel Sheets and Their Welded Joints', SAE Paper 830032, Feb. 1983.

25. Sawhill, J. M., Jr., and Furr, S. T., 'Spot Weldability Tests for High-Strength Steels', SAE Paper 810352, Feb. 1981.

26. Freytag, N. A., 'A Compressive Study of Spot Welding Galvanized Steel', Welding Journal, pp 145-156s, April 1965.

27. Matsoukas, G., Stevens, G. P. and Mai, Y. W., 'Fatigue of Spot-Welded lap Joints', International Journal of Fatigue, Vol 6, No.1, Jan. 1984.

28. Frost, N. E., 'The Effect of Environment on The Propagation of fatigue Crack in Mild Steel', Applied Material Research, p131, 3, 1964.

29. Choquet, A., Krivobok, V. N. and Welter, G., 'Effect of Prestressing on Fatigue Strength of Spot-Welded Stainless Steels', Welding J., 33 (10), Research Suppl. pp 509-523s, 1954.

30. Lawrence, F. V., Jr., Wang, P. C., Ho, N. J. and Corten, H. T., 'The Fatigue Resistance of Thin Gauge Automotive Weldments', Technical Reports to General Motors Corporation, March 1984.

31. Welter, G. and Choquet, J. A., 'Internal Stress Distribution of Single Spotwelds in Relation to Their Fatigue Life', Welding Journal, 38(4), Research Suppl., pp 145-158s, 1959.

32. Chandel, R. S. and Garber, S., 'Mechanical Aspects of Spot-Welded Joints in Heat-Treated Low-Carbon Mild-Steel Sheets', Metals Technology, pp 37-44, Jan. 1977.

33. Balasubramanian, S., Sundaresan, S. and Vasudevan, R., 'Improvement of Resistance Spot Weld Characteristics', Welding Research Abroad, pp 45-63, Nov. 1978.

34. Hiratsuka, K. and Ito, C., 'Determination of The Heat Treatment Conditions of Spot Welds on Anti-Corrosion High Strength Steels', J. of Japan Welding Society, Vol. 39, No. 3, pp. 39-49, March, 1970.

35. Parks, D. M., 'A Stiffness Derivation Finite Element Technique for Determination of Crack Tip Stress Intensity Factors', International Journal of Fracture, Vol. 10, No. 4, pp.487-502, December, 1974.

36. Munse, W. H., Wilbur, T. W., Tellalian, M. L., Nicoll, K. and Wilson, K., 'Fatigue Characterization of Fatigue Ship Details for Design', Ship Structure Committee Report, SSC-318, Aug., 1982.

37. Ang, A. H.-S. and Munse, W. H., 'Practical Reliability Basis for Structure Fatigue', ASCE National Structure Engineering Convention, April, 1975, Reprint No. 2494.

38. Pook, L. P., 'Approximate Stress Intensity Factor for Spot Weld and Similar Welds', National Engineering Laboratary Report No. 588, April, 1975.

39. Creager, M., 'The Elastic Stress Field Near the Tip of a Blunt Crack', M. S. Thesis, Lehigh University, 1966.

40. Basquin, O. H., 'The Expotential Law of Endurance Tests', Proce. ASTM ,10:625, 1910.

41. Lawrence, F. V., Mattos, R. J., Higashida, Y., and Burk, J. D., 'Estimation of Fatigue Crack Initiation Life of Weld', ASTM STP 648, P. 420 , American Society of Testing and Materials, 1978.

42. Socie, D. F., Mitchell, M. R., Caulfield, E. M., 'Fundamental of Modern Fatigue Analysis', FCP Report No. 26, University of Illinois at Urbana-Champaign, Jan., 1978.

43. Topper, T. H., Wetzel, R. M., and Morrow, J., 'Neuber's Rule Applied to Fatigue Notched Specimens', J. of Materials, Vol. 4 , P. 200, 1969.

44. Mattos, R. J., 'Estimation Fatigue Initiation Life of Weld', Ph.D. Thesis, University of Illinois at Urbana-Champaign, 1973.

45. Burk, J. D., 'Effect of Residual Stresses on Weld Fatigue Life', Ph.D. Thesis, Department of Metallurgy and Mining, University of Illinois at Urbana-Champaign, 1978.

46. Morrow, JoDean, (ed.) and Graham, J. A., SAE Fatigue Design Handbook,

Society of Automotive Engineers, 1968.

47. Peterson, R. E., 'Notch Sensitivity', Metal Fatigue, Chap. 13, Sines and Waisman (ed.) McGraw-Hill, New York, 1959.

48. Paris, P. C. and Erdogan, F., 'A Critical Analysis of Crack Propagation Law', J. of Basic Engineering, Vol. 85, p.528, 1963.

49. Maddox, S. J., 'An Analysis of Fatigue Crack in Fillet Welded Joints', British Welding Institute, Report No. E4972, 1972.

50. Zheng, X. and Hirt, M. A., 'Fatigue Crack Propagation in Steels', Engineering Fracture Mechanics, Vol.18, No.5, pp965-973, 1983.

51. Emery, A. F., 'Stress Intensity Factor for Thermal Stress in Thick Hollow Cyclinder', J. of Basic Engineering, ASME Trans., Series D, Vol. 88, pp.45, 1966.

52. Smith, G. A., 'Fatigue Crack Development in Tensile-Shear Spot Weldments', M. S. Thesis, Department of Metallurgy and Mining, University of Illinois at Urbana-Champaign, 1984.

53. Broek, D., Elementary Engineering Fracture Mechanics, 2nd, Ed., Sijthoff and Noordhoff, pp77-80, 1978.

54. Burk, J. D. and Lawrence, F. V., Jr., 'Influence of Bending Stresses on Fatigue Crack Propagation Life in Butt Joint Welds', Welding J., Vol. 56, p. 43s, 1977.

55. Mcmahon, J. C., 'Predicting Fatigue Properties Through Hardness Measurements', M. S. Thesis, Department of Metallurgy and Mining Eng., University of Illinois at Urbana-Champaign, 1983.

56. Miller, G. A. and Reemsnyder, H. S., 'Strain-Cycle Fatigue of Sheet and Plate Steels II: Some Practical Considerations in Applying Strain-Cycle Fatigue Concepts', SAE Paper No. 830173, 1983.

57. MDS-247, 'Specification and Procedure for Determination The Weldability of Body Steel Materials', Fisher Body Division, General Motors Corporation.

58. Ewing, K. M., Private Communication, Department of Sheet Forming, Welding and Painting, General Motors Co., 1983.

59. Kurath, P., Private Communication, Department of Theoretical and Applied Mechanics, University of Illinois, 1983.

60. Landgraf, D., Private Communication, Ford Motors Co., 1983.

61. Ho, N. J., Private Communication, Department of Metallurgy and Mining, University of Illinois at Urbana-Champaign, 1983.

62. Pook, L. P., 'Fracture Mechanics Analysis of The Fatigue Behavior of Spot Welds', International Journal of Fracture, Vol. 11, pp 173-176,

1975.

63. Hibbitt, Karlsson and Sorensen INC., ABAQUS, Rhode Island 02906.

64. Newman, J. C., Jr., 'A Review and Assessment of The Stress Intensity Factors for Surface Cracks', ASTM STP 687, 1979.

65. Raju, I. S. and Newman, J. C., Jr., 'Stress Intensity Factors for A Wide Range of Semi-Elliptical Surface Cracks in Finite- Thickness Plates', Engineering Fracture Mechanics 11 pp 817-829 1979.

66. Fuchs, H. O., Metal Fatigue (Eds Sines, G. and Waisman, J. L.) P.197, McGraw-Hill, New York, 1959.

67. Rosenthal, D., Metal Fatigue (Eds Sines, G. and Waisman, J. L.) p.170, McGraw-Hill, New York, 1959.

68. Rolfe, S. T. and Barsom, J. M., Fracture and Fatigue Control in Structure, Prentice-Hall, New Jersey, 1977.

69. Chang, S.-T., 'Improvement of Weld Fatigue Resistance', Ph.D. Thesis, Department of Metallurgy and Mining Engineering, University of Illinois at Urbana-Champaign, Jan. 1983.

70. Smith, I. F. C. and Hirt, M. A., 'Methods of Improving the Fatigue Strength of Welded Joints', Publication ICON 114, Ecole Polytechnique Federale de Lausanne, 1983.

71. Maddox, S. J., 'Fracture Mechanics to Fatigue in Welded Structures', Welding Institute Conference on Fatigue of Welded Structures, july, 1970.

72. Tada, H., Paris, P. C. and Irwin, G. R., The Stress Analysis of Cracks Handbook, Del Research Corporation, PA. 1973.

73. Rooke, D. P. and Cartwright, D. J., Compendium of Stress Intensity Factors, London Her Majesty's Stationery Office, Hillingdon Press, pp 314-315, 1976.

Table 1

Chemical Composition of DQSK G-90, B60XK G-90 and Galvanized SAE 960X Sheet Steels

Element*	DQSK G-90	B60XK G-90	Galv. SAE 960X
C	0.024	0.033	0.07
Mn	0.24	0.56	0.06
P	0.009	0.08	0.11
S	0.017	0.005	0.016
Si	0.026	0.34	0.02
Al	0.041	0.072	0.08
N	0.007	--	--
Cb	--	0.043	--
Nb	--	--	0.029
Ce	--	--	0.026

* weight percent

Table 2

Average Tensile Properties for DQSK G-90, B60XK G-90 and Galv. SAE 960X

Material	0.2% Offset Yield Strength MPa (ksi.)		Tensile Strength MPa (ksi.)		% Elongation (in 50.8 mm)	
	Longitudinal Orientation	Transverse Orientation	Longitudinal Orientation	Transverse Orientation	Longitudinal Orientation	Transverse Orientation
DQSK G-90 (Low Carbon)	212 (30.7)	257 (37.2)	298 (43.2)	306 (44.3)	37.5	32.5
B60XK G-90 (HSLA)	431 (62.5)	471 (68.3)	533 (77.3)	541 (78.5)	24.0	21.5
Galv. SAE 960X (HSLA)	424 (61.5)	---	501 (72.6)	---	27.0	--

Table 3

Estimated Cyclic and Fatigue Properties of Heat-Affected-Zone Materials for DQSKG-90, B60XKG-90 and Galv. SAE960X

Material	DQSKG-90	B60XKG-90	Galv. SAE960X
Cyclic Strain Hardening Exponent, n'	.175	.17	.17
Cyclic Strength Coefficient, K', MPa (Ksi.)	1000 (145)	1338 (194)	1200 (174)
Fatigue Strength Coefficient, σ'_f, MPa (Ksi.)	827 (120)	1103 (160)	1020 (148)
Fatigue Ductility Coefficient, ε'_f	.28	.32	.31
Fatigue Strength Exponent, b	-.095	-.077	-.081
Fatigue Ductility Exponent, C	-.542	-.453	-.476

Table 4

Welding Procedures

Material	Electrode Force KN (lb.)	Hold Time (Cycles)	Weld Time (Cycles)	Weld Current (Kamps)
DQSK G-90	3.0 (675)	30	18	10
B60XK G-90	3.8 (850)	30	20	11.5
Galv. SAE 960X	3.7 (825)	30	20	12.7

Table 5

Test Matrix

Materials	Conditions	Loading History
B60XK G-90 (HSLA)	As-Welded	Constant Amplitude (R=-1), Variable Load
	Elliptical Nugget	Constant Amplitude (R=-1)
	Preloaded	Constant Amplitude (R=-1), Variable Load
	Coined	Constant Amplitude (R=-1), Variable Load
DQSK G-90 (Low Carbon)	As-Welded	Constant Amplitude (R=-1), Variable Load
	Preloaded	Constant Amplitude (R=-1), Variable Load
Galv. SAE 960X (HSLA)	As-Welded	Constant Amplitude (R=0)

Table 6

Fatigue Test Results for As-Welded B60XK G-90 Tensile-Shear Spot Weld (R = -1)

Specimen	ΔS MPa (Ksi.)	N_T Predicted Cycles	N_T Observed Cycles
HG-1	54 (7.8)	1,789,000	2,280,000
HG-2	54 (7.8)	1,789,000	10,200,000+
HG-3	90 (13.0)	85,600	143,000
HG-4	90 (13.0)	85,600	245,000
HG-5	90 (13.0)	85,600	181,000
HG-6	127 (18.4)	15,760	29,200
HG-7	127 (18.4)	15,760	34,400
HG-8	127 (18.4)	15,760	31,500
HG-9	54 (7.8)	1,789,000	3,070,000
HG-10	127 (18.4)	15,760	23,400
HG-11	127 (18.4)	15,760	32,300
HG-12	90 (13.0)	85,600	144,000

Table 6 Cont.

Specimen	ΔS MPa (Ksi.)	N_T Predicted Cycles	N_T Observed Cycles
HG-13	90 (13.0)	85,600	107,000
HG-14	163 (23.6)	4,770	8,200
HG-15	163 (23.6)	4,770	8,700
HG-16	163 (23.6)	4,770	8,800

+ no failure

Table 9

Fatigue Test Results for As-Welded
B60XK G-90 Tensile-Shear Spot Weld Subjected to Ford Weld History

Specimen	S_A MPa	max / min (ksi.)	N_T Predicted Blocks (50% reliability)	N_T Observed Blocks
HGV-2	+135 / -135	(+19.6) / (-19.6)	---	7
HGV-3	+108 / -108	(+15.7) / (-15.7)	36	23
HGV-4	+81 / -81	(+11.8) / (-11.8)	150	64
HGV-5	+68 / -68	(+9.8) / (-9.8)	390	132
HGV-6	+54 / -54	(+7.8) / (-7.8)	1250	655
HGV-7	+108 / -108	(+15.7) / (-15.7)	36	20
HGV-8	+81 / -81	(+11.8) / (-11.8)	150	61
HGV-9	+68 / -68	(+9.8) / (-9.8)	390	132
HGV-10	+54 / -54	(+7.8) / (-7.8)	1250	670
HGV-11	+81 / -81	(+11.8) / (-11.8)	150	83
HGV-12	+81 / -81	(+11.8) / (-11.8)	150	93
HGV-13	+68 / -68	(+9.8) / (-9.8)	390	186

Table 10

Fatigue Test Results for As-Welded DQSK G-90
Tensile-Shear Spot Welds Subjected to Ford Weld History

Specimen	S_A MPa	max / min (ksi.)	N_T Predicted Blocks	N_T Observed Blocks
LGV-1	+61 / -61	(+8.9) / (-8.9)	200	158
LGV-2	+77 / -77	(+11.1) / (-11.1)	62	38
LGV-3	+77 / -77	(+11.1) / (-11.1)	62	49
LGV-4	+61 / -61	(+8.9) / (-8.9)	200	58
LGV-5	+61 / -61	(+8.9) / (-8.9)	200	72
LGV-6	+46 / -46	(+6.7) / (-6.7)	1,030	514
LGV-7	+46 / -46	(+6.7) / (-6.7)	1,030	694
LCV-8	+77 / -77	(+11.1) / (-11.1)	62	37
LGV-9	+92 / -92	(+13.3) / (-13.3)	21	18

Table 11

Uncertainty, Random Load Factor and Reliability Factor Corresponding to the Level of Reliability for DQSK G-90 and B60XK G-90 Tensile-Shear Spot Weld.

Material	SN-Curve Slope, m	Level of Reliability, R	Uncertainty in Fatigue Life, ΩN	Random Load Factor, ξ	Reliability Factor, R_F
DQSK G-90	5.497	.50	.772	2.902	.923
	5.497	.95	.772	2.902	.672
B60XK G-90	5.181	.50	.698	2.970	.931
	5.181	.95	.698	2.970	.688

Table 12

Fatigue Test Results for As-Welded B60XK G-90 Tensile-Shear Spot Weld with Different Nugget Ellipticity (R=-1).

Ellipticity	Specimen	ΔS MPa (ksi.)	N_T Observed Cycles
b/a = 1.7	HB-1	90 (13.0)	74,790
	HB-2	90 (13.0)	84,060
	HB-3	72 (10.4)	149,350
	HB-4	54 (7.8)	334,800
	HB-5	54 (7.8)	567,700
	HB-6	54 (7.8)	438,700
b/a = .6	HA-1	90 (13.0)	75,990
	HA-2	54 (7.8)	3,170,800
	HA-3	54 (7.8)	2,664,900
	HA-4	54 (7.8)	524,500
	HA-5	54 (7.8)	773,200
	HA-6	54 (7.8)	524,400

Table 13

Fatigue Test Results for Pre-Loaded* B60XK G-90 Tensile-Shear Spot Weld (R=-1).

Specimen	ΔS MPa (ksi.)	N_T Predicted Cycles	N_T Observed Cycles
HGP-1	163 (23.6)	42,700	22,700
HGP-2	163 (23.6)	42,700	26,900
HGP-3	135 (19.6)	171,000	174,700
HGP-4	135 (19.6)	171,000	147,900
HGP-5	108 (15.6)	1,086,500	2,317,200
HGP-6	108 (15.6)	1,086,500	2,709,900
HGP-7	95 (13.8)	---	9,999,990+
HGP-8	81 (11.8)	---	6,465,000+

* 75% ultimate tensile load
\+ no failure

Table 14

Fatigue Test Results for Pre-Loaded* DQSK G-90 Tensile-Shear Spot Weld (R=-1).

Specimen	ΔS MPa (ksi.)	N_T Predicted Cycles	N_T Observed Cycles
LPG-1	123 (17.8)	38,970	27,700
LPG-2	123 (17.8)	38,970	33,850
LPG-3	92 (13.4)	247,900	385,700
LPG-4	92 (13.4)	247,900	423,800
LPG-5	81 (11.8)	566,200	773,800
LPG-6	81 (11.8)	566,200	1,380,500
LPG-7	81 (11.8)	566,200	2,860,000
LPG-8	72 (10.4)	---	9,345,600+
LPG-9	51 (7.4)	---	10,485,500+

* 75% ultimate tensile load
\+ no failure

Table 15

Fatigue Test Results for Pre-Loaded* B60XK G-90
Tensile-Shear Spot Weld Subjected to Ford Weld History

Specimen	S_A Mpa	max / min (ksi.)	N_T Predicted Blocks	N_T Observed Blocks
HPV-1	+108 / -108	(+15.7) / (-15.7)	---	44
HPV-2	+68 / -68	(+9.8) / (-9.8)	---	803†
HPV-3	+81 / -81	(+11.8) / (-11.8)	---	779
HPV-4	+95 / -95	(+13.7) / (-13.7)	---	161
HPV-5	+81 / -81	(+11.8) / (-11.8)	---	928
HPV-6	+95 / -95	(+13.7) / (-13.7)	---	176

* 75% ultimate tensile load

† no failure

Table 16

Fatigue Test Results for Pre-Loaded* DQSK G-90
Tensile-Shear Spot Weld Subjected to Ford Weld History

Specimen	S_A MPa	max / min (ksi.)	N_T Predicted Blocks	N_T Observed Blocks
LPV-1	+61 / -61	(+8.9) / (-8.9)	---	477
LPV-2	+92 / -92	(+13.3) / (-13.3)	---	32
LPV-3	+77 / -77	(+11.1) / (-11.1)	---	57
LPV-4	+61 / -61	(+8.9) / (-8.9)	---	342

* 75% ultimate tensile load

Table 17

Fatigue Test Results for Coined B60XK G-90 Tensile-Shear Spot Weld (R=-1).

Specimen	ΔS MPa (ksi.)	N_T Predicted Cycles	N_T Observed Cycles	Remark
HGL-1	90 (13)	---	515,000	5,000 lb. compressive load without oil
HGL-2	90 (13)	---	347,400	5,000 lb. compressive load with oil
HGL-3	90 (13)	2,318,800	1,666,300	10,000 lb. compressive load without oil
HGL-4	90 (13)	2,318,800	928,600	10,000 lb. compressive load without oil
HGL-5	90 (13)	2,318,800	769,100	10,000 lb. compressive load without oil
HGL-6	90 (13)	2,318,800	2,001,500	10,000 lb. compressive load with oil
HGL-7	90 (13)	2,318,800	1,196,700	10,000 lb. compressive load with oil
HGL-8	127 (18.4)	123,400	143,870	10,000 lb. compressive load without oil
HGL-9	127 (18.4)	123,400	126,370	10,000 lb. compressive load without oil
HGL-10	127 (18.4)	123,400	194,100	10,000 lb. compressive load without oil
HGL-11	127 (18.4)	123,400	173,400	10,000 lb. compressive load with oil

Table 18

Fatigue Test Results for Coined B60XK G-90
Tensile-Shear Spot Weld Subjected to Ford Weld History

Specimen	S_a MPa	max / min (ksi.)	N_T Predicted Blocks	N_T Observed Blocks	Remark
HCV-1	+81 / -81	(+11.8) / (-11.8)	---	309	10,000 lb. compressive load with oil
HCV-2	+68 / -68	(+9.8) / (-9.8)	---	1291†	10,000 lb. compressive load without oil
HCV-3	+108 / -108	(+15.7) / (-15.7)	---	56	10,000 lb. compressive load without oil
HCV-4	+81 / -81	(+11.8) / (-11.8)	---	745	10,000 lb. compressive load with oil
HCV-5	+108 / -108	(+15.7) / (-15.7)	---	114	10,000 lb. compressive load without oil
HCV-6	+95 / -95	(+13.7) / (-13.7)	---	259	10,000 lb. compressive load without oil
HCV-7	+95 / -95	(+13.7) / (-13.7)	---	274	10,000 lb. compressive load without oil
HCV-8	+81 / -81	(+11.8) / (-11.8)	---	500	10,000 lb. compressive load without oil

† no failure

Table 19

Residual Stresses Measured for the Dimpled Surface of Tensile-Shear Spot Weld.

Condition	Materials	Specimen	Measured Value MPa (ksi.)	Average MPa (ksi.)
As-Welded	B60XKG-90	BR-1	+390 (56.5)	+415 (60.2)
		BR-2	+455 (66)	
		BR-3	+402 (58.3)	
	DQSKG-90	DR-1	+32 (4.6)	+163 (23.6)
		DR-2	+295 (42.7)	
Pre-Loaded	B60XKG-90	BR-4	+70 (10.1)	+11 (1.6)
		BR-5	-48 (7.0)	
	DQSKG-90	DR-3	+92 (13.3)	+92 (13.3)
Coined	B60XKG-90	BR-6	-232 (33.7)	-332 (48.2)
		BR-7	-432 (62.7)	

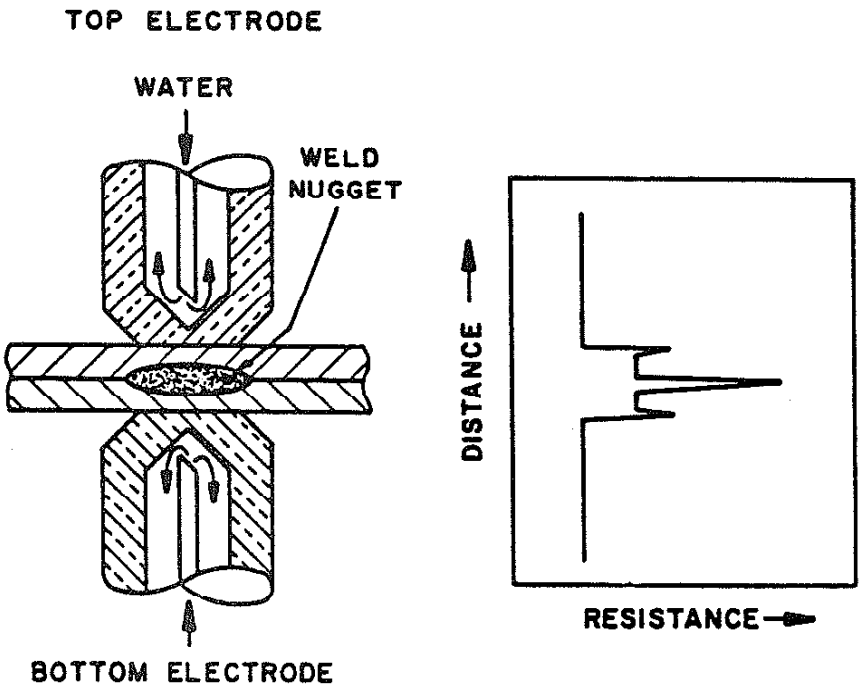

Fig. 1 Schematic Diagram of the Spot Welding Process

Table 7

Fatigue Test Results for As-Welded DQSK G-90 Tensile-Shear Spot Weld (R = -1)

Specimen	ΔS MPa (Ksi.)	N_T Predicted Cycles	N_T Observed Cycles
LG-2	143 (20.8)	7,600	3,530
LG-3	143 (20.8)	7,600	3,780
LG-4	102 (14.8)	37,300	16,500
LG-5	102 (14.8)	37,300	28,500
LG-6	102 (14.8)	37,300	20,600
LG-7	102 (14.8)	37,300	31,900
LG-8	143 (20.8)	7,600	6,620
LG-9	143 (20.8)	7,600	4,320
LG-10	61 (8.8)	496,800	282,000
LG-11	61 (8.8)	496,800	206,000
LG-12	61 (8.8)	496,800	449,000
LG-13	51 (7.4)	1,469,300	1,530,000
LG-14	51 (7.4)	1,469,300	1,256,000
LG-15	51 (7.4)	1,469,300	1,513,000

Table 8

Fatigue Test Results for As-Welded Galvanized SAE 960X Tensile-Shear Spot Weld (R=0)

Specimen	ΔS MPa (ksi.)	N_T Predicted Cycles	N_T Observed Cycles
SG-1	67 (9.7)	46,000	95,000
SG-2	67 (9.7)	46,000	117,000
SG-3	67 (9.7)	46,000	115,000
SG-4	42 (6.1)	652,400	705,000
SG-5	42 (6.1)	652,400	721,000
SG-6	42 (6.1)	652,400	741,000
SG-7	33 (4.8)	3,383,000	994,000
SG-8	33 (4.8)	3,383,000	2,389,000
SG-9	33 (4.8)	3,383,000	3,100,000
SG-10	33 (4.8)	3,383,000	3,110,000
SG-11	33 (4.8)	3,383,000	3,400,000
SG-12	29 (4.2)	11,094,000	4,299,000
SG-13	29 (4.2)	11,094,000	6,381,000
SG-14	29 (4.2)	11,094,000	9,218,000
SG-15	29 (4.2)	11,094,000	9,527,000
SG-16	29 (4.2)	11,094,000	19,311,000

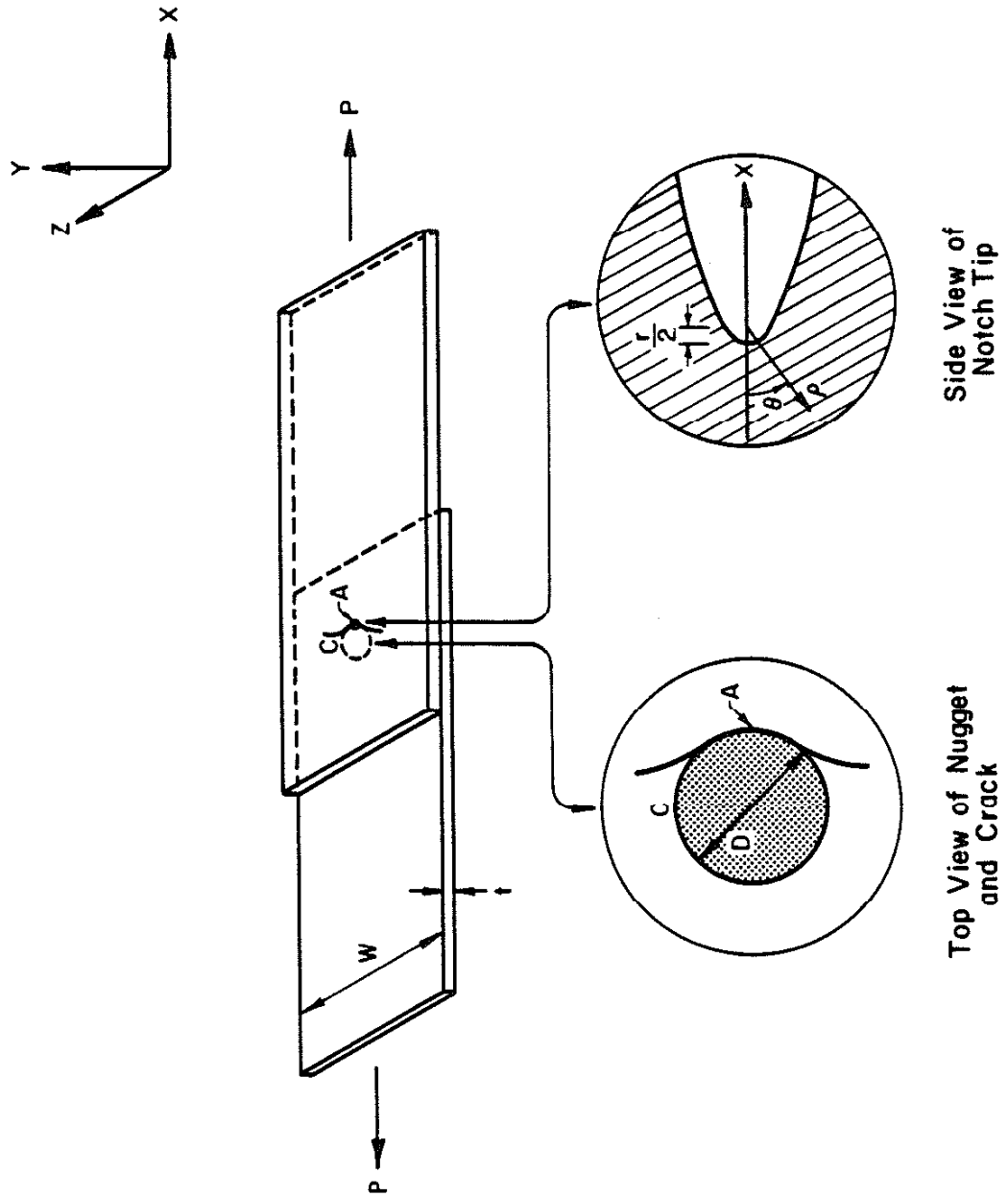

Fig. 2 Geometry of the Tensile-Shear Spot Weld. γ is the Notch Tip Radius.

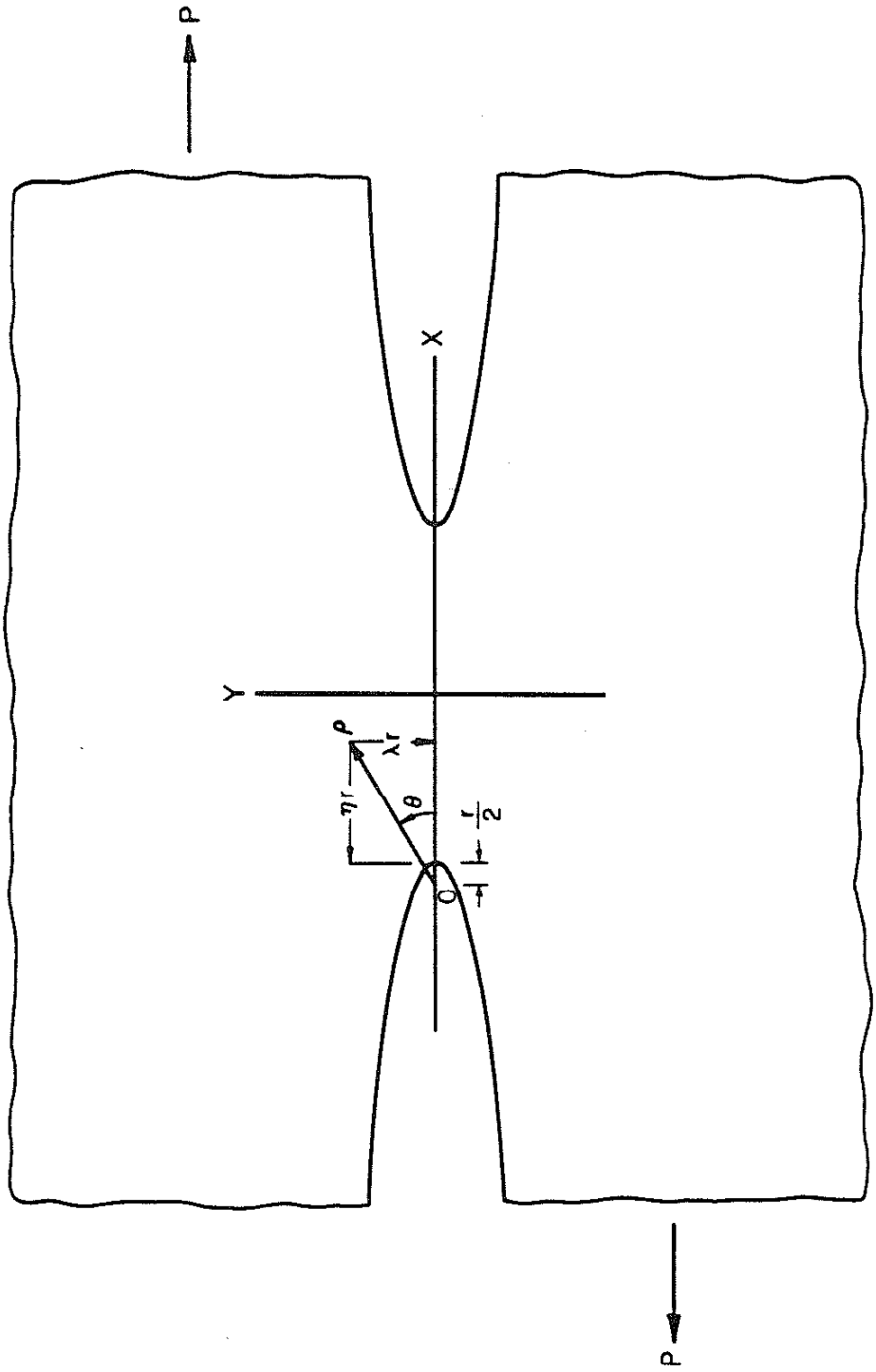

Fig. 3 The Hyperbolic Notch with Tip Radius (γ).

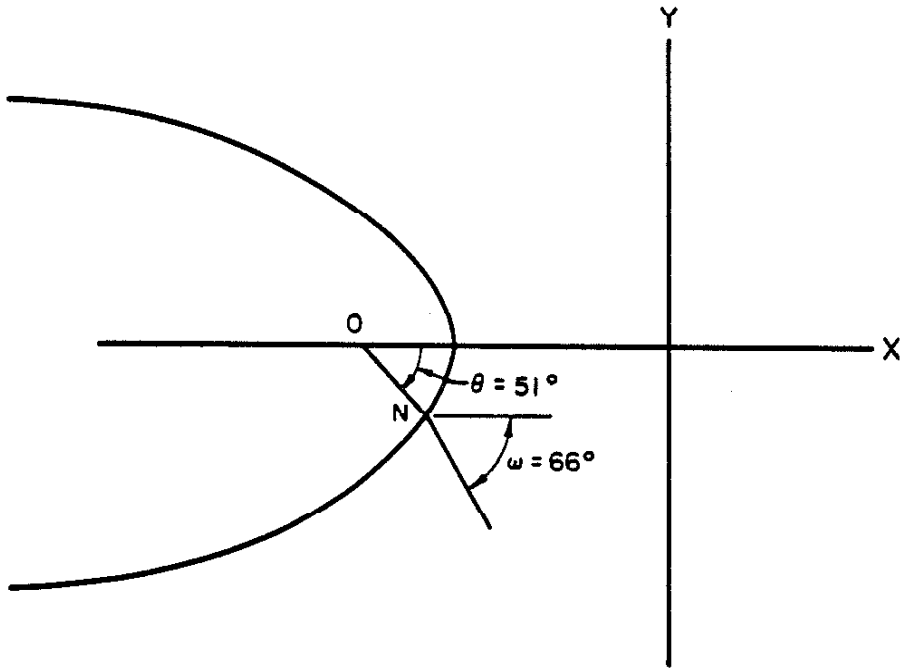

Fig. 4 The Initial Angle of Crack Growth.

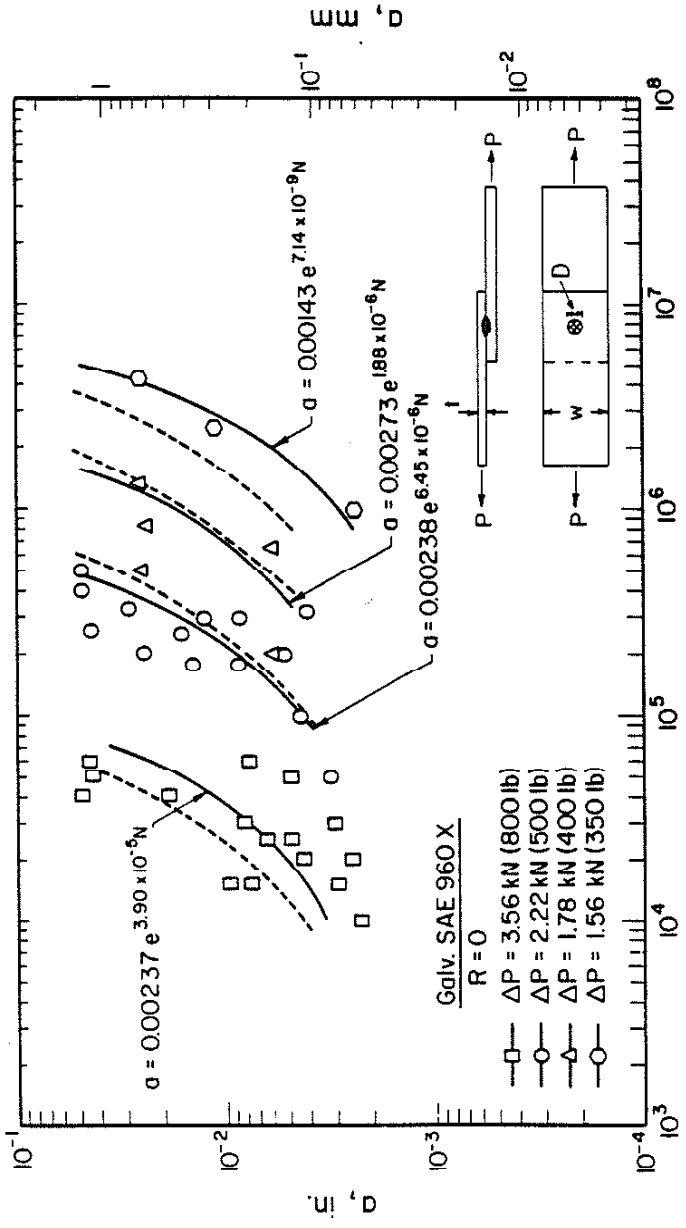

Fig. 5 Fatigue Crack Depth (a) Versus Cycles for Four Load Levels. The Solid Line Is the Curve Fitted Relationship and the Dashed Line Is the Calculated Crack Depth Versus Life Using 2.22 kN Load Level Data (See Section 2.5).

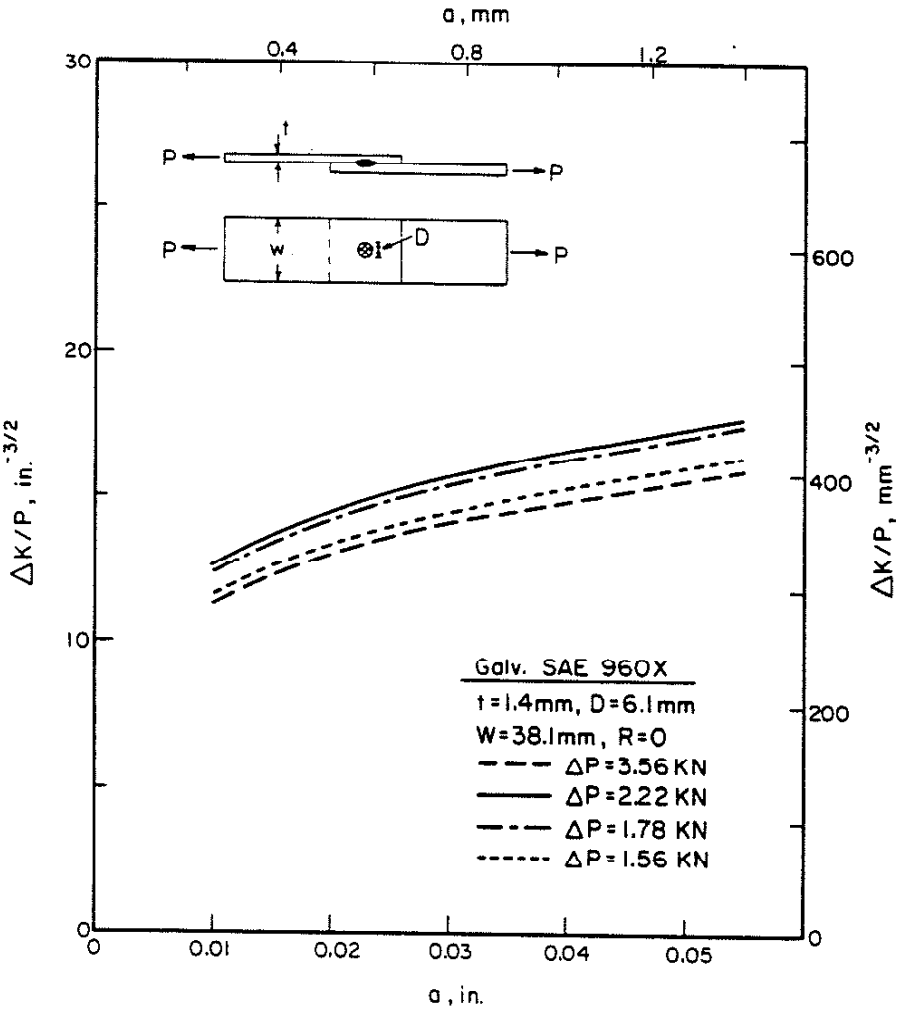

Fig. 6 The Calculated Variation of ΔK/p Versus Crack Depth (a) of Four Different Load Levels for Tensile-Shear Spot Weld.

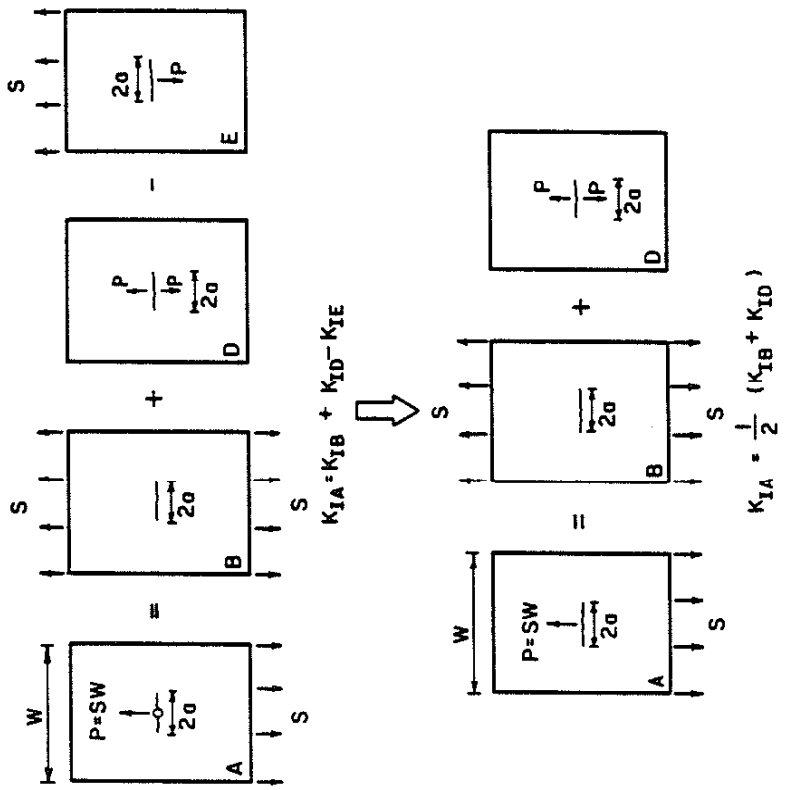

Fig. 7 Crack Emanating from Loaded Rivet Hole (53).

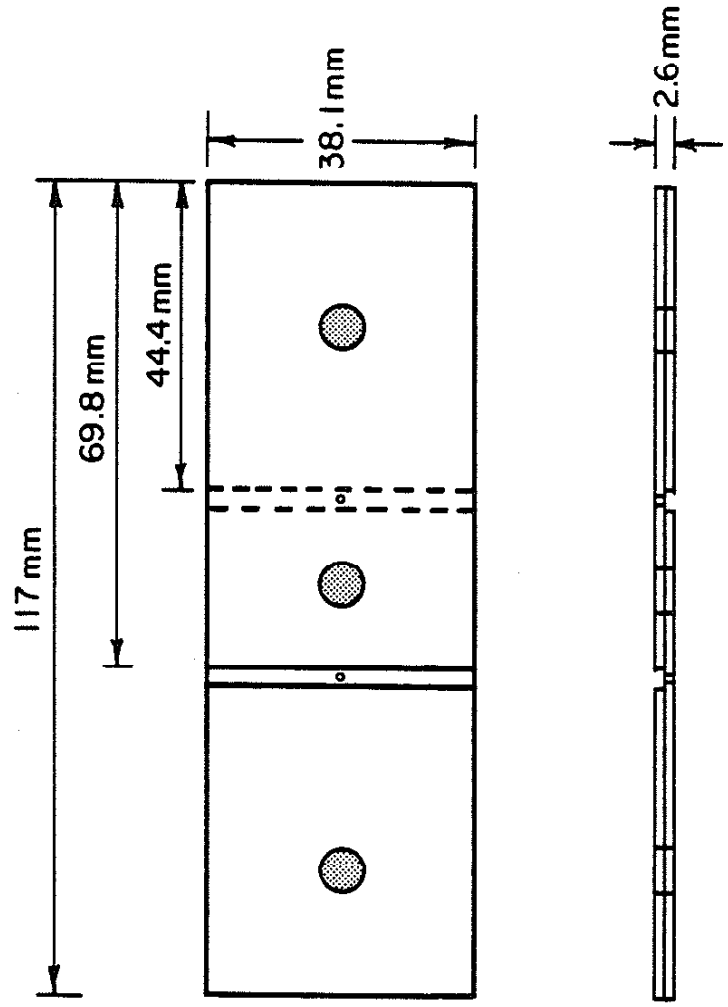

Fig. 8 Tensile-Shear Spot Weld Fatigue Test Specimen for R=-1 Loading Condition. Small Holes are for Specimen Alignment.

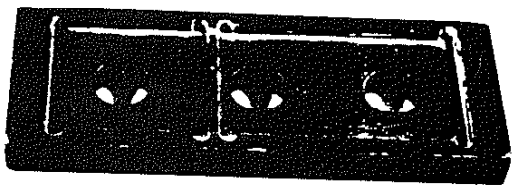

Fig. 9 Photograph of A Fixture for Spot Weld Preparation.

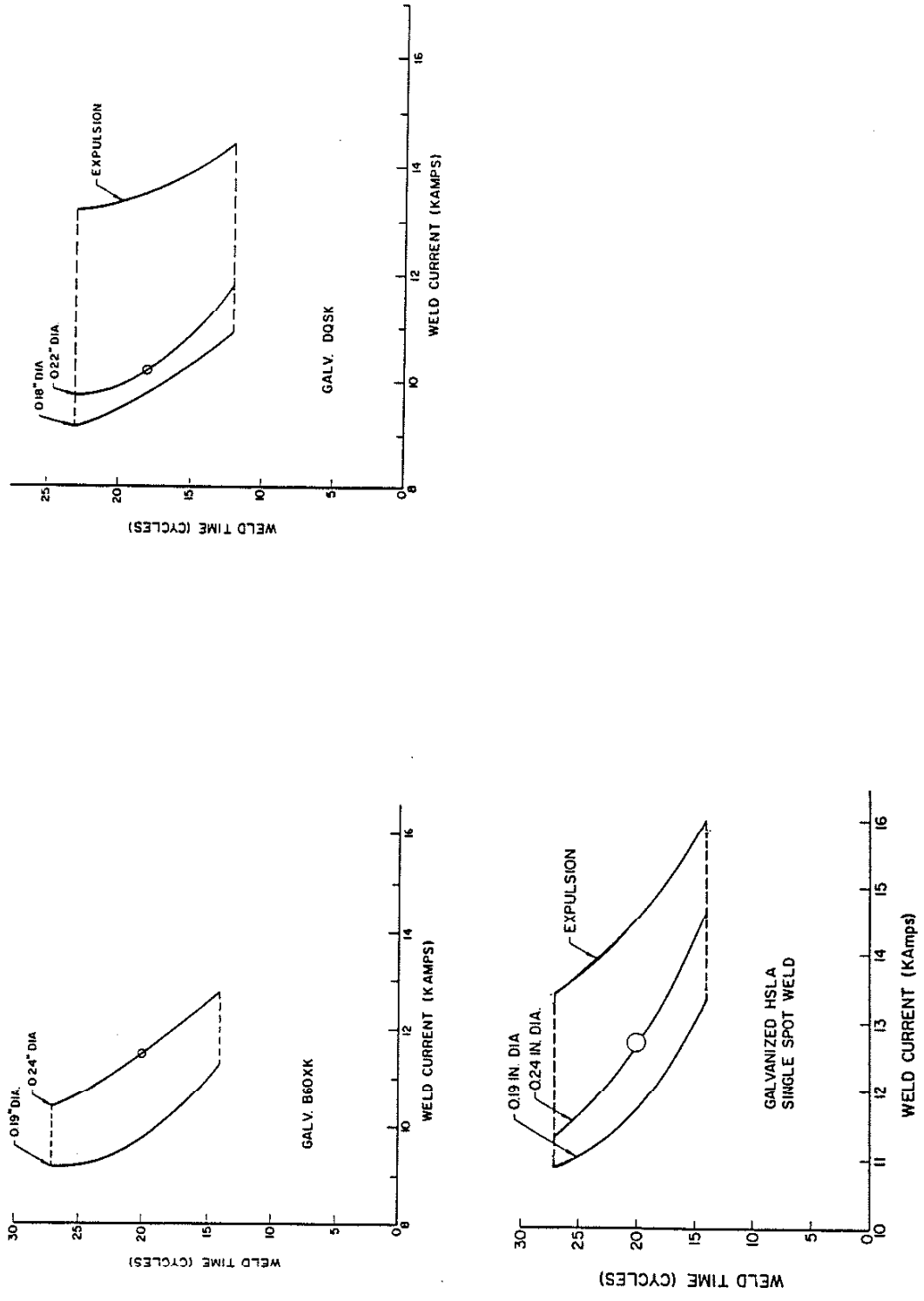

Fig. 10 Welding Lobe Diagram for DQSK G-90 (Low Carbon), B60XK G-90 (HSLA) and Galvanized SAE 960X (HSLA).

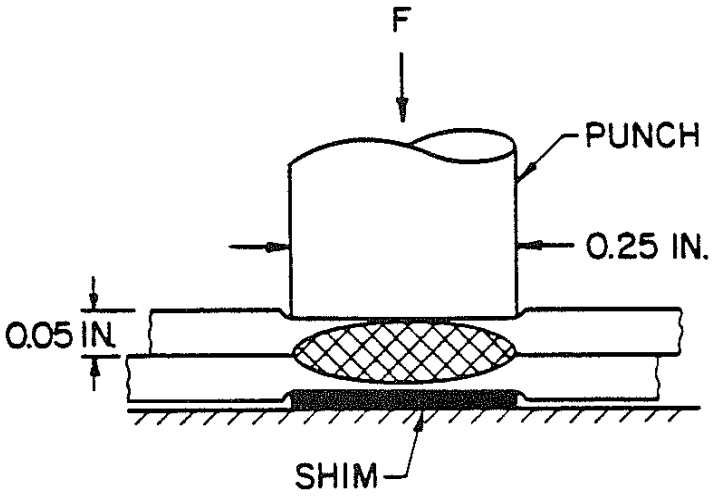

Fig. 11 Schematic Drawing of Coining Post-Weld Treatment.

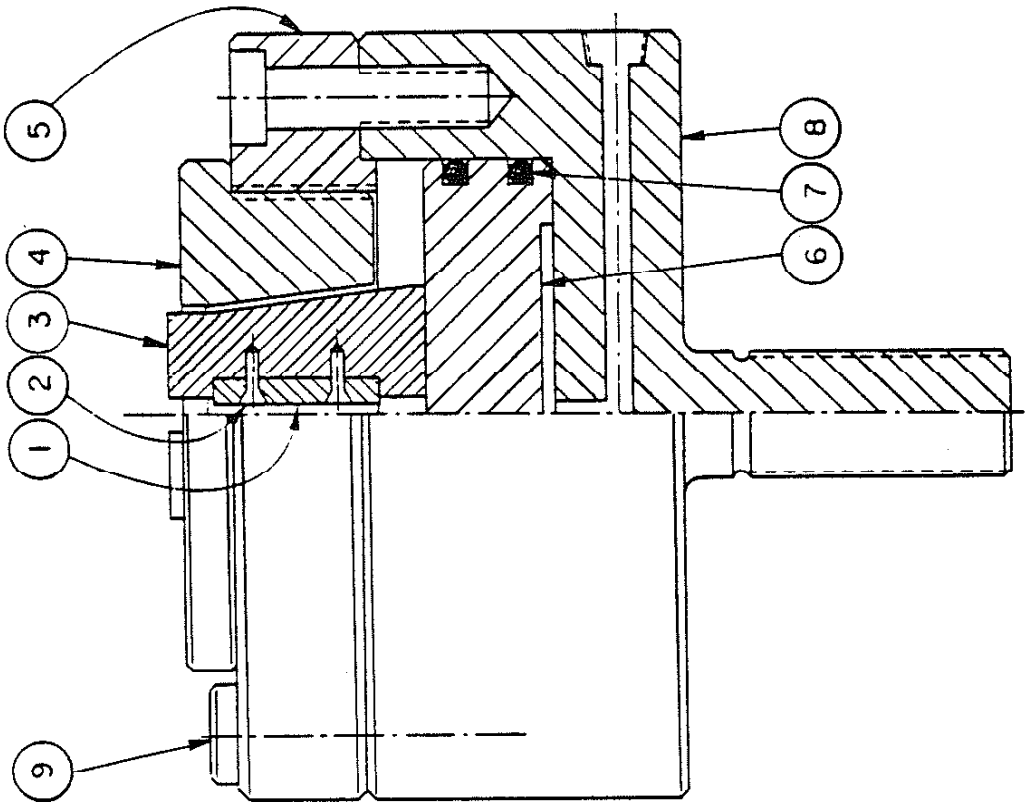

Fig. 12 Schematic Diagram of Hydraulic Grip for R=-1 Test on Tensile-Shear Spot Weld.

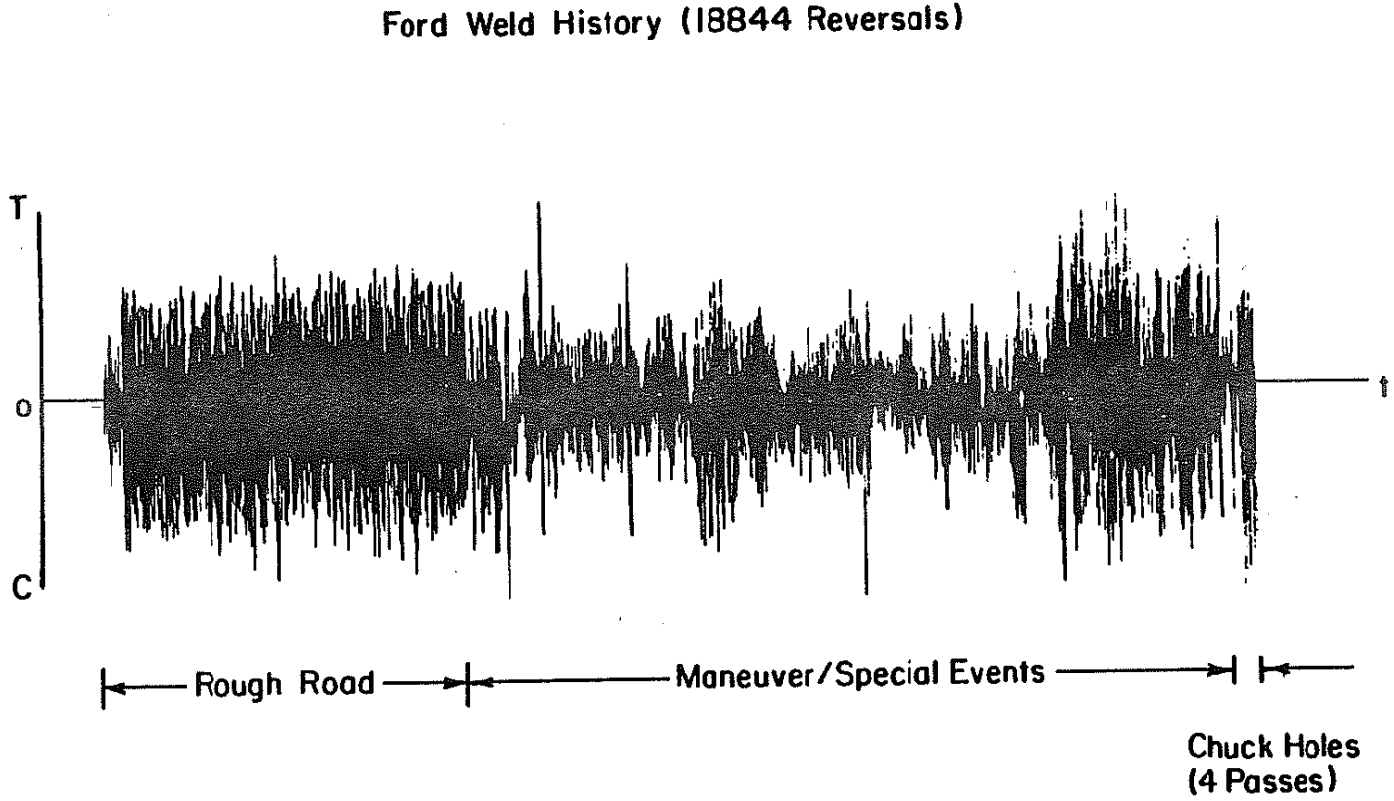

Fig. 13 Amplitude-Time Display of Ford Weld History.

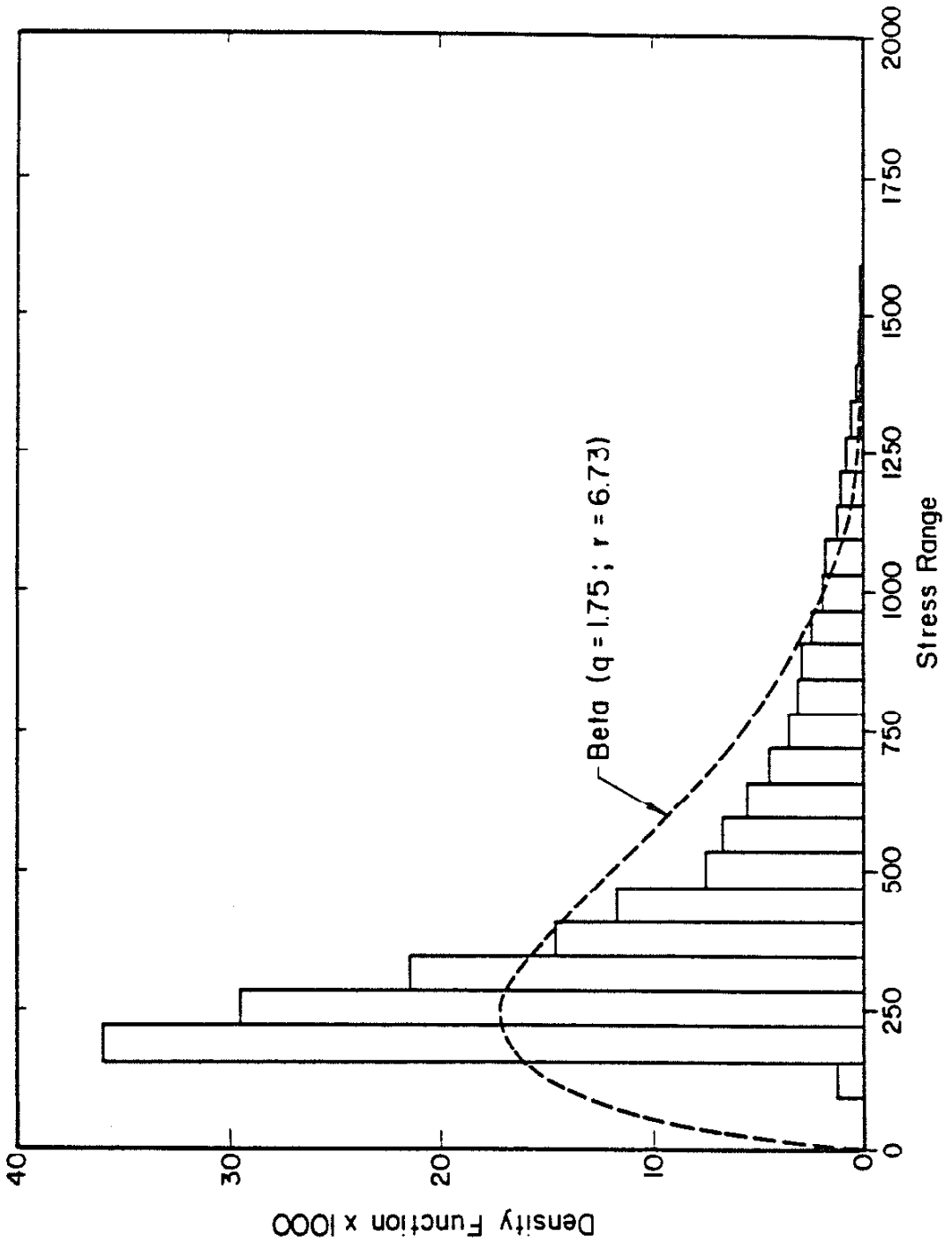

Fig. 14 Histogram of the Ford Weld Load History. The Dashed Line is a Beta Distribution Fitted to the Load Spectrum (See Appendix B).

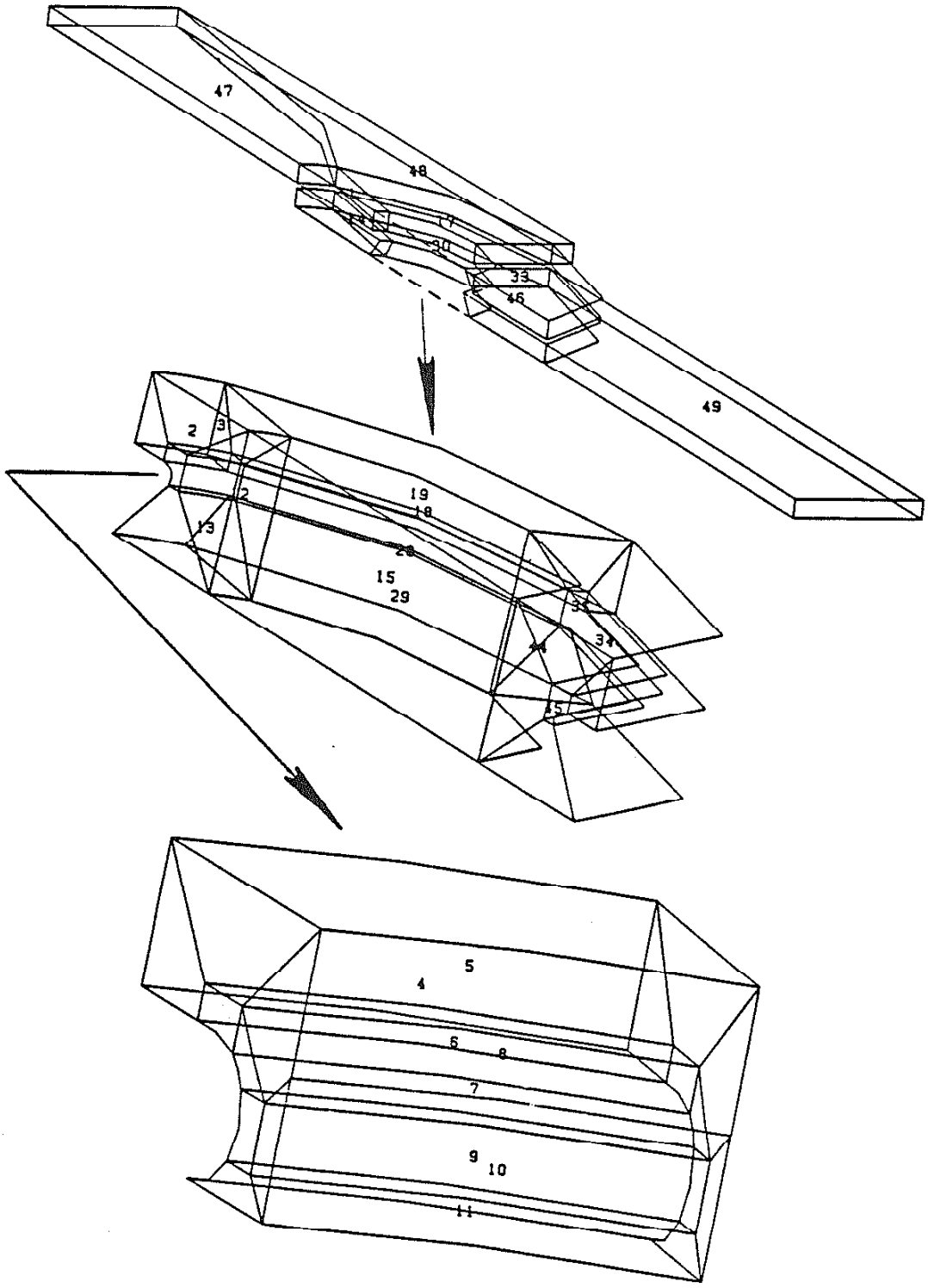

Fig. 15 Finite Element Mesh for the Tensile-Shear Spot Weld. The Inset Drawings Show the Details of the Finite Element Modelling at the Nugget Notch Root.

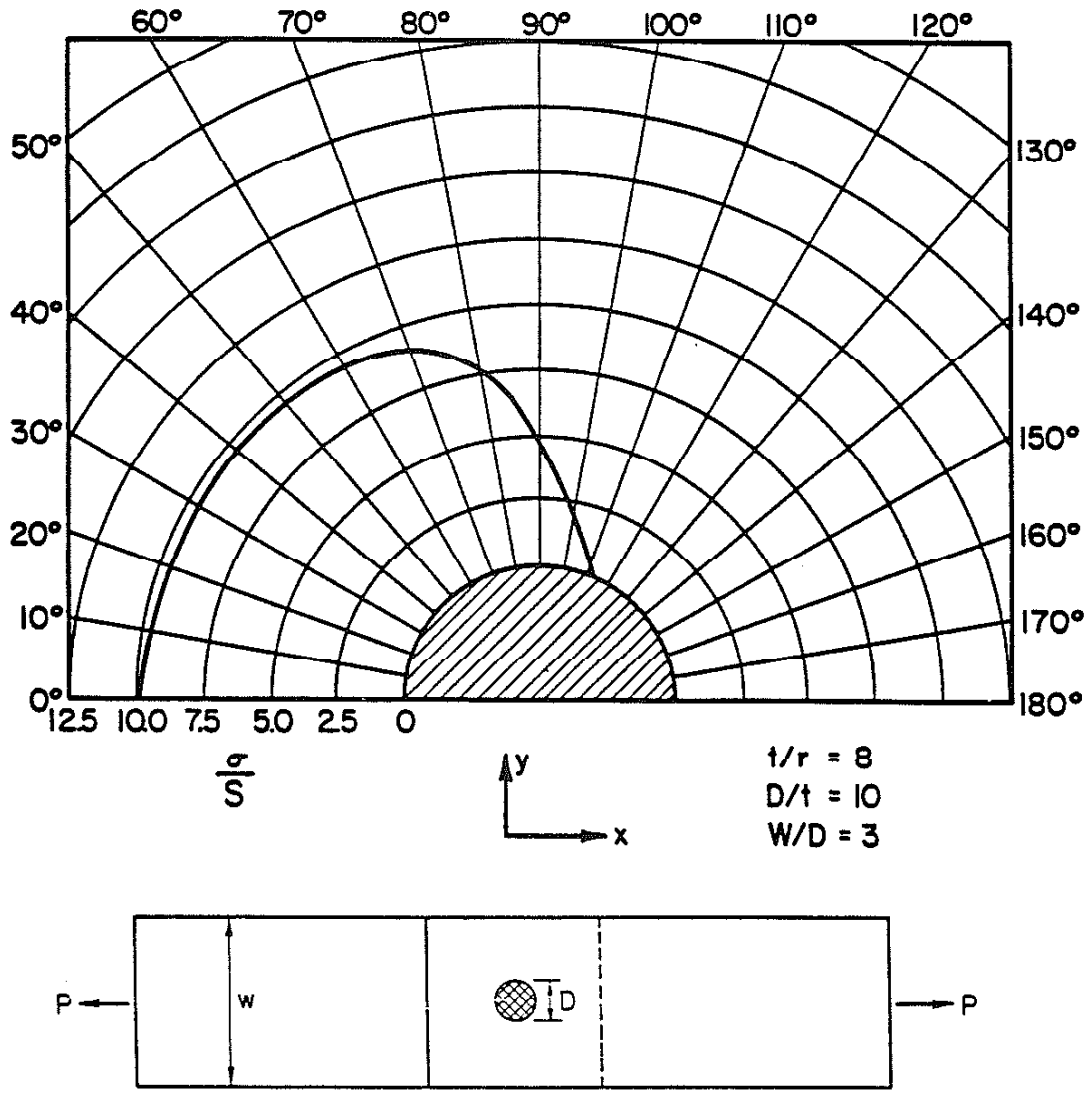

Fig. 16 Principal Stress Distribution Around the Nugget Circumference.

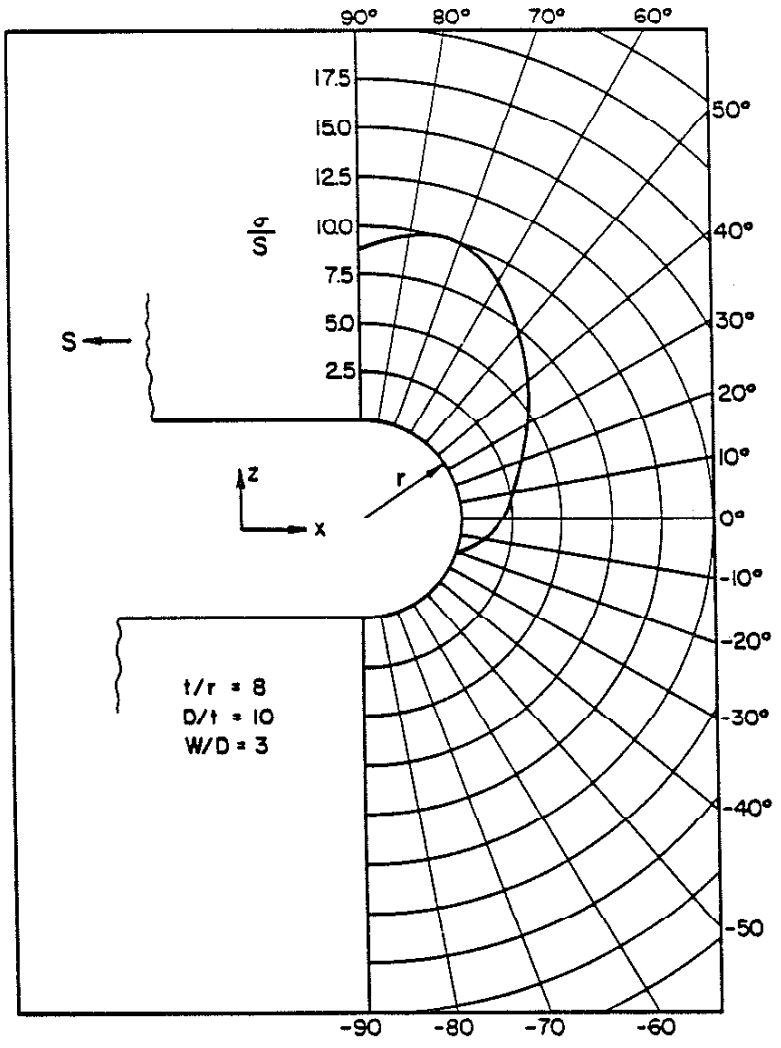

Fig. 17 Principal Stress Distribution at the Notch Root.

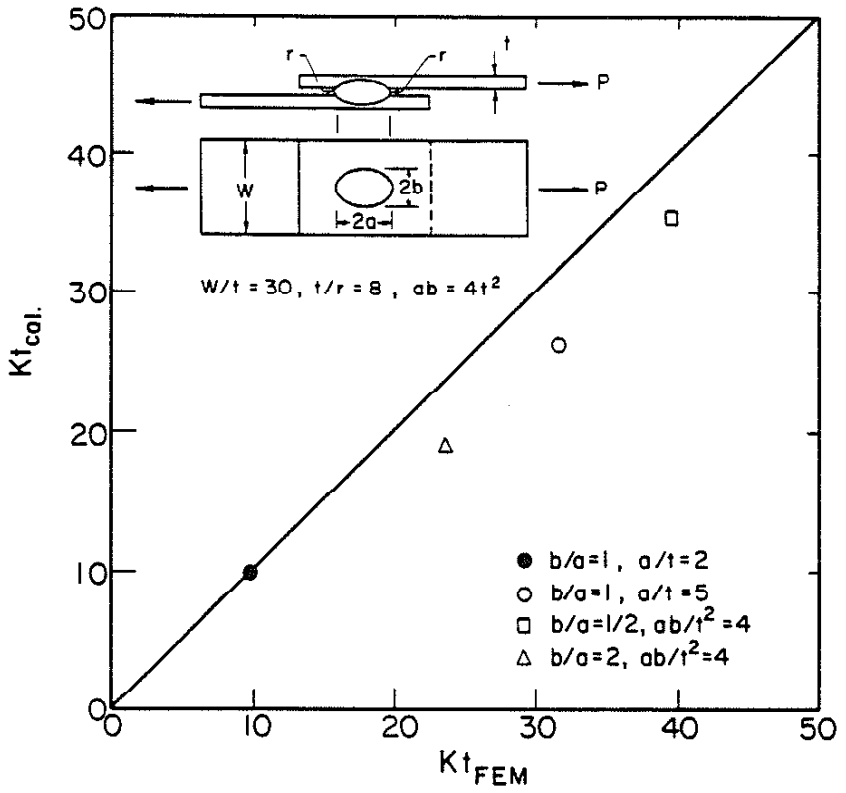

Fig. 18 A Comparison of the Calculated Stress Concentration Factor Using Eq. 7 and Computed Stress Concentration Factor Using FEM for Various Ellipticity.

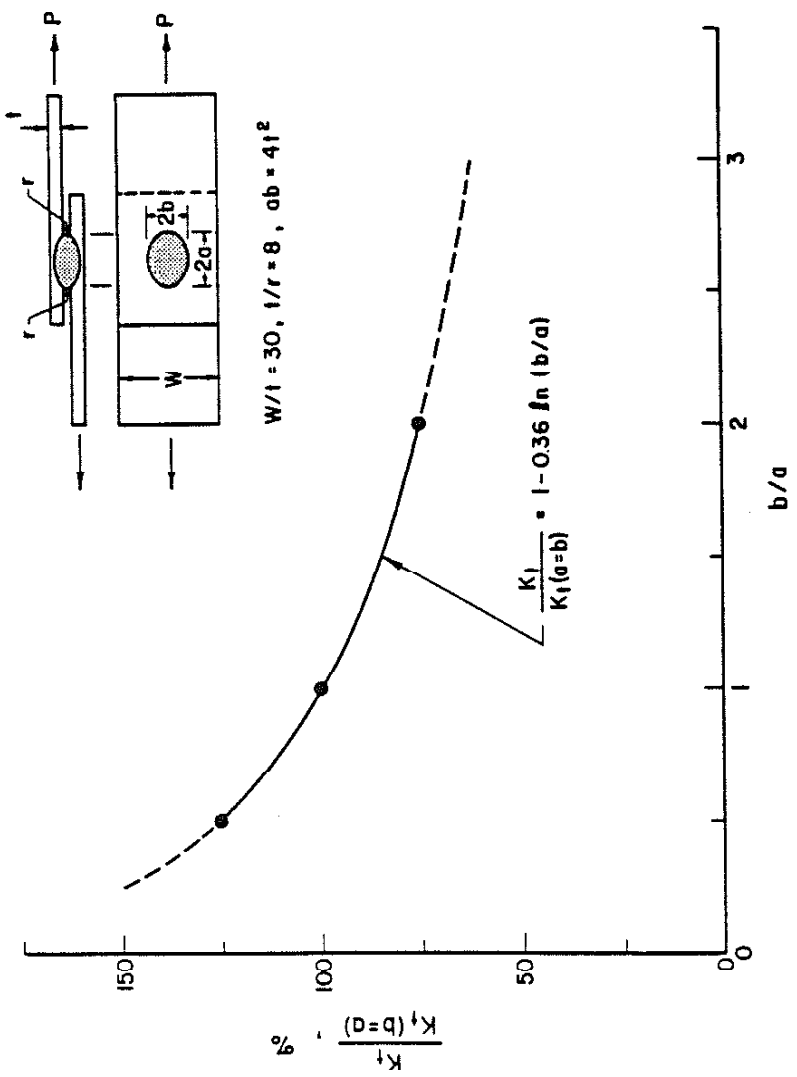

Fig. 19 Effect of Nugget Shape (b/a) on the Elastic Stress Concentration Factor ($K_t/K_{t(b=a)}$). Close Circles Are the Finite Element Calculations.

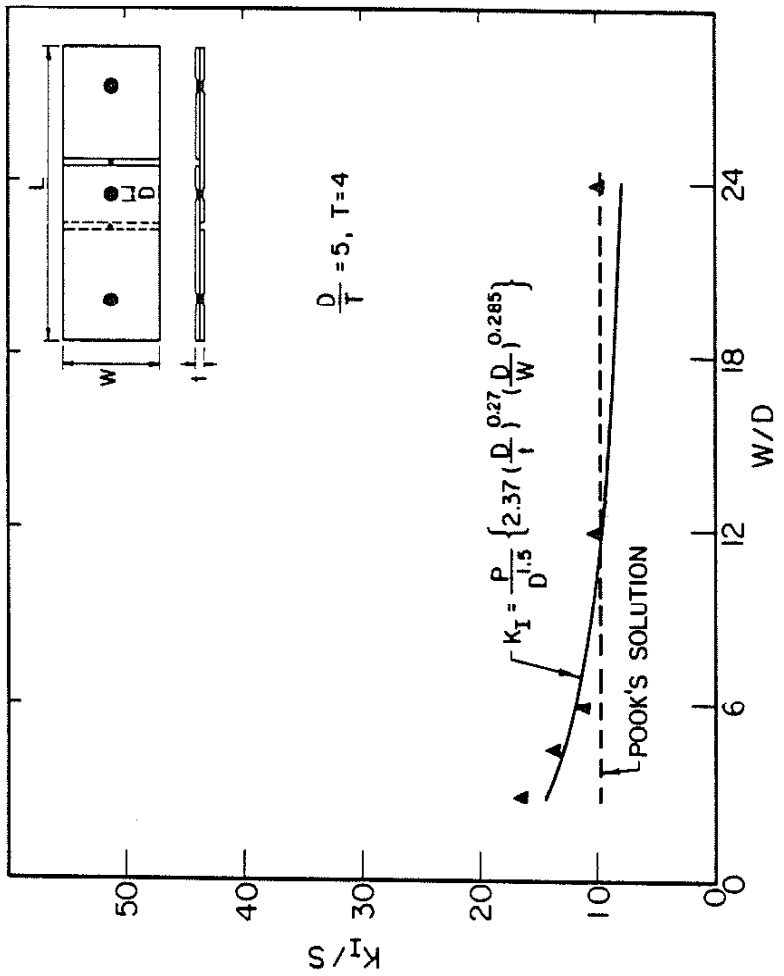

Fig. 20 Effect of Sheet Width on Stress Intensity Factor (K_I) of Tensile-Shear Spot Weld. Triangles Are the Finite Element Calculations.

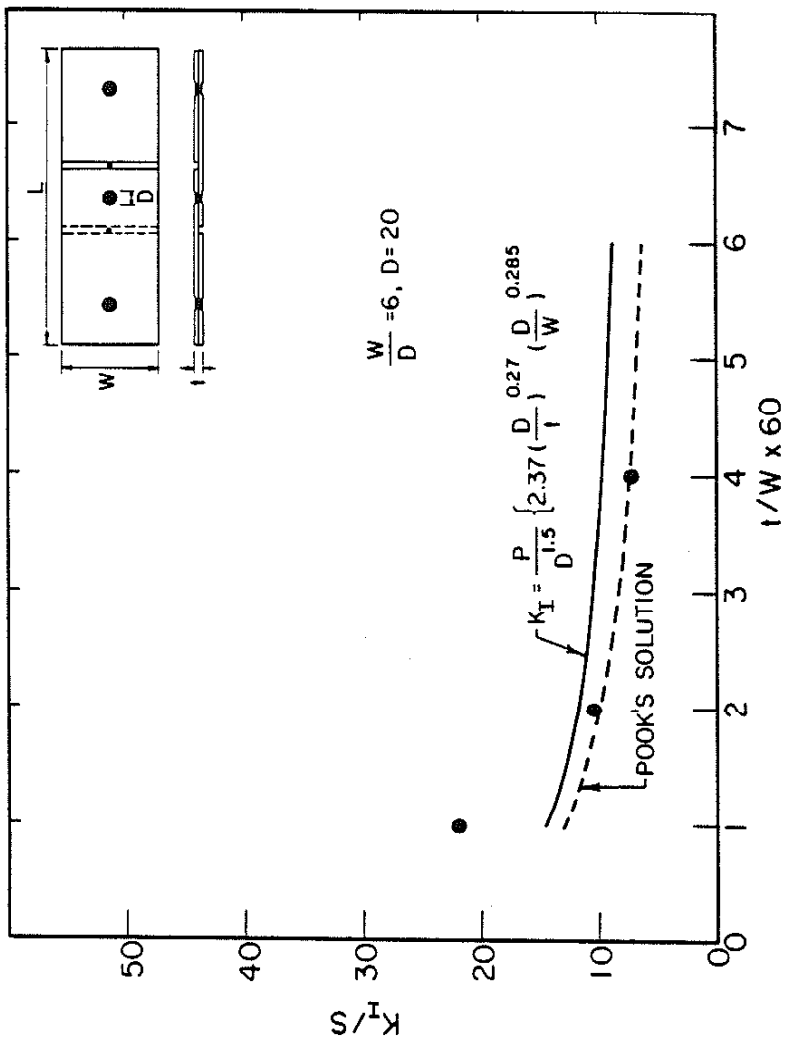

Fig. 21 Effect of Sheet Thickness on Stress Intensity Factor (K_I) of Tensile-Shear Spot Weld. Circulars Are the Finite Element Calculations.

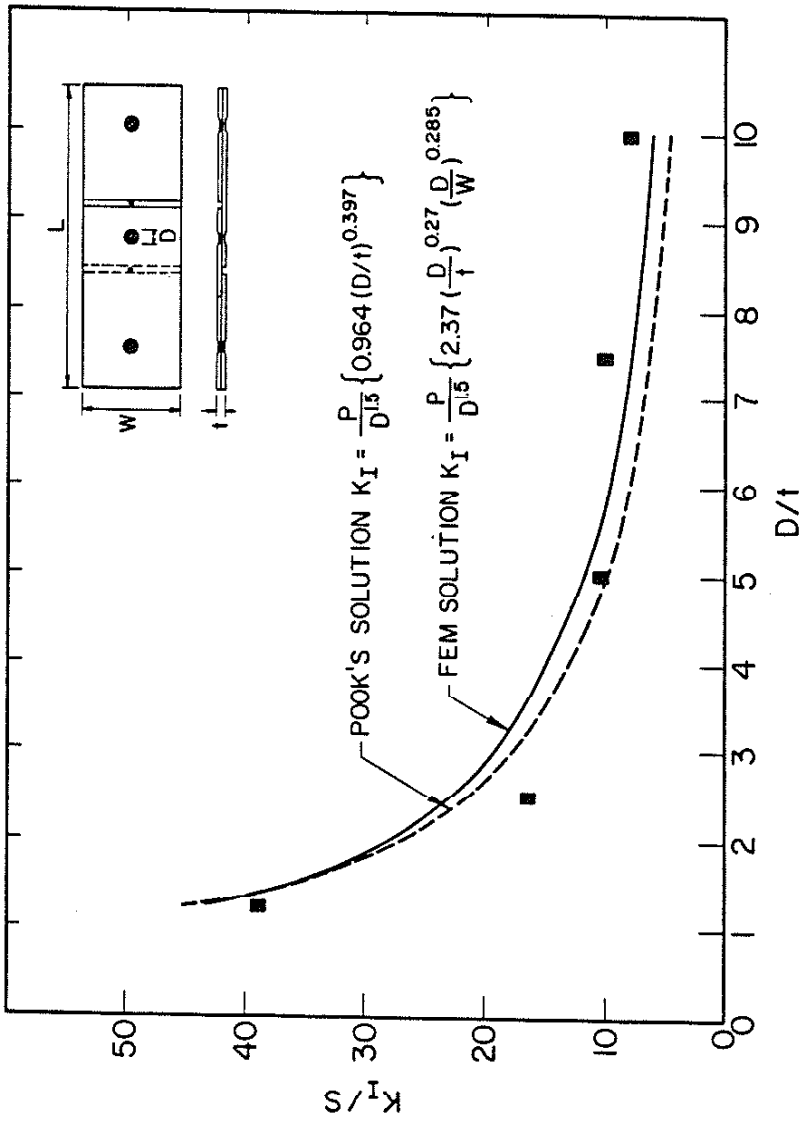

Fig. 22 Effect of Nugget Diameter on Stress Intensity Factor (K_I) of Tensile-Shear Spot Weld. Squares Are the Finite Element Calculations.

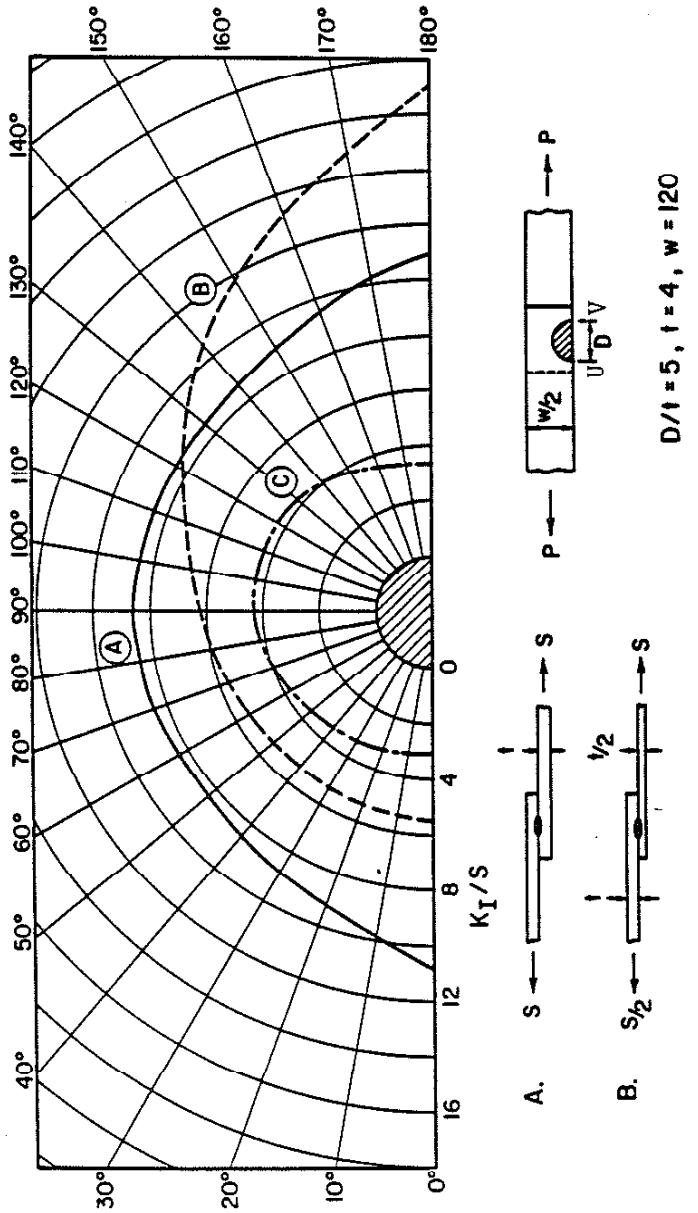

Fig. 23 Finite Element Calculations for the Tensile-Shear Spot Weld Having Equal Thickness, Dissimilar Thickness, and Triple-Sheet Configurations.

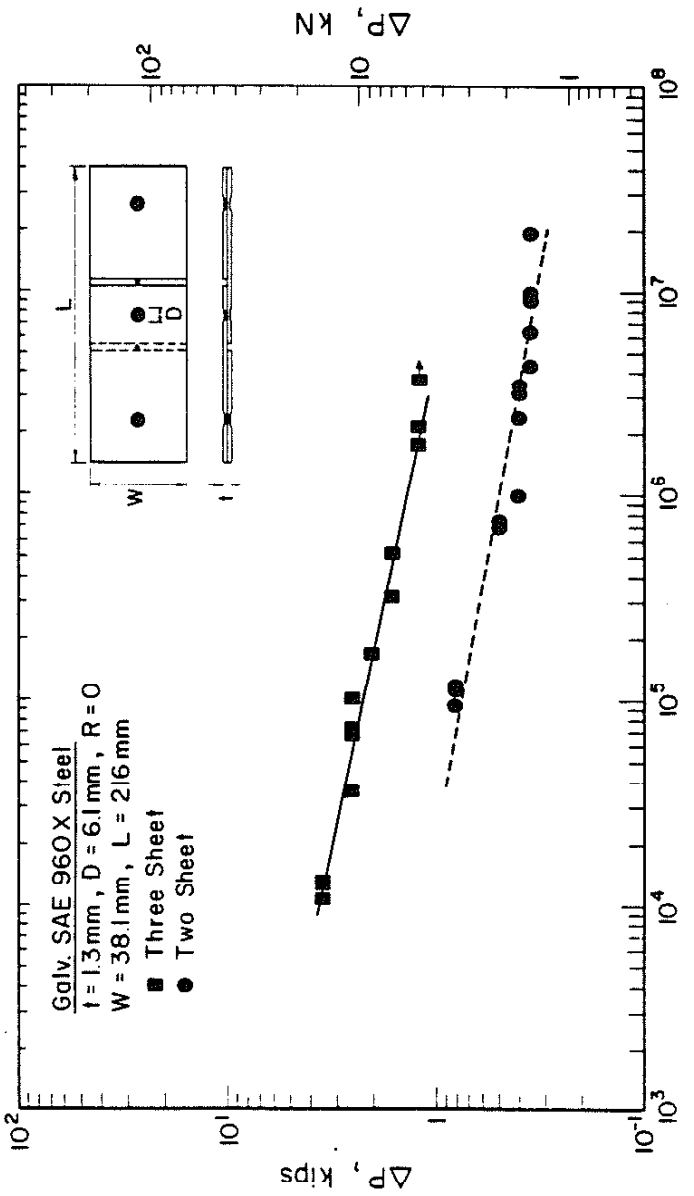

Fig. 24 Fatigue Test Results for Galvanized SAE 960X (HSLA) Two Sheet and Three-Sheet Tensile-Shear Spot Weld.

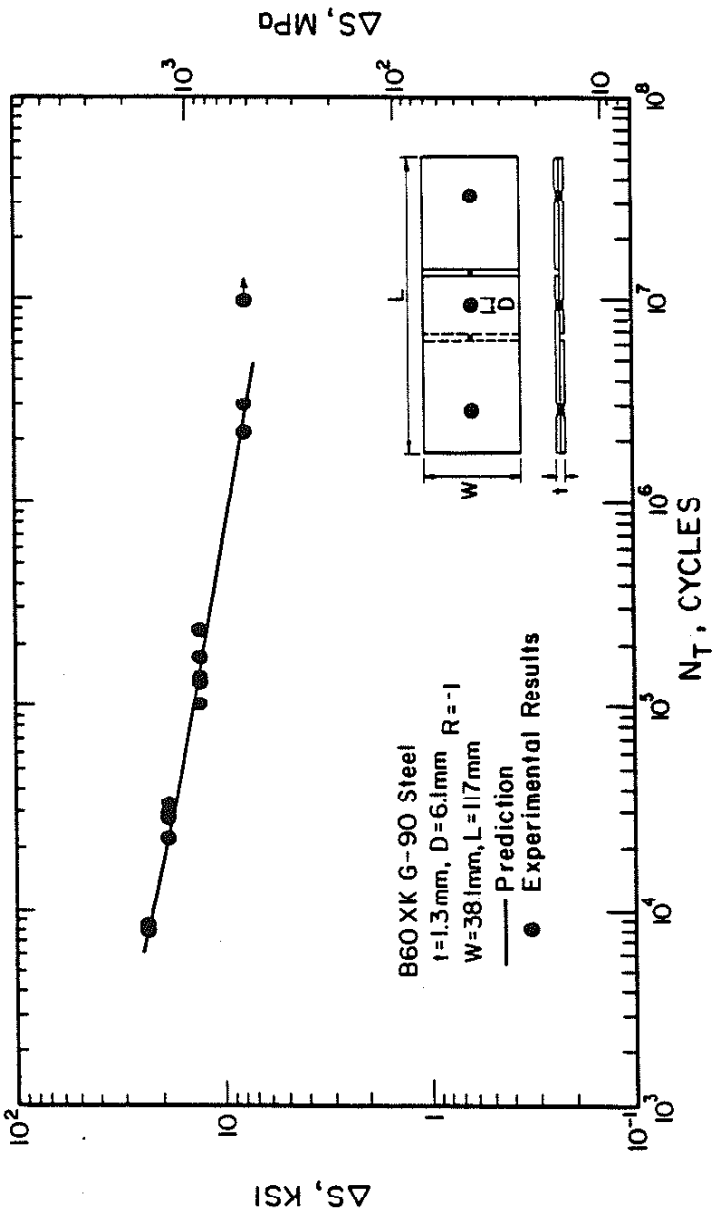

Fig. 25 Total Fatigue Life Predictions Using TSIP Model and Experimental Results for B60XK G-90 (HSLA) Tensile-Shear Spot Weld Under R=-1 Loading Condition.

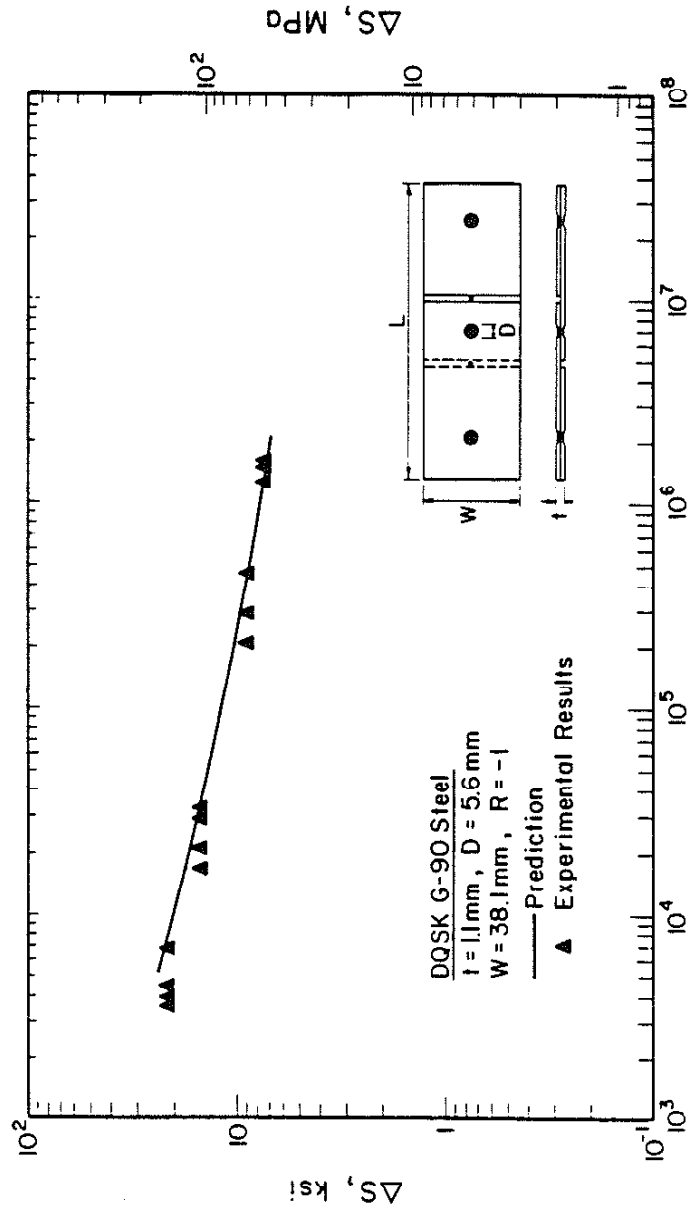

Fig. 26 Total Fatigue Life Predictions Using TSIP Model and Experimental Results for DQSK G-90 (Low Carbon) Tensile-Shear Spot Weld Under R=-1 Loading Condition.

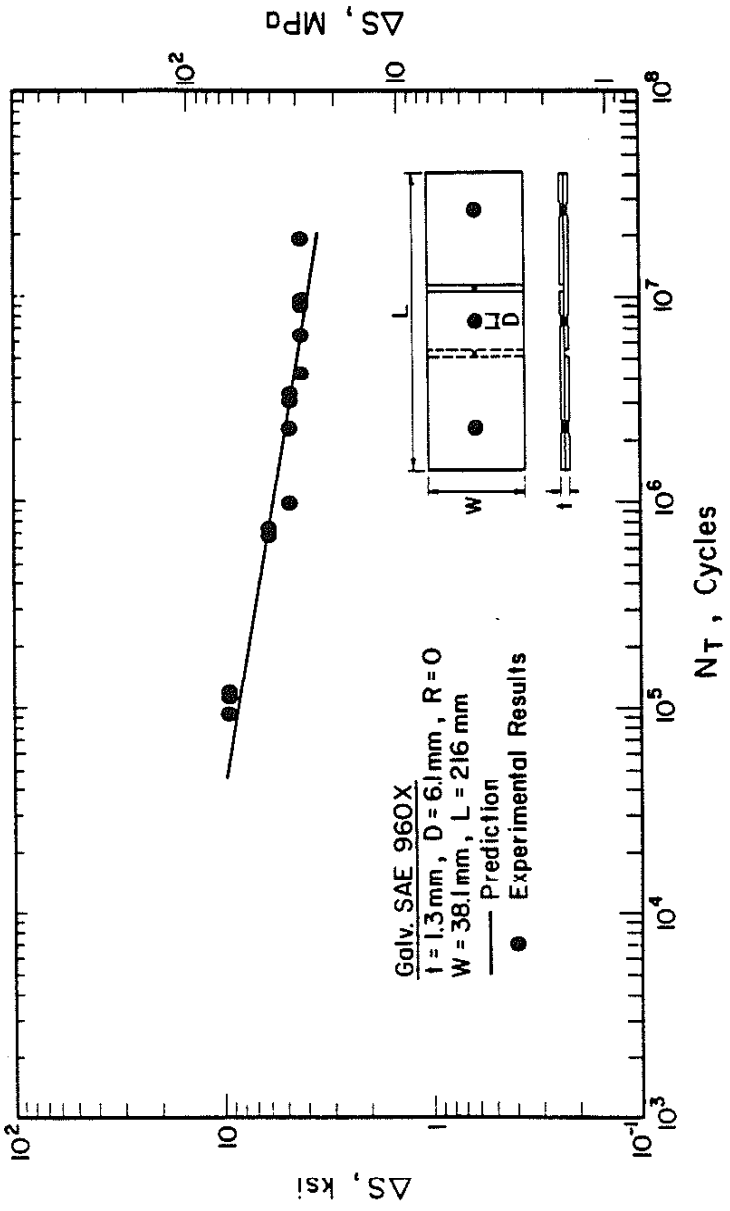

Fig. 27 Total Fatigue Life Predictions Using TSIP Model and Experimental Results for Galvanized SAE 960X (HSLA) Tensile-Shear Spot Weld Under R=0 Loading Condition.

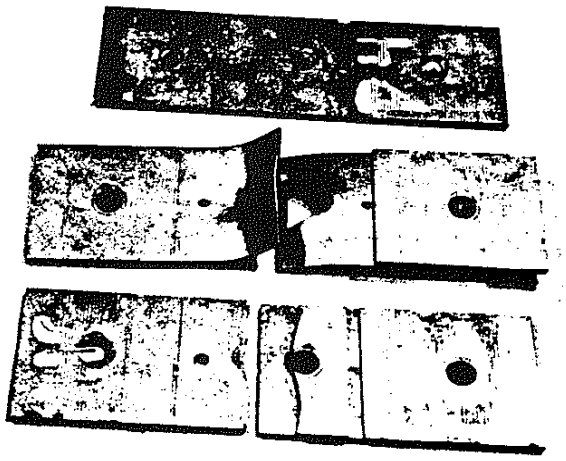

Fig. 28 Photograph of Untested and Fatigue Tested B60XK G-90 (HSLA) Spot Weld Specimens. Top Untested Specimen, Middle Pull-Out Failure and Bottom Separation Failure.

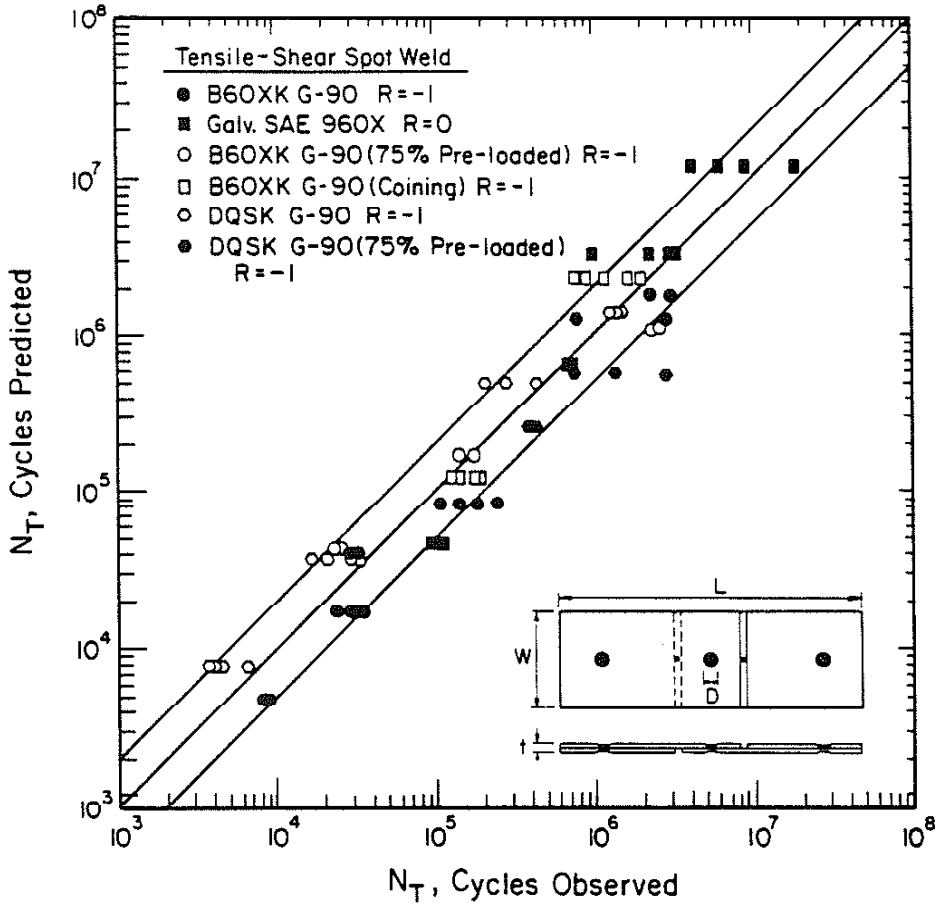

Fig. 29 Comparison of Predicted Using TSIP Model and Summary of Data Observed in this Study for Galvanized SAE 960X (HSLA), B60XK G-90 (HSLA) and DQSK G-90 (Low Carbon) Tensile-Shear Spot Weld Under the Constant Amplitude Fatigue Tests.

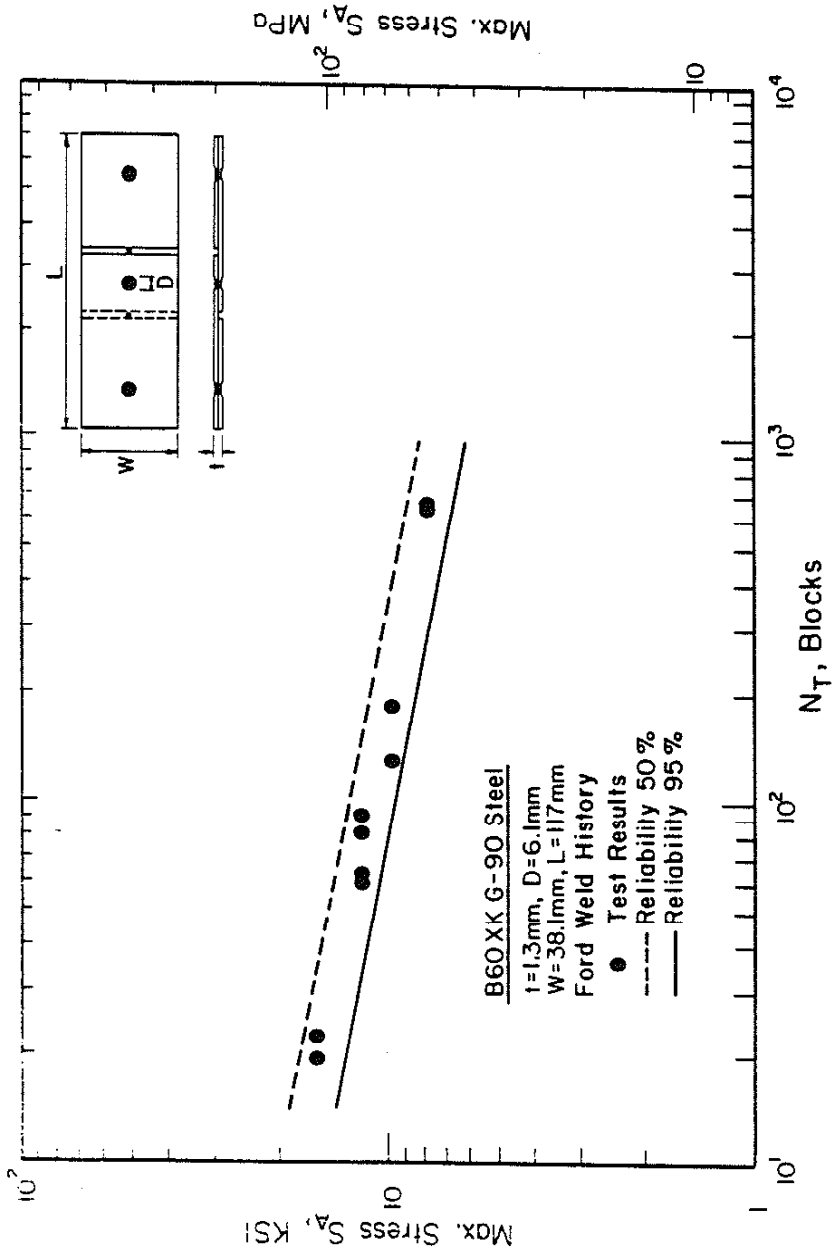

Fig. 30 Fatigue Test Results and Predictions Using the Munse Fatigue Criterion for the B60XK G-90$_i$ (HSLA) Tensile-Shear Spot Weld Subjected to the Ford Variable Load History.

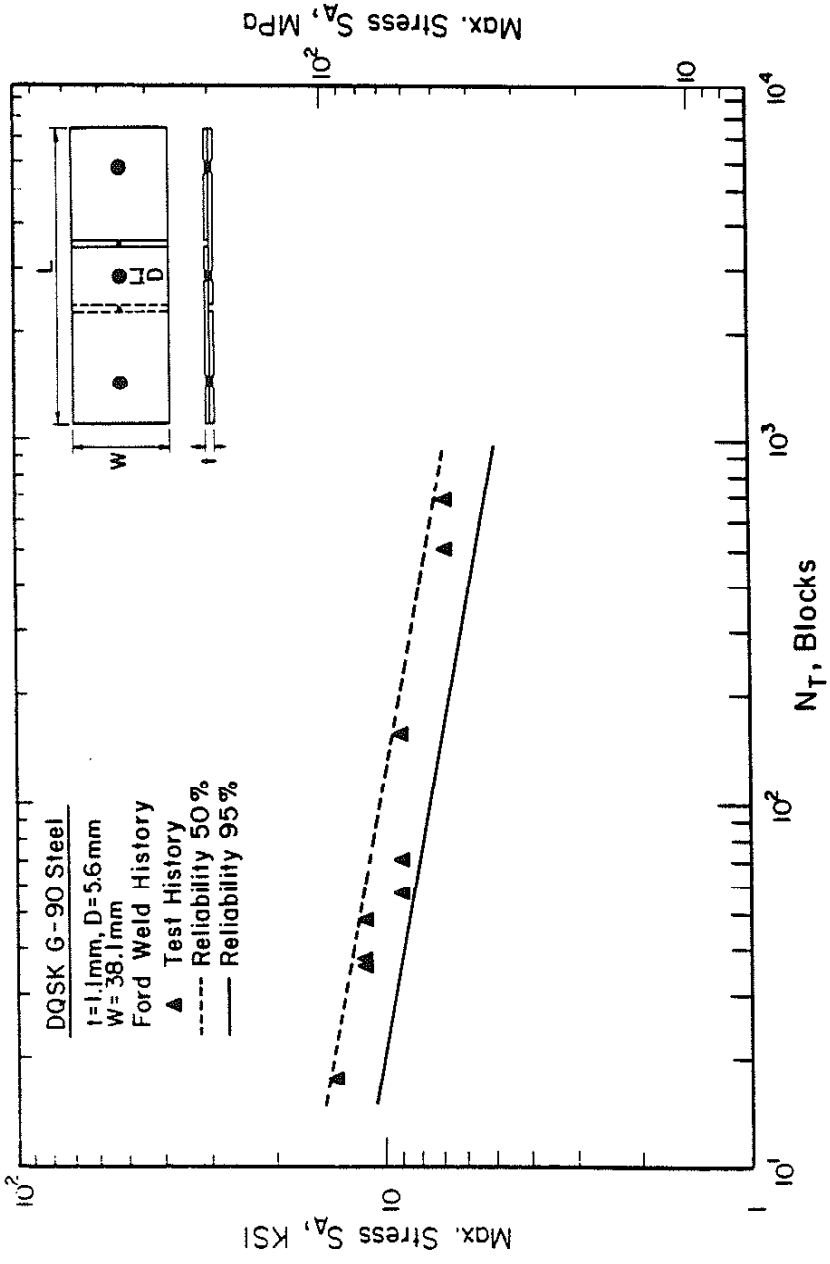

Fig. 31 Fatigue Test Results and Predictions Using the Munse Fatigue Criterion for the DQSK G-90 (Low Carbon) Tensile-Shear Spot Weld Subjected to the Ford Variable Load History.

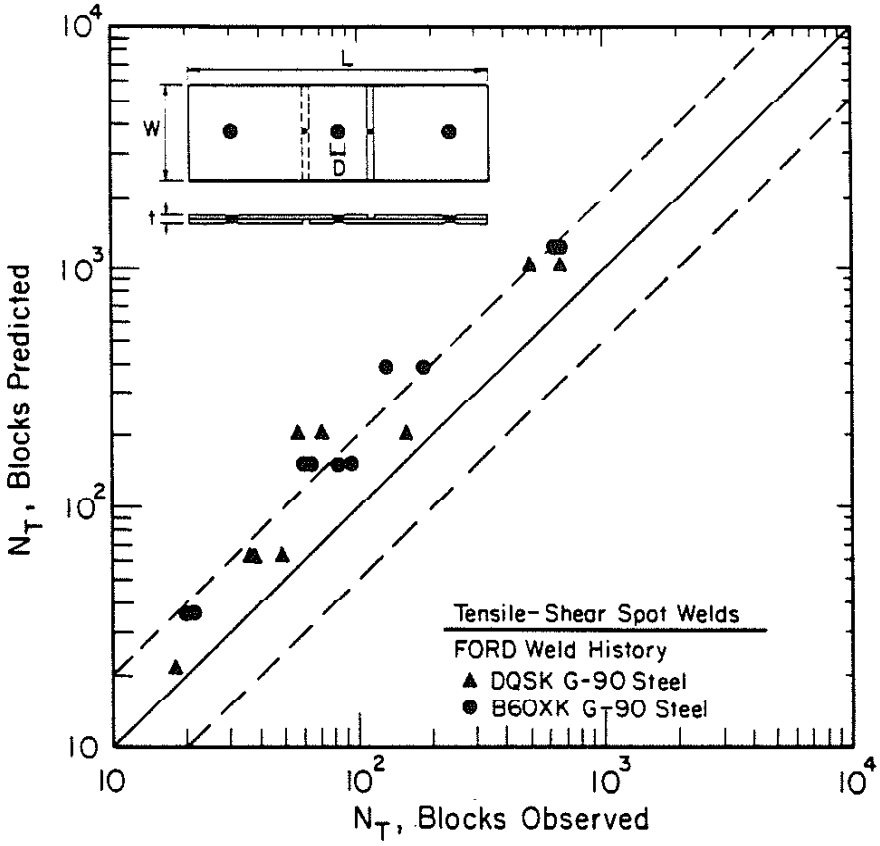

Fig. 32 The Observed and Predicted Total Fatigue Life of B60XK G-90 (HSLA) and DQSK G-90 (Low Carbon) Tensile-Shear Spot Weld. The Predictions of Total Life Were Made Using the Munse Fatigue Criterion.

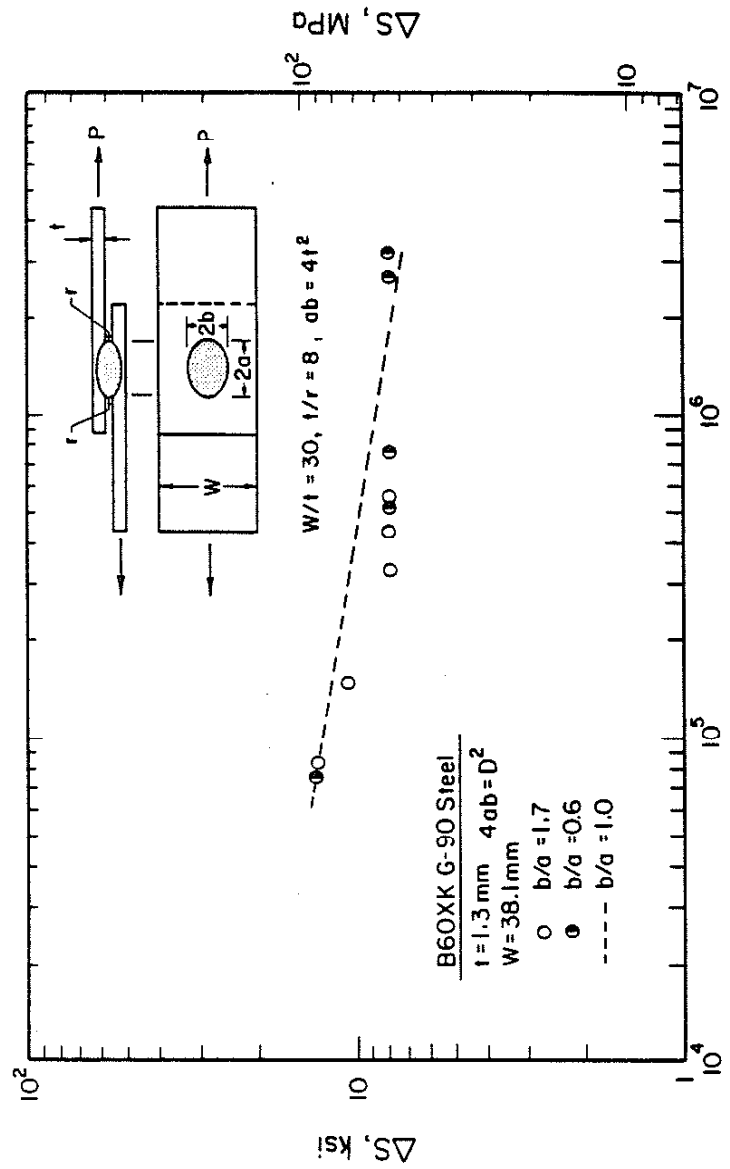

Fig. 33 Effect of Ellipticity on the Fatigue Resistance of B60XK G-90 (HSLA) Tensile-Shear Spot Weld Under R=-1 Loading Condition.

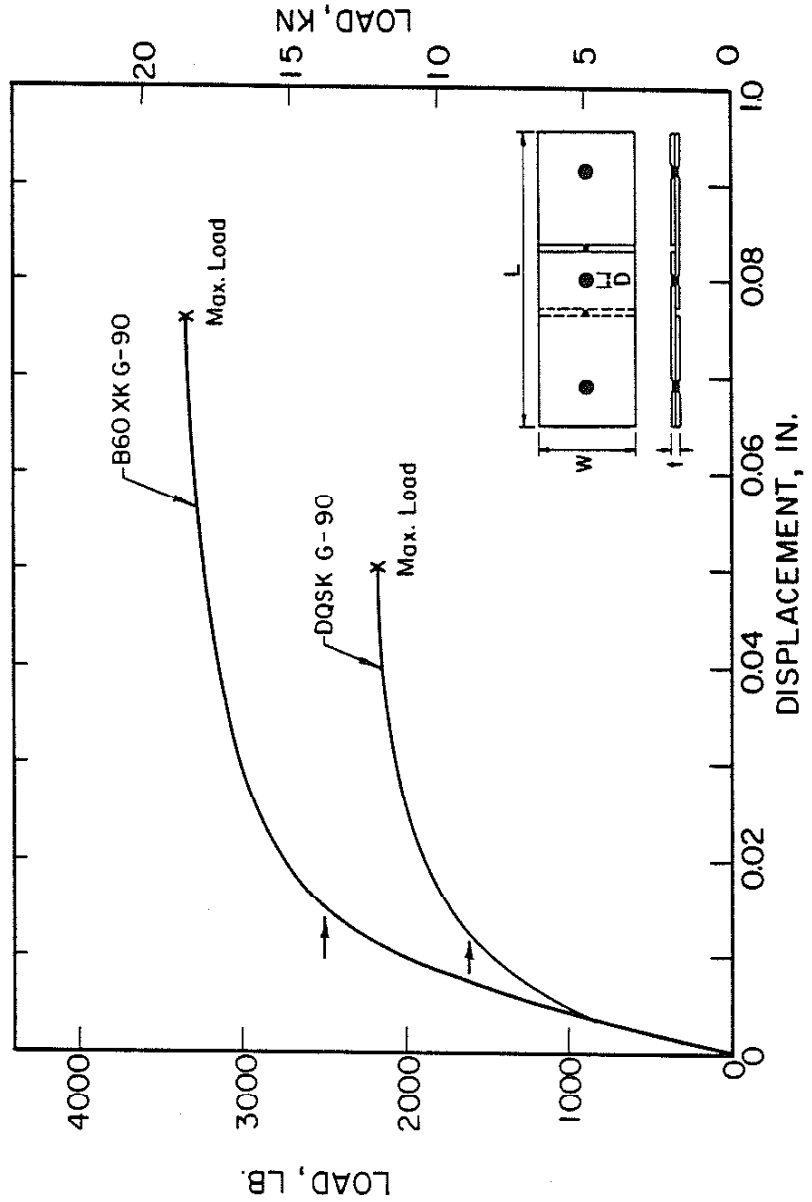

Fig. 34 Load-Displacement Diagrams for B60XK G-90 (HSLA) and DQSK G-90 (Low Carbon) Tensile-Shear Spot Welds. Arrows Indicate 75% of Ultimate Tensile Load.

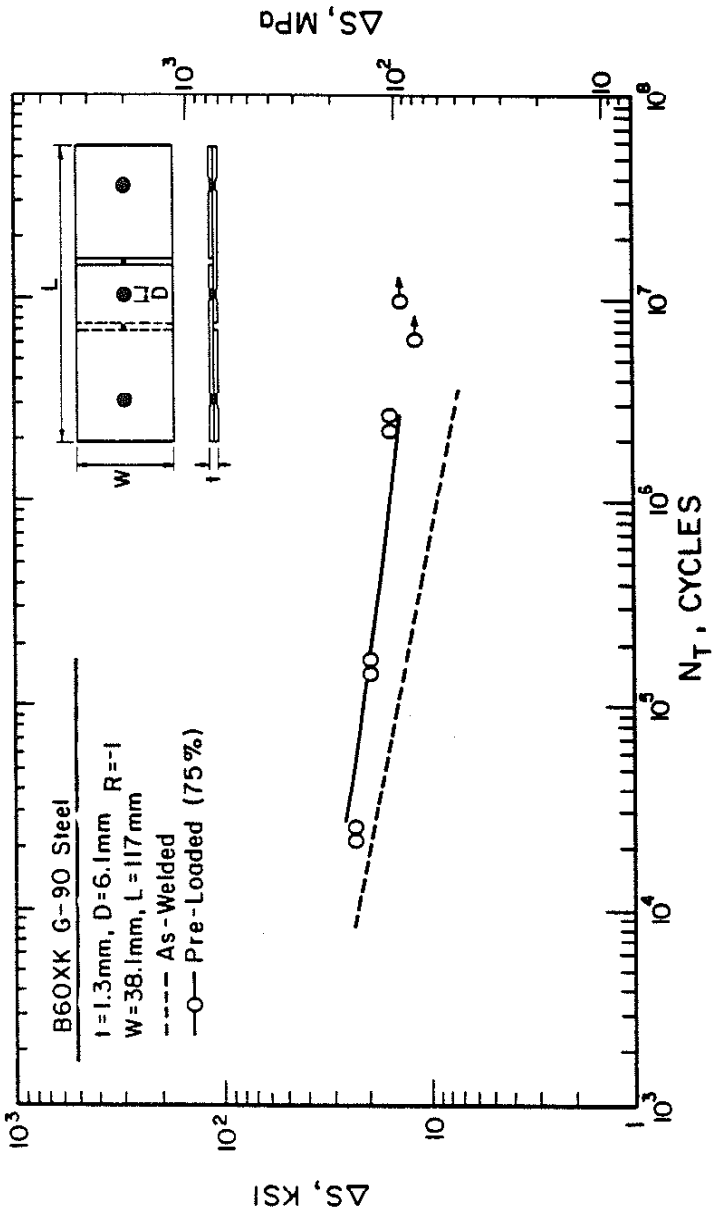

Fig. 35 Total Fatigue Life Predictions (Solid Line) and Fatigue Test Results of R=-1 Loading Condition for Preloaded B60XK G-90 (HSLA) Tensile-Shear Spot Weld.

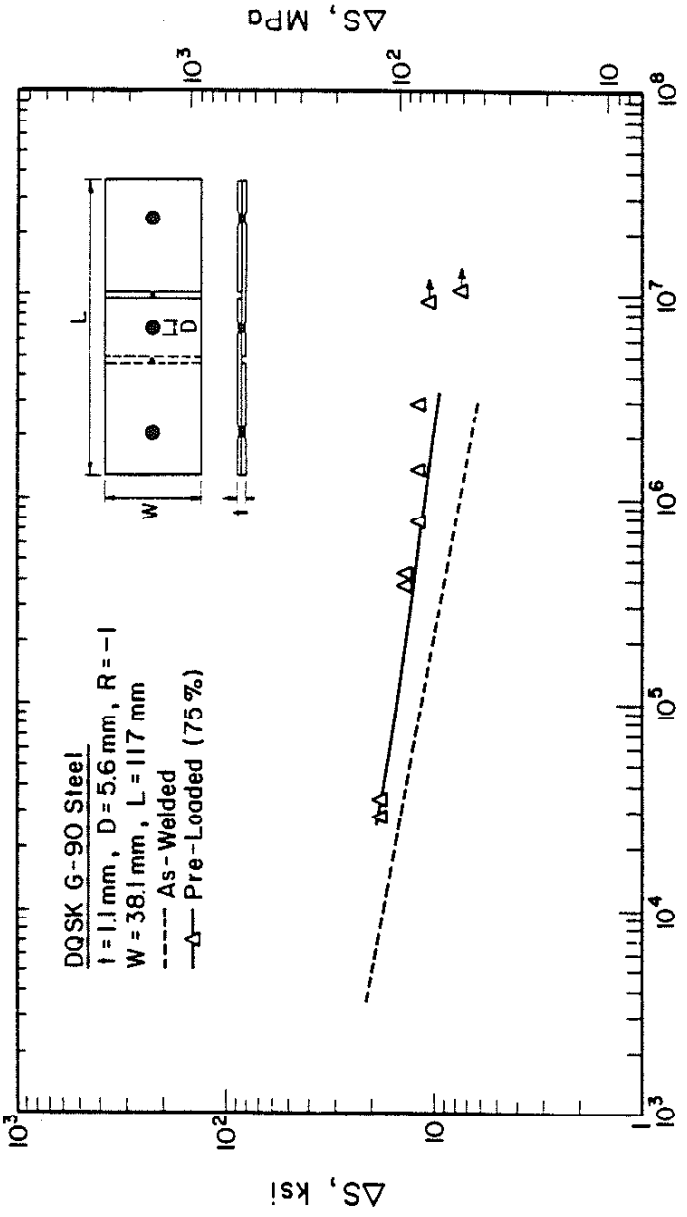

Fig. 36 Total Fatigue Life Predictions (Solid Line) Using TSIP Model and Fatigue Test Results of R=-1 Loading Condition for Preloaded DQSK G-90 (Low Carbon) Tensile-Shear Spot Weld.

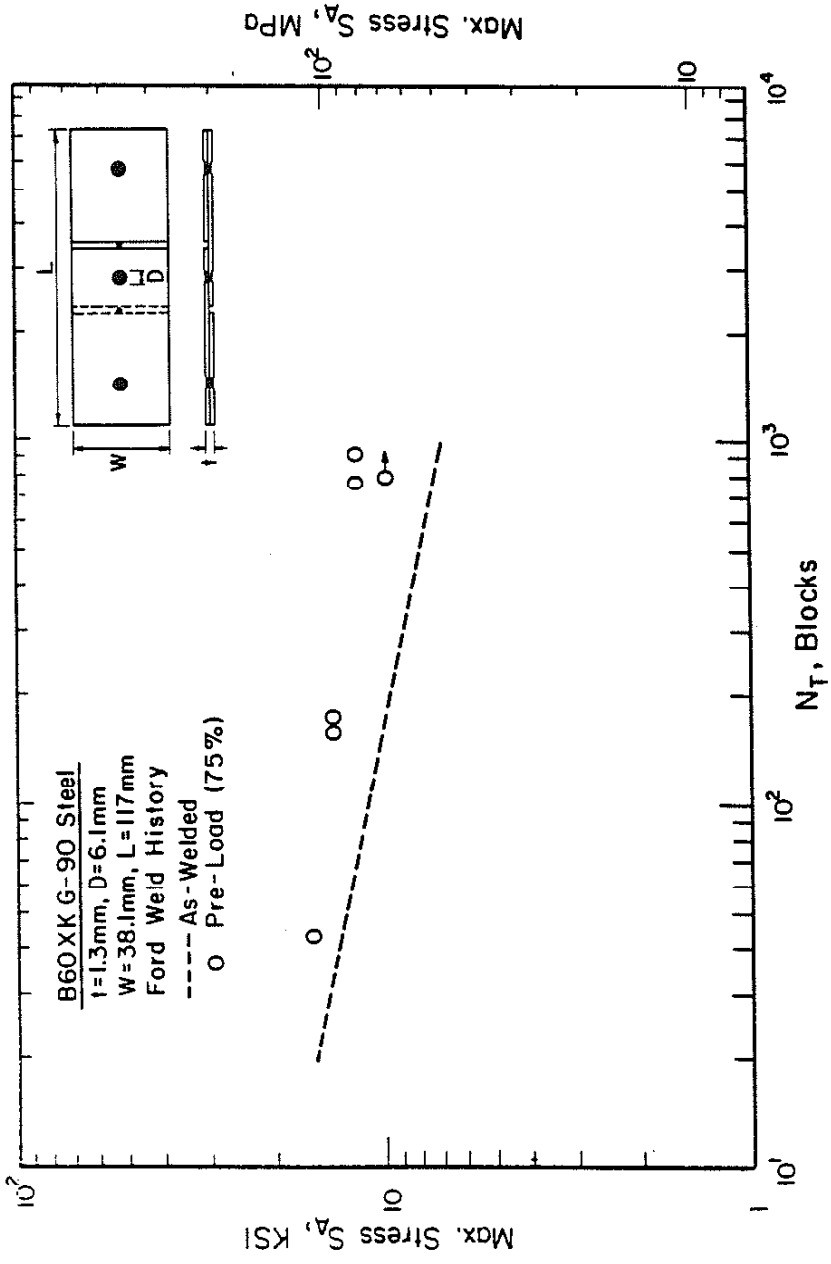

Fig. 37 The Effect of Preloading B60XK G-90 (HSLA) Tensile-Shear Spot Weld Subjected to the Ford Variable Load History.

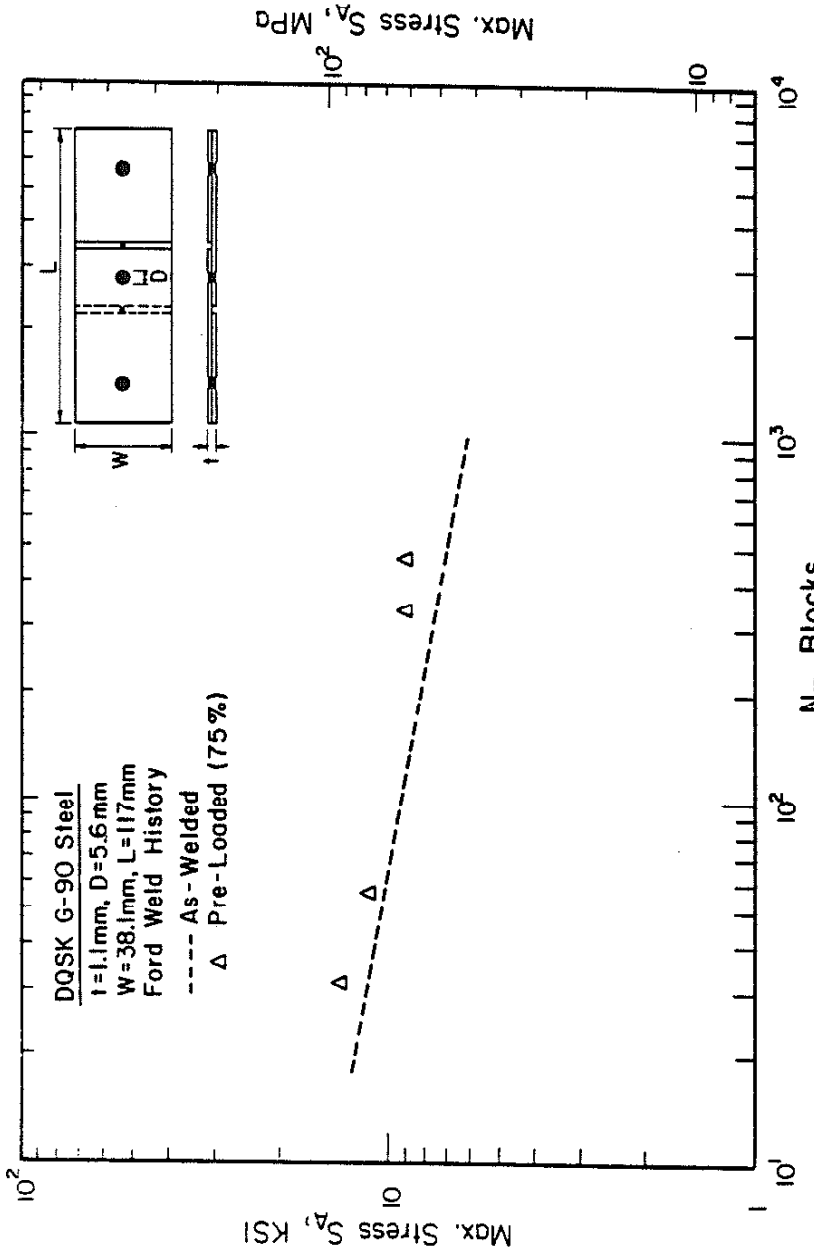

Fig. 38 The Effect of Preloading DQSK G-90 (Low Carbon) Tensile-Shear Spot Weld Subjected to the Ford Variable Load History.

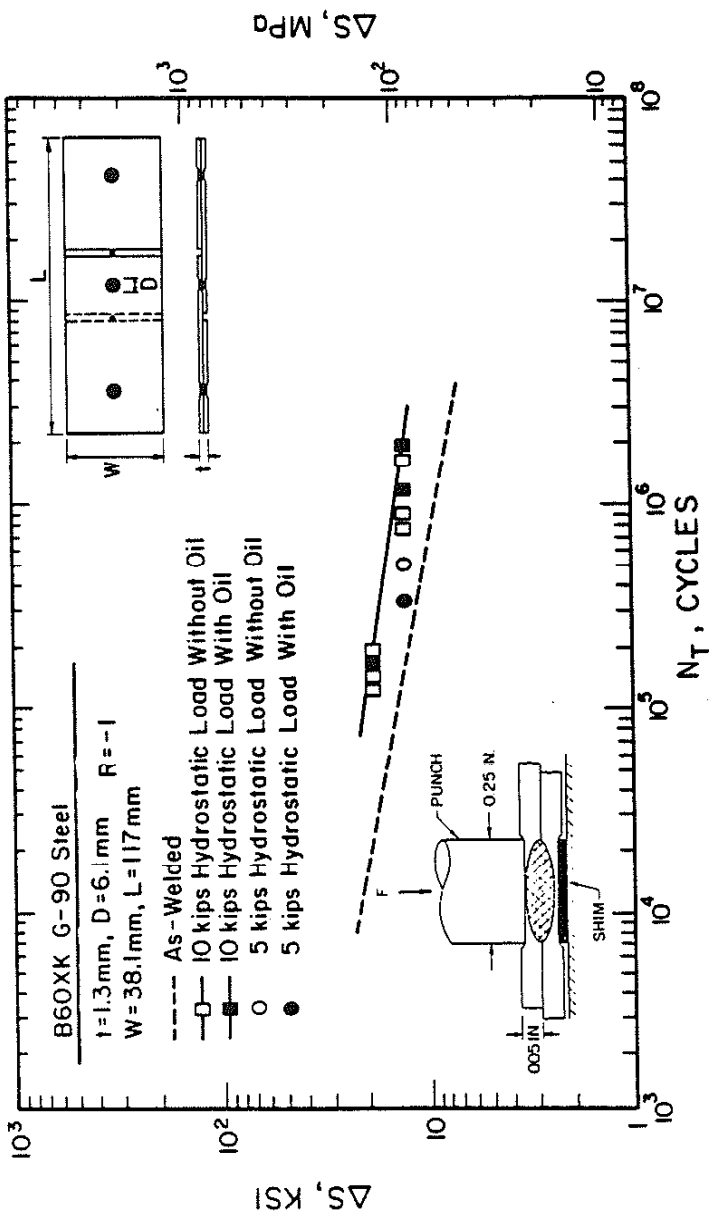

Fig. 39 Total Fatigue Life Predictions (Solid Line) Using TSIP Model and Fatigue Test Results of R=-1 Loading Condition for Coined B60XK G-90 (HSLA) Tensile-Shear Spot Weld.

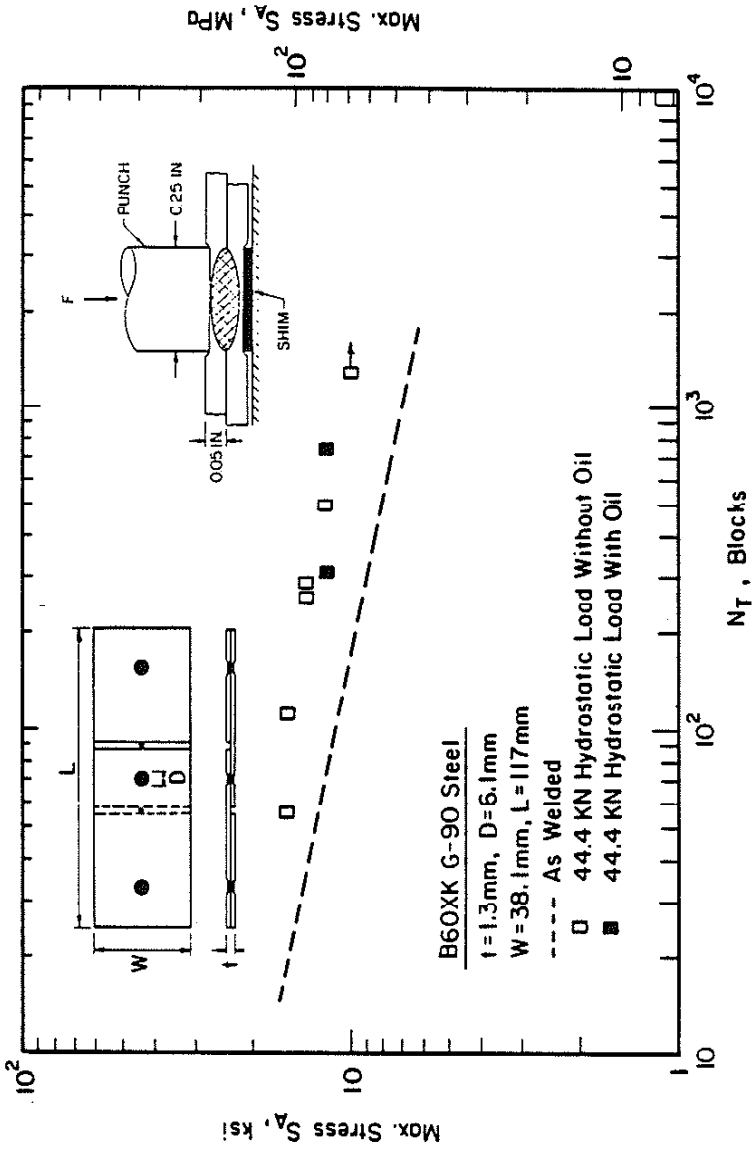

Fig. 40 The Effect of Coining B60XK G-90 (HSLA) Tensile-Shear Spot Weld Subjected to the Ford Variable Load History.

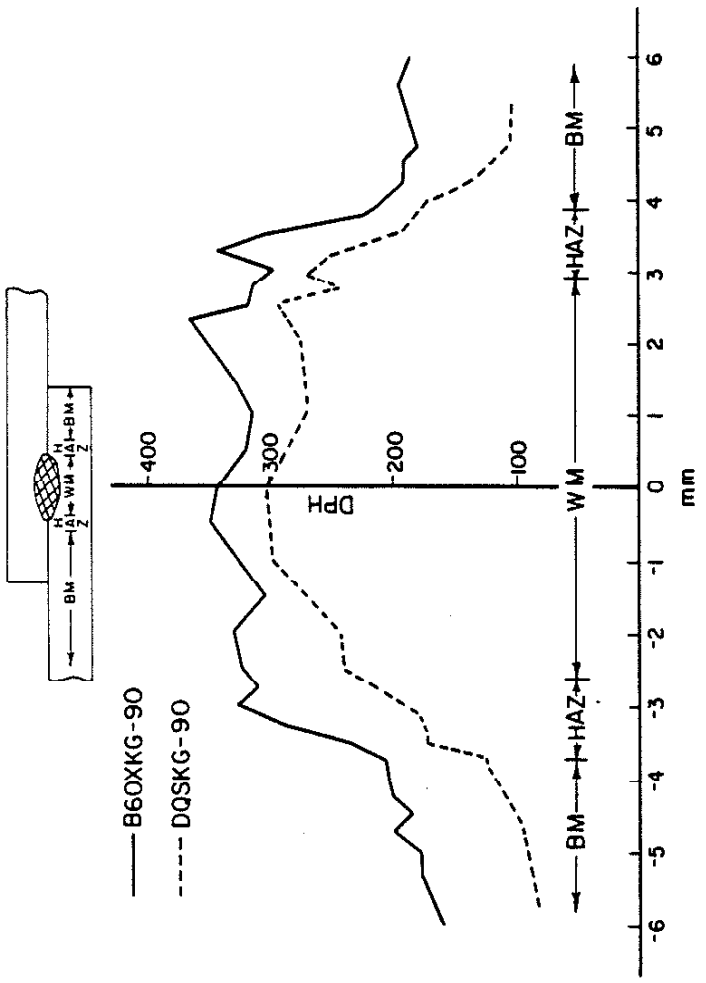

Fig. 41 Microhardness Traverse in the Region of the Fatigue Crack Initiation for B60XK G-90 (HSLA) and DQSK G-90 (Low Carbon) Tensile-Shear Spot Weld.

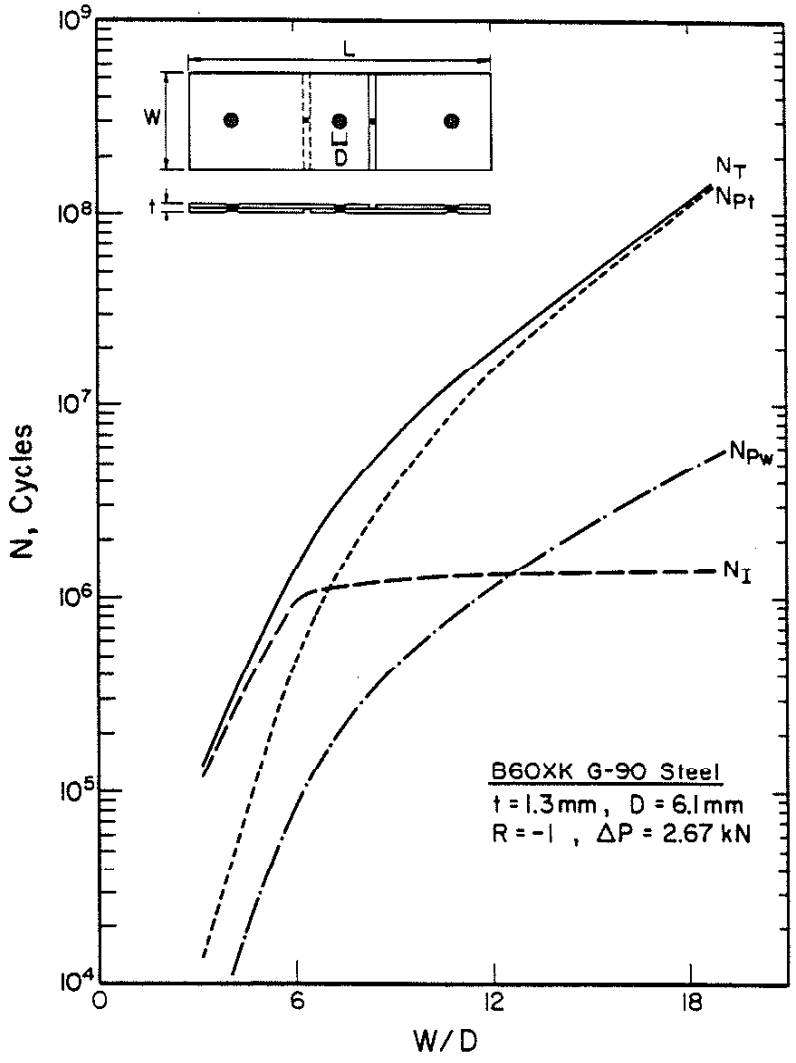

Fig. 42 The Predicted Effect of Sheet Width (W) Using TSIP Model on the Fatigue Life for B60XK G-90 (HSLA) Tensile-Shear Spot Weld.

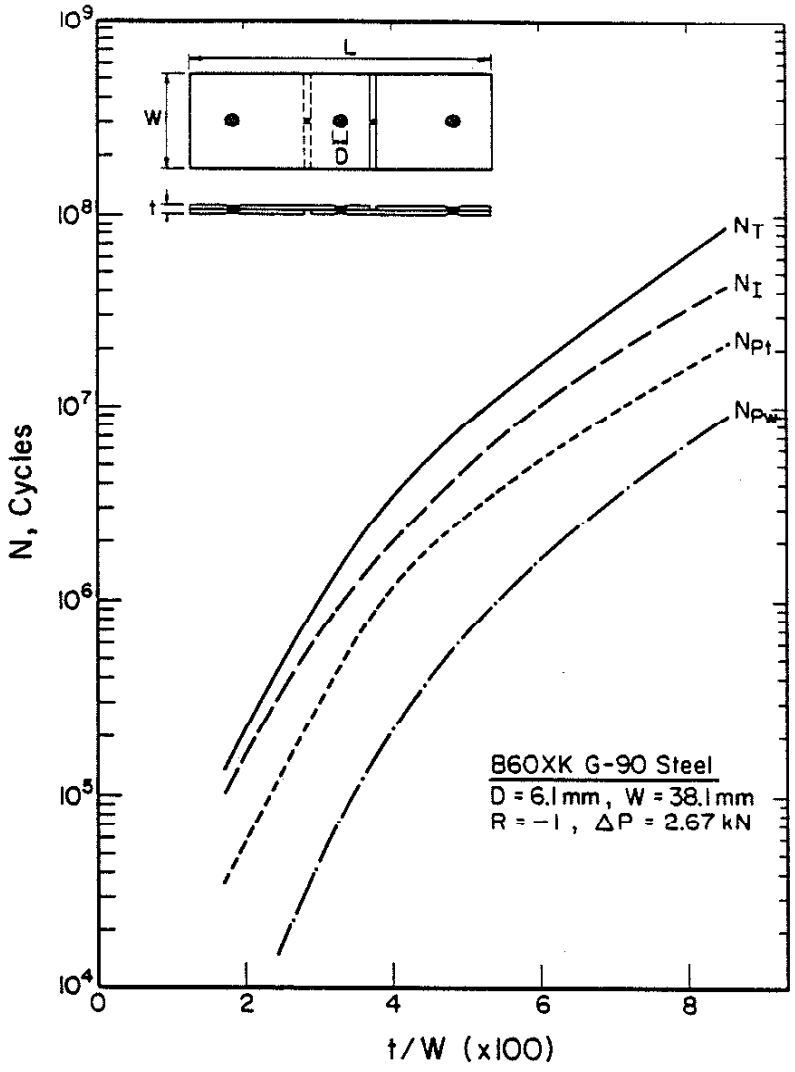

Fig. 43 The Predicted Effect of Sheet Thickness (t) Using TSIP Model on the Fatigue Life for B60XK G-90 (HSLA) Tensile-Shear Spot Weld.

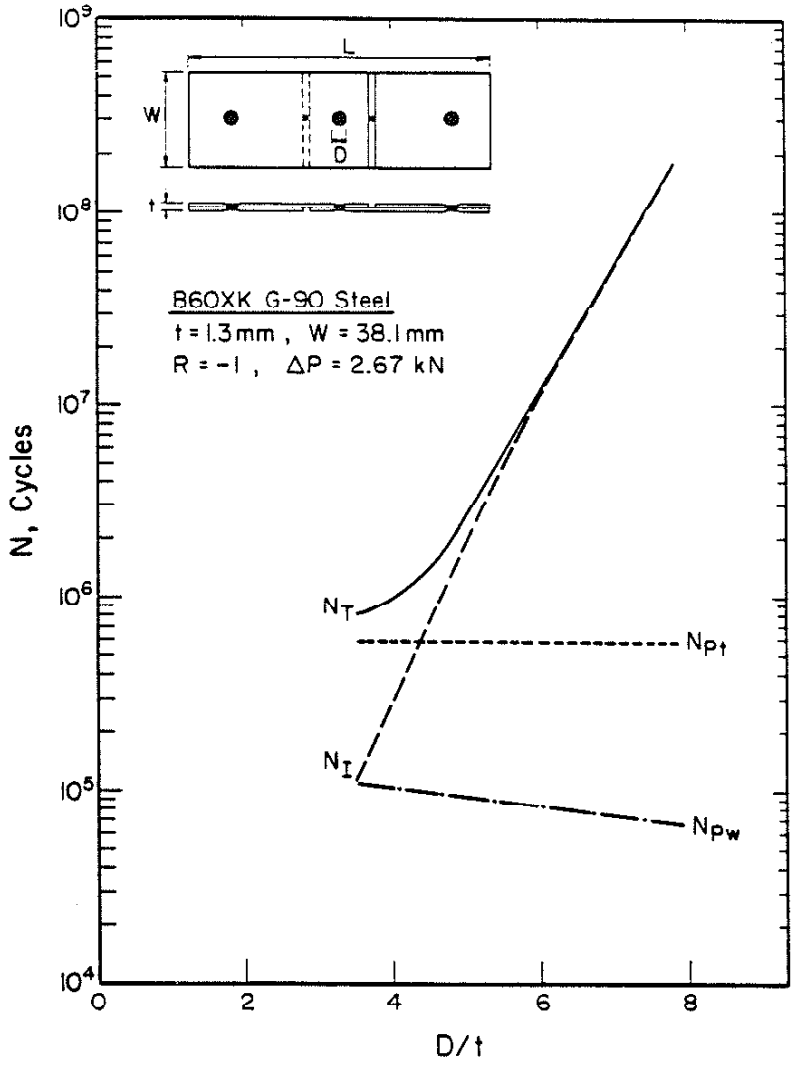

Fig. 44 The Predicted Effect of Nugget Diameter (D) Using TSIP Model on the Fatigue Life for B60XK G-90 (HSLA) Tensile-Shear Spot Weld.

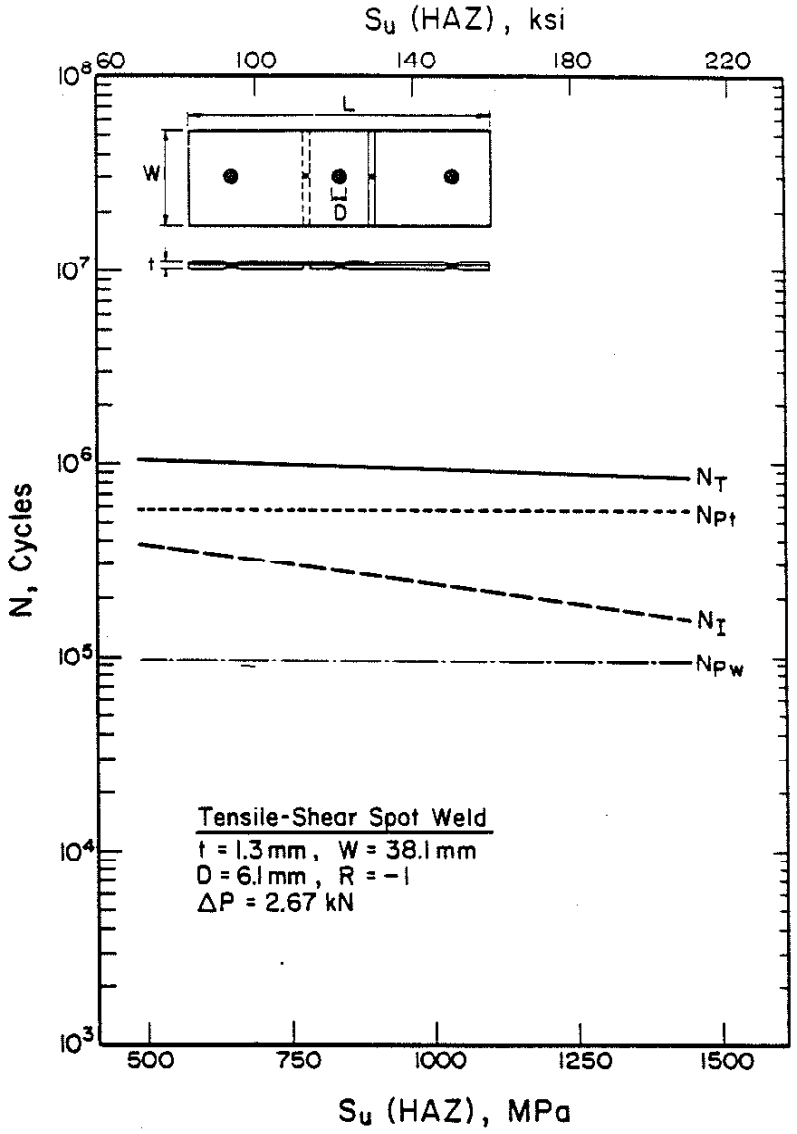

Fig. 45 The Predicted Effect of Material Properties Using TSIP Model on Fatigue Life for B60XK G-90 (HSLA) Tensile-Shear Spot Weld. The HAZ Residual Stresses Are Assumed to be Equal to the Yield Strength of the Base Metal.

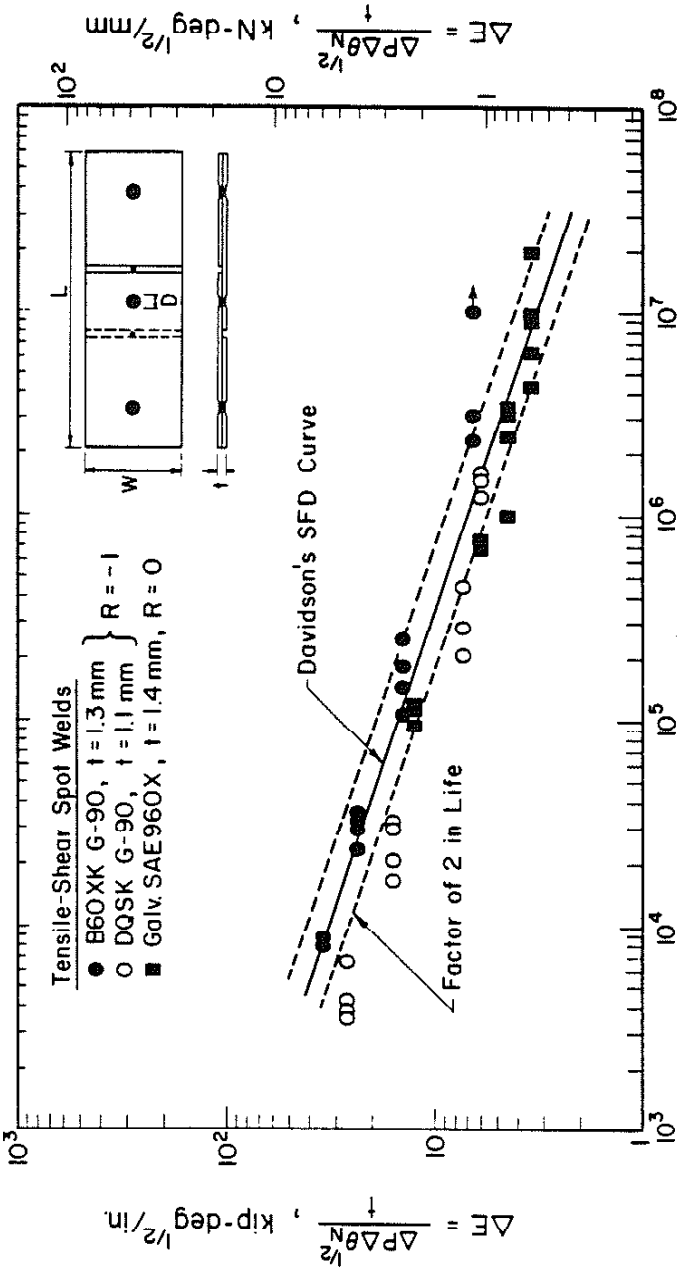

Fig. 46 Comparison of the Predicted Total Fatigue Life Using the SFD Method and the Observed Total Fatigue Life (See Section 6.6).

APPENDIX A

Estimation of Stress Intensity Factor of a Central Crack Subjected to Axial and Bending Load

As seen in Fig. A.1, the stress intensity factor of a central crack (Stage III) subjected to the axial and bending loads can be obtained using superposition (see Section 2.6):

$$\Delta K_{IA} = .5(\Delta K_{IBa} + \Delta K_{IBb} + \Delta K_{IDa} + \Delta K_{IDb}) \tag{A.1}$$

In Fig. A.1, ΔK_{IBa} is the stress intensity factor of structure B under the axial loading and is expressed as:

$$\Delta K_{IBa} = S\sqrt{\pi a}\, Y_{IBa} \tag{A.2}$$

where Y_{IBa} is geometrical factor (72).

$$Y_{IBa} = [1 - .5(2a/W)^3 + .37(2a/W)^2 - .044(2a/W)]/[1 - (2a/W)] \tag{A.3}$$

where W is the sheet width and a the crack length.

The quantity ΔK_{IBb} is the stress intensity factor of structure B subjected to the bending moment and is expressed as:

$$\Delta K_{IBb} = \left(\frac{1 + \nu}{3 + \nu}\right)\frac{6M}{t^2}\sqrt{\pi a}\, Y_{IBb} \tag{A.4}$$

$$= \left(\frac{1 + \nu}{3 + \nu}\right) 3S\sqrt{\pi a}\, Y_{IBb} \tag{A.5}$$

where ν is the Possion's ratio, and Y_{IBb} is the geometrical factor (73), given by

$$Y_{IBb} = -.595(2a/W)^3 + .244(2a/W)^2 + .738(2a/W) - .034(2a/W) + 1 \tag{A.6}$$

The quantity ΔK_{IDa} is the stress intensity factor of structure D subjected to the axial loading and is expressed as:

$$\Delta K_{IDa} = \frac{P}{\sqrt{\pi a}} Y_{IDa} \tag{A.7}$$

$$= \frac{SW}{\sqrt{\pi a}} Y_{IDa} \tag{A.8}$$

where Y_{IDa} is geometrical factor (72), given by

$$Y_{IDa} = 29.71(2a/W)^3 - 36.07(2a/W)^2 + 16.32(2a/W) - 1.56(2a/W) + 1 \tag{A.9}$$

Finally, the quantity ΔK_{IDb} is the stress intensity factor of structure D subjected to the bending moment. Since this stress intensity solution is not available in a closed form, an estimate of ΔK_{IDb} is:

$$\Delta K_{IDb} \approx .25\ \Delta K_{IDa} \tag{A.10}$$

As seen in an infinite plate containing a crack subjected to a centrally located force P at the edge is shown in Fig. A.2. This loading condition is equilvalent to a central located force P at crack center and a bending moment M also shown in Fig. A.2. Due to bending, the crack will get longer on top surface but closure at bottom surface should cause no extension. Combined with the opening due to uniform (axial) force, closure will be reduced on the bottom surface and the crack opening on the top surface will be increased by combined effect of tension and bending. When a stable crack shape is established (dotted line in Fig. A.2), it is anticipated that it will propagate to critical size maintaining approximate geometrical similitude.

Using the average crack length to characterize the crack length and anticipating that the total stress intensity factor K is largest on the top face, smallest on the bottom face. A stress intensity factor K that can be associated with the midplane crack growth rate is expected to be equal to the stress intensity factor K due to the central (axial) force plus a small contribution from bending. As seen in Fig. A.2, the tensile part of bending stresses contribution to cause crack growth may be approximated as one quarter of the axial forces. The bending stresses lead to a triangular shaped stress distribution having an area approximately one-quarter of the area of the axial stress distribution. Also, the bending stresses have a direction parallel to the axial forces. Thus, the stress intensity factor range ΔK for the surface load P (see Fig. A.2) was estimated using superposition and taking $\Delta K_{bending}$ to be approximately .25 ΔK_{axial} :

$$\begin{aligned} \Delta K &= \Delta K_{axial} + \Delta K_{bending} \\ &\approx \Delta K_{axial} + .25\ \Delta K_{axial} \\ &\approx 1.25\ \Delta K_{axial} \end{aligned} \qquad \text{(A.11)}$$

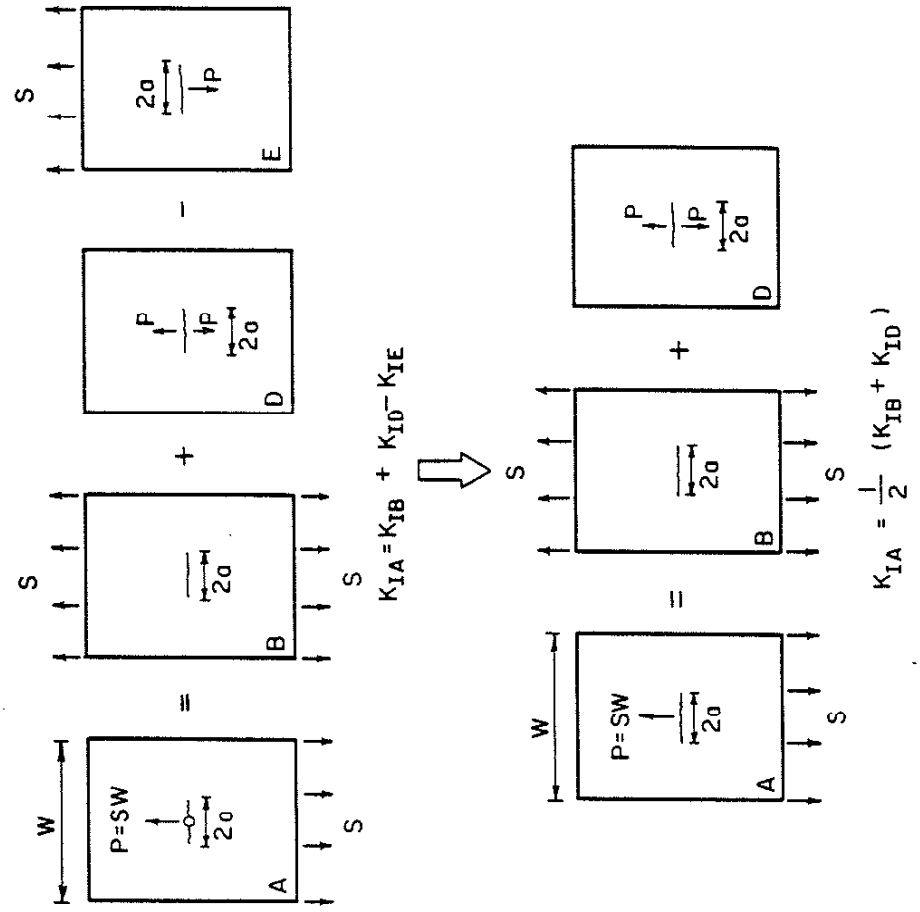

Fig. A.1 Crack Emanating from a Loaded Rivet Hole.

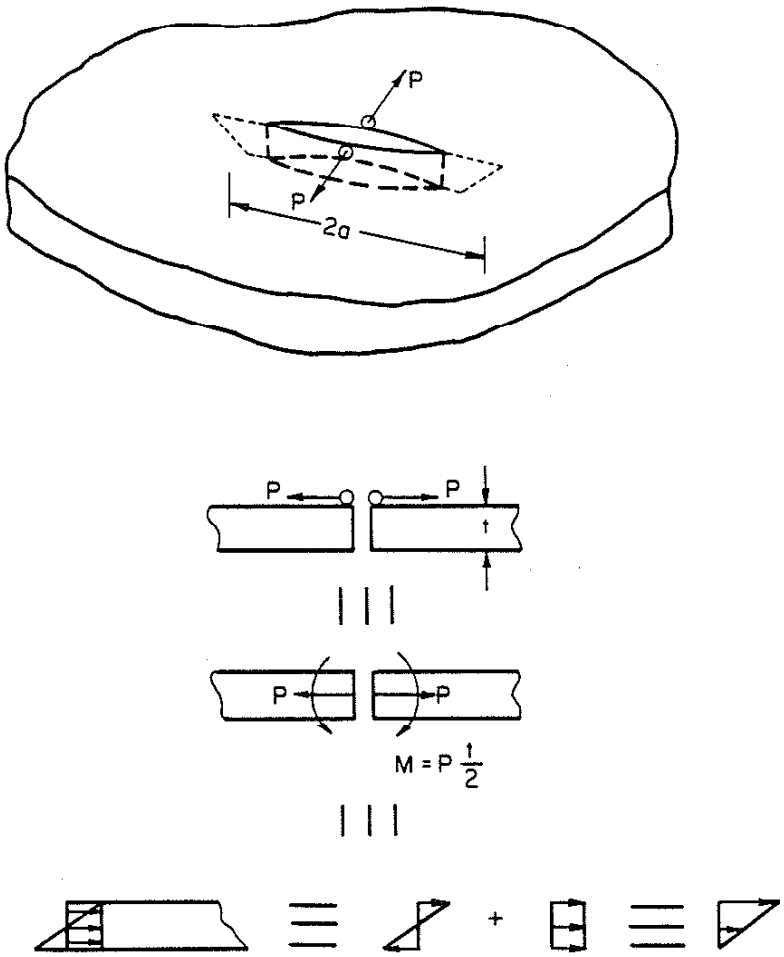

Fig. A.2 Through Crack in an Infinite Sheet Subjected to a Surface Force.

APPENDIX B

Munse Fatigue Criterion for Estimating the Fatigue Resistance of Spot Welds Subjected to Variable Loading

A simple random-load fatigue criterion was proposed by Munse (36) to estimate the maximum stress range of weld under the variable loading. The maximum stress range S_D is obtained from the following equation:

$$S_D = S_N \quad \xi \quad R_F \tag{B.1}$$

where S_N is the constant cycle stress range for detail, the quantity ξ is the random load factor, and R_f is the reliability factor. The procedure of this criterion is shown in Fig. B.1 and may be recapitulated by the following steps:

1. Establish the appropriate loading history for the detail
2. Obtain the S-N curve of detail
3. Find random load factor ξ
4. Find reliability factor R_f
5. Compute the maximum stress range S_D

When a detail is subjected to a constant stress range S, the mean fatigue life N is given by the straight line S-N relationship:

$$\overline{N} = \frac{C}{S^m} \tag{B.2}$$

where C and m are constants that can be determined from a regression analysis of the constant stress range fatigue data. These constants C and m are, respectively, the intercept and (negative) slope of the regression of logN on logS.

The Munse Fatigue Criterion requires that the loading history be represented by a probability distribution function. Consequently, it was necessary to find a distribution or distributions which provide the best fit to the weld loading histories. If a histogram is available for the loading to which a structure will be subjected, it is possible then to establish a Beta distribution such that the mean value and standard deviation for the Beta distribution and the histogram are equal. Beta distribution is a very versatile function and can be made symmetrical or skewed depending on the values of q and r selected.

The random load factor which is based on the assumption that the loading history can be modelled by a Beta distribution is given by:

$$\xi = \left[\frac{\Gamma(q)\Gamma(m+q+r)}{\Gamma(q+r)\Gamma(m+q)}\right]^{1/m} \qquad (B.3)$$

where q and r are the shape parameters of the Beta distribution, m is slope of S–N regression analysis line, and (q) is gamma function of q.

The reliability factor is given by:

$$R_F = \left[\frac{(P_F)^{\Omega_N^{1.08}}}{\Gamma(1+\Omega_N^{1.08})}\right]^{1/m} \qquad (B.4)$$

where P_F is the probability of failure, and Ω_N is the total uncertainity in fatigue life (37). The maximum fatigue stress range for a detail subjected to random loading can be estimated using Eq. B.2, B.3 and B.4.

The advantage of using the Munse Fatigue Criterion is the rational and simple way in which it deals with several complex problems. The method deals with the complexity of a weldment by relying on laboratory tests on welds. The method copes with the problem of variable load distributions which model service histories. The influence of these histories is

reflected in the value of the variable load factor ξ in Eq. B3. The uncertainities in design, testing, fabrication, and stress analysis are dealt with in an elegant but simple way through the reliability factor R_F in the Eq. B.4. The Munse Fatigue Criterion ignores sequence and mean stress effects.

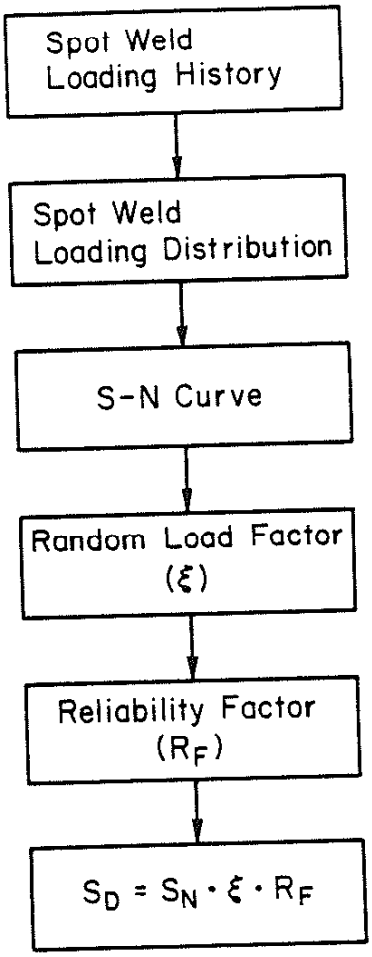

Fig. B.1 The Procedure of Munse Fatigue Criterion.

VITA

Pei-Chung Wang was born at Taiwan in 1953. He received a Bachelor of Science degree in Metallurgy and Materials Engineering in 1976 from National Cheng Kung University of Taiwan.

After obtaining the Bachelor's degree he joined the China Steel Corporation as a shift supervisor of steelmaking and the continuous casting mill. In August, 1977 he entered the University of Wisconsin-Milwaukee, Wisconsin to continue his education. During this time, he served as a graduate research assistant in the Department of Materials Science. He received a Master of Science degree in July, 1979. He then joined the University of Illinois at Urbana-Champaign in August, 1979 to pursue studies leading to the Doctor of Philosophy in Metallurgy and Mining Engineering.

Mr. Wang is a student member of the American Society of Metals.